The

PHILOSOPHICAL MAGAZINE

FIRST PUBLISHED IN 1798

ol. 1 Eighth Series No. 9 September 1956

A Journal of Theoretical Experimental and Applied Physics

PRICE £1 0s. 0d.
Annual Subscription £10 10s. 0d. payable in advance

ALERE FLAMMAM.
Printed and Published by
TAYLOR & FRANCIS LTD.
RED LION COURT, FLEET STREET, LONDON, E.C.4

CONTENTS OF No. 9.

***All communications for the Philosophical Magazine should be addressed, post-paid, to the Editors, c/o Messrs. Taylor and Francis, Ltd., Red Lion Court, Fleet Street, London, England.

LXXXI. *Lattice Vibrations and Specific Heat of Graphite*

By G. R. Baldock
Department of Applied Mathematics, University of Liverpool†

[Received February 2, 1956]

Abstract

The vibrations of the graphite lattice can be treated approximately by ignoring the interaction between displacements parallel and perpendicular to the layer planes. The normal modes then separate into two types, which may be called planar and transverse. The complete frequency distribution of the transverse modes is calculated, and, with the aid of an approximate calculation of the distribution of the planar modes, the specific heat is deduced and compared with experimental results from 1·5° to 1000°K. Above 200° the atomic model gives results close to those obtained by superimposing two Debye two-dimensional continuum models, but below 100° the interaction between layers becomes important. Below 20°, the transverse modes are dominant, and the result is very sensitive to the coefficient of interaction between second neighbours in the layer. This coefficient is close to a critical value which it would attain if the transverse restoring forces on the atoms of a single layer could be considered as acting only against out-of-plane bending of the bonds. It is shown that for any two-dimensional crystal the spectrum of the transverse vibrations is anomalous at low frequencies whenever the potential energy function satisfies certain conditions, and that these conditions are satisfied if the function is independent of any uniform small rotation of the crystal.

§ 1. Introduction

The graphite lattice has four atoms in the unit cell situated at the points $(0, 0, 0)$, $(0, a, 0)$, $(0, 0, c)$, $(0, -a, c)$, and the lattice is generated by the vectors

$$(a\sqrt{3}, 0, 0), (\tfrac{1}{2}a\sqrt{3}, a, 0), (0, 0, 2c),$$

The crystal thus consists of plane layers in each of which the atoms are arranged in a hexagonal pattern. Within each layer the distance between first neighbours is a, while the distance between adjacent layers is c. From the cell dimensions determined by x-ray analysis (Bacon 1951), we obtain

$$a = 1{\cdot}42 \times 10^{-8} \text{ cm}, \qquad c = 3{\cdot}35 \times 10^{-8} \text{ cm}.$$

The interaction between atoms in adjacent layers is much weaker than that between atoms in the same layer, and consequently the Debye

† Communicated by the Author.

three-dimensional continuum approximation fails to predict the observed relation between the specific heat and the temperature. Below 100° the specific heat varies roughly as T^2, instead of T^3 as would be expected.

Because of the weak interaction between layers it is natural, as a first approximation, to neglect it, which is equivalent to assuming that the crystal is effectively just a single hexagonal layer. The normal modes separate into planar and transverse vibrations, both of which make contributions proportional to T^2 to the specific heat at sufficiently low temperatures. By adjusting the characteristic temperatures of the two types of vibration it is possible to obtain good agreement with experiment above 100°. The shape of the frequency distribution curve depends critically on the force constants assumed (Rosenstock 1953), but the specific heat is much less sensitive. No choice of constants, however, will give good agreement at low temperatures. Evidently the interaction between layers must be taken into account. This has been done by Krumhansl and Brooks (1953) (henceforward abbreviated to KB), who calculated the frequency distribution of the transverse modes perturbed by weak interaction between adjacent layers. By assuming the planar vibrations to have a similar distribution, they calculated the specific heat and showed that at low temperatures, where the interaction between layers becomes important, it would vary as T^3. The transition from T^2 to T^3 dependence was predicted in the range between 80° and 20°.

Recent measurements (Bergenlid *et al.* 1954) have produced no evidence for a T^3 law at temperatures down to 1·5°. From 1·5° to 3° the specific heat varies approximately as $T^{2\cdot4}$.

In this paper it is shown that the behaviour of the specific heat at low temperatures can be explained if both interaction between layers and interaction between second neighbours in the same layer is included. The frequency distribution of the transverse vibrations is studied in detail. The distribution of the planar vibrations is estimated approximately, and the specific heat is calculated. The results are compared with experiment and with earlier calculations, and the significance of the second-neighbour interaction is discussed in relation to the binding forces. In the final section there is a discussion of the conditions to be satisfied by the potential energy of a general two-dimensional crystal for it to give rise to a frequency distribution function which behaves anomalously at the origin.

§ 2. The Frequency Distribution of the Transverse Modes

Let the displacement of a typical atom i from its equilibrium position be (u_i, v_i, w_i), where u_i, v_i are components in the layer plane and w_i is the component normal to the plane. The potential energy is a homogeneous quadratic form in the displacement components of all the atoms (terms of higher degree will be neglected). We make the following assumptions.

(*a*) The potential energy contains no terms of the form $u_i w_j$ or $v_i w_j$. This separates the normal modes into those involving only u_i's and v_i's (planar vibrations) and those involving only w_i's (transverse vibrations).

(*b*) The terms of the form $w_i w_j$ are non-zero only if (i) $i=j$, (ii) i and j are first or second neighbours in the same layer or (iii) i and j are first neighbours in adjacent layers.

Figure 1 represents part of a single layer. The atoms 1, 5, 6, 7, 8, 9, 10 have first neighbours in the adjacent layers, while 2, 3, 4 have not. The part of the potential energy function which involves the transverse displacement of atom 1 may be written

$$V_1=\tfrac{1}{2}\alpha \sum_{i=2}^{4} (w_1-w_i)^2+\tfrac{1}{2}\beta \sum_{i=5}^{10} (w_1-w_i)^2+\tfrac{1}{2}\gamma \sum_{i=11}^{12} (w_1-w_i)^2, \qquad (1)$$

where α, β, and γ are constants and 11 and 12 are the first neighbours of atom 1 in the adjacent planes.

Fig. 1

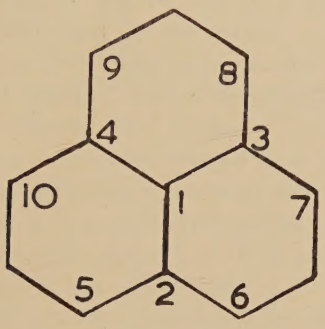

For atom 2 the function is similar but without the last term.

The nature of the binding forces of the layer, which is discussed in § 6, suggests the approximate relation

$$\beta \simeq -\tfrac{1}{6}\alpha.$$

Let $$\kappa=1+6\beta/\alpha.$$

It will be shown that when κ is small its value critically affects the form of the lower end of the frequency distribution.

Let the atomic mass be m, and write

$$2\pi^2\nu^2 m/3\alpha=r, \quad \gamma/\alpha=\rho.$$

The frequencies ν of the normal modes are obtained from the potential energy by writing down the equations of motion of the four atoms in the unit cell and substituting a periodic wave solution for the displacements w_i. This leads to the following determinantal equation

$$\begin{vmatrix} 3+2\rho+\frac{1}{6}(1-\kappa)z-6r & 2\cos\theta+\exp(i\phi) & 2\rho\cos\psi & 0 \\ 2\cos\theta+\exp(-i\phi) & 3+\frac{1}{6}(1-\kappa)z-6r & 0 & 0 \\ 2\rho\cos\psi & 0 & 3+2\rho+\frac{1}{6}(1-\kappa)z-6r & 2\cos\theta+\exp(-i\phi) \\ 0 & 0 & 2\cos\theta+\exp(i\phi) & 3+\frac{1}{6}(1-\kappa)z-6r \end{vmatrix} =0,$$

where θ, ϕ, and ψ are components (multiplied by convenient factors) of the wave-vector in reciprocal lattice space, and

$$z=4\cos\theta(\cos\theta+\cos\phi)-8.$$

The quartic equation in r factorizes into two quadratics, giving

$$r=\tfrac{1}{2}+\tfrac{1}{36}(1-\kappa)z+\tfrac{1}{6}\rho(1\pm\cos\psi)\pm\tfrac{1}{6}\{\rho^2(1\pm\cos\psi)^2+z+9\}^{\frac{1}{2}},$$

in which the first and third ambiguities are taken together but the second is independent.

If the number of atoms in the crystal is large and the Born cyclic condition is used, the density of the normal modes in the reciprocal lattice is uniform. Since the frequency is a function of $\cos\theta$, $\cos\phi$, and $\cos\psi$, the cell $0<\theta<\pi$, $0<\phi<\pi$, $0<\psi<\pi$ contains all the frequencies with their correct density. Moreover, a change in the sign of $\cos\psi$ only reproduces the same set of frequencies, so the ambiguities $\pm\cos\psi$ are unnecessary.

The quantity ρ represents the interaction between layers and may be assumed small compared with unity ; the value chosen in the numerical calculations is $\rho=0{\cdot}18$. Therefore ρ^2 may be neglected except when $z+9$ is small. This occurs near the middle of the frequency band, where the density of modes happens to be low. Hence the effect on the general shape of the distribution is small, and certainly unimportant in the specific heat calculation, and we are justified in neglecting ρ^2 altogether.

In the calculation of the frequency distribution we use the following notation. Let $f(\theta, \phi, \psi)$ be any function of θ, ϕ, and ψ, and let V be the proportion of the volume of (θ, ϕ, ψ)-space occupied by points satisfying $f(\theta, \phi, \psi)<f_0$. Then V is a non-decreasing function of f_0, and its derivative dV/df_0 is the value of the density distribution of the function f at the point f_0. We denote the density distribution in general by the symbol $\mathscr{D}f$, and its value when $f=f_0$ by $\mathscr{D}f(f_0)$.

It is instructive to calculate the frequency distribution first on the assumption that $\kappa=1$ and $\rho=0$ (single layer with only first-neighbour interaction), then to modify it by introducing arbitrary κ (second-neighbour interaction in the plane), and finally to modify it again to include ρ (interaction between layers).

Let $\quad p=\tfrac{1}{2}\pm\tfrac{1}{6}(z+9)^{\frac{1}{2}}$, and $q=\kappa p+(1-\kappa)p^2$,

so that $\quad r=q+\tfrac{1}{6}\rho(1-\cos\psi)$.

If we assume $\kappa=1$ and $\rho=0$, then $\nu^2\propto p$. The distribution of p has been evaluated by several authors (see Rosenstock 1953). It is

$$\begin{aligned}
&p<0 \text{ or } p>1, && \mathscr{D}p=0,\\
&0<p\leqslant\tfrac{1}{3}, && \mathscr{D}p=\frac{9(1-2p)}{\pi^2 B}K\left(\frac{A}{B}\right)\\
&\tfrac{1}{3}\leqslant p\leqslant\tfrac{1}{2}, && \mathscr{D}p=\frac{9(1-2p)}{\pi^2 A}K\left(\frac{B}{A}\right)\\
&\tfrac{1}{2}\leqslant p<1, && \mathscr{D}p=\mathscr{D}(1-p),
\end{aligned}$$

where $A^2=3p(2-3p)^3$, $B^2=3(1-2p)$, and $K(k)=\int_0^{\pi/2}(1-k^2\sin^2\xi)^{-1/2}\,d\xi$ (Legendre's complete elliptic integral of the first kind).

This function is illustrated by the solid curve in fig. 2. It contains logarithmic singularities at $p=\frac{1}{3}$ and $p=\frac{2}{3}$, and falls to zero at $p=\frac{1}{2}$. At $p=0$ it is approximately constant, and the resulting frequency distribution $\mathscr{D}\nu$ would be proportional to ν at low frequencies, as is expected for a two-dimensional lattice.

Fig. 2

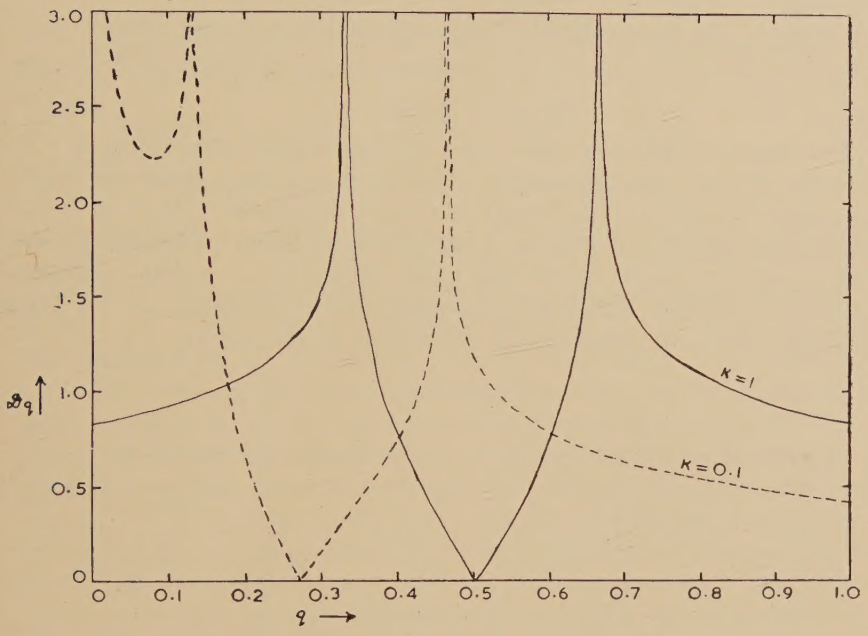

Since q is an increasing function of p, the distribution of q is simply

$$\mathscr{D}q=(dp/dq)\mathscr{D}p=\{\kappa+2(1-\kappa)p\}^{-1}\mathscr{D}p.$$

If $\kappa>1$, the effect on the distribution is to shift the singularities and the zero to the right and to produce a sharp maximum at $q=1$, extending but not otherwise distorting the first portion of the curve. The general features of the distribution for values of κ from 1 to ∞ have been described by Rosenstock (1953). If $0<\kappa<1$, the opposite effect is obtained. The broken line in fig. 2 is the graph of $\mathscr{D}q$ for $\kappa=0{\cdot}1$. When κ is small, the resulting frequency distribution $\mathscr{D}\nu$ is of the form $C\nu$ when ν is very small, C being a large constant. As ν increases, there comes a point at which the gradient of the curve suddenly falls to a low value, and there follows a frequency range for which $\mathscr{D}\nu$ is approximately constant. Beyond this range the curve rises to the first infinite discontinuity. In the special case $\kappa=0$, $\mathscr{D}q$ has an infinity at the origin of the form $q^{-1/2}$, and $\mathscr{D}\nu$ has the same form as $\mathscr{D}p$, since $\nu\propto p$. So $\mathscr{D}\nu$ is approximately constant for small values of ν, which is the result which would normally be expected for a one-dimensional lattice.

The distribution of r is

$$\mathscr{D}r=\pi^{-1}\int_0^{\pi}\mathscr{D}q\{r-\tfrac{1}{6}\rho(1-\cos\psi)\}d\psi.$$

It is positive for $0<r<1+\frac{1}{3}\rho$, and zero elsewhere. It resembles $\mathscr{D}q$, but the infinite discontinuities are cut off, and $\mathscr{D}r\propto r^{1/2}$ when r is small, except in the special case $\kappa=0$, when $\mathscr{D}r$ is approximately constant near the origin. In addition there is a sharp peak at $r=\frac{1}{3}\rho$.

Writing ν_m for the maximum frequency and $\nu/\nu_m=\bar{\nu}$, we obtain

$$r=(1+\tfrac{1}{3}\rho)\bar{\nu}^2$$

and

$$\mathscr{D}\bar{\nu}=2(1+\tfrac{1}{3}\rho)\bar{\nu}\mathscr{D}r.$$

This function, with $\kappa=0{\cdot}01$ and $\rho=0{\cdot}18$, is illustrated in fig. 3. For $\bar{\nu}<0{\cdot}005$, $\mathscr{D}\bar{\nu}\propto\bar{\nu}^2$ approximately. The curvature then decreases, and in the range $0{\cdot}01<\bar{\nu}<0{\cdot}1$ the graph is almost rectilinear. Beyond $\bar{\nu}=0{\cdot}1$, $\mathscr{D}\bar{\nu}$ increases rapidly to a sharp maximum at $\bar{\nu}=0{\cdot}24$. The intermediate linear range is a result of the low value chosen for κ. With a larger κ, the range is shorter, and with κ as high as $0{\cdot}1$ it disappears. The range is longest when $\kappa=0$, and in this case $\mathscr{D}\bar{\nu}\propto\bar{\nu}$ at the origin.

Fig. 3

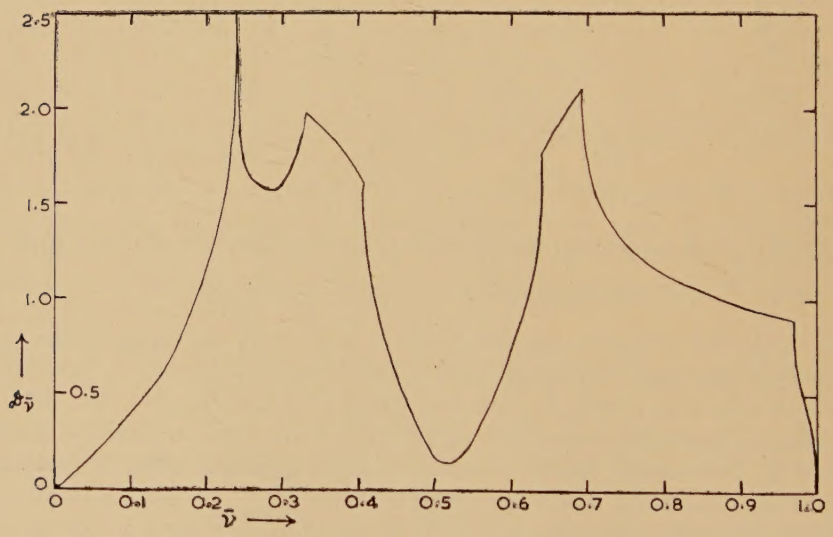

§ 3. Frequency Distribution of the Planar Modes

The planar modes, like the transverse modes, will have a distribution similar to that for a single layer, but corrected for the small interaction between layers. The secular determinant for the planar modes of the single layer is of the fourth order, but in this case the quartic equation does not factorize. We therefore approximate by the method of KB, which is equivalent to assuming the crystal to be a set of weakly coupled elastic sheets.

Let $\bar{\nu}'$ be the ratio of the frequency ν' of a normal mode to the frequency ν'_m of the highest mode. Then it is easily shown that the distribution has the following form

$$0<\bar{\nu}'<\sigma, \qquad \mathscr{D}\bar{\nu}'=2\pi^{-1}A\bar{\nu}'\sin^{-1}\bar{\nu}',$$
$$\sigma<\nu'<1, \qquad \mathscr{D}\bar{\nu}'=A\bar{\nu}'.$$

Here A is a constant adjusted so that $\int_0^1 \mathscr{D}\bar{\nu}'d\bar{\nu}'=1$, and σ corresponds to a low frequency below which the interaction between layers takes effect. To simplify the calculation the following slightly different function is used.

$$0<\bar{\nu}'<0{\cdot}9\sigma, \qquad \mathscr{D}\bar{\nu}'=2\pi^{-1}A\nu'^2,$$
$$0{\cdot}9\sigma<\bar{\nu}'<1, \qquad \mathscr{D}\bar{\nu}'=A\bar{\nu}',$$

the coefficient 0·9 being chosen so that $\int_0^\sigma \mathscr{D}\bar{\nu}'d\bar{\nu}'$ is the same in both cases.

Although this distribution is a coarse approximation to the true distribution, its use for specific heat calculations has some justification. The specific heat is not sensitive to the exact form of the distribution except at low temperatures, where the lower end of the spectrum is of most importance. If the approximation is used (as in KB) for both the planar and the transverse vibrations, the disagreement between the predicted and the experimental specific heats is serious at low temperatures. But the planar modes have a higher average frequency than the transverse modes, so that the lower end of the planar spectrum is masked by the more accurately computed transverse spectrum. Errors in the planar spectrum are therefore less important in the derivation of the specific heat.

In KB it is assumed that $\sigma=0{\cdot}1$. The value chosen here is $\sigma=0{\cdot}01$, on the ground that the interaction between layers, which is responsible for forces tending to prevent slipping between adjacent layers, is known to be very weak in graphite. It can therefore be expected to be much smaller than the corresponding interaction for the transverse vibrations.

§ 4. Calculation of the Specific Heat

The specific heat at constant volume, expressed in calories per degree per gramme-atom, is

$$c_v=c_{vt}+c_{vp}+c_{ve},$$

where c_{vt} and c_{vp} are the contributions due to transverse and planar vibrations, and c_{ve} is due to the electronic motion.

We have $$c_{vt}=R\int_0^1 x^2e^x(e^x-1)^{-2}\mathscr{D}\bar{\nu}d\bar{\nu}$$

and $$c_{vp}=2R\int_0^1 x^2e^x(e^x-1)^{-2}\mathscr{D}\bar{\nu}'d\bar{\nu}',$$

where R is the gas constant and $x=h\nu/kT$ or $h\nu'/kT$.

The second expression contains the factor 2 because the number of normal modes is twice the number of atoms.

Define the characteristic temperatures of the vibrations

$$\Theta_t = h\nu_m/k \quad \text{and} \quad \Theta_p = h\nu'_m/k.$$

Then, in the two expressions,

$$x = \bar{\nu}\Theta_t/T \quad \text{and} \quad x = \bar{\nu}'\Theta_p/T.$$

The characteristic temperatures, chosen to give the best fit with the experimental results, are

$$\Theta_t = 1300, \qquad \Theta_p = 2500.$$

The electronic contribution c_{ve} is significant only at the extreme ends of the temperature range (1·5°–1000°) considered. The expression derived by Komatsu and Nagamiya (1951) (henceforward abbreviated to KN), using the theory of Wallace (1947), is

$$c_{ve} = 6{\cdot}7 \times 10^{-7} T(3{\cdot}29 + 0{\cdot}49 \times 10^{-2} T + 0{\cdot}14 \times 10^{-5} T^2 + \ldots\ldots).$$

At 1000° the contribution amounts to 0·006. At low temperatures c_{ve} is proportional to T, and it gives a contribution to the second significant figure below 3°.

The total specific heat thus calculated is given in the second column of table 1. In the third column are the observed values, which have been taken from the following sources: 1·5°–80°, Bergenlid *et al.* 1954; 100°–300°, De Sorbo and Tyler 1953; 500°–1000°, Spencer 1948.

Table 1

T (°K)	c_v (calories per degree per mole)	
	Calculated	Observed
1·5	0·0000356	0·0000377
2	0·0000751	0·0000750
3	0·000194	0·000193
4	0·000392	0·000395
8	0·0021	0·0024
10	0·0034	0·0039
15	0·0082	0·0094
20	0·0159	0·0183
30	0·038	0·044
50	0·120	0·124
80	0·316	0·279
100	0·476	0·409
150	0·874	0·778
200	1·30	1·20
300	2·11	2·05
500	3·47	3·47
800	4·59	4·66
1000	5·03	5·04

§ 5. Features of the Specific Heat Curve

The calculated specific heats are in good agreement with the observed results over the whole range. The parameters determining the function $c_v(T)$ in the approximation used here are Θ_p, σ, Θ_t, κ, and ρ. The values chosen are listed in table 2, together with the corresponding quantities used by previous authors.

Table 2

Parameter	Present calculation	Komatsu and Nagamiya	Krumhansl and Brooks
Θ_p	2500	2440	2500
σ	0·01	0	0·1
Θ_t	1300	1430	950
κ	0·01	0	1
ρ	0·18	0·4	0·04

Above 500° the specific heat is governed by Θ_p. The frequency distribution of the planar modes has the same form in all three approximations, and consequently the values chosen for Θ_p are about the same. In KN, Θ_p is calculated from force constants derived from the planar vibrations of benzene, so that in this range there is a good fit between the specific heat theory and the optical spectrum data.

The maximum frequency of the transverse vibrations determines Θ_t, which in all the approximations has been chosen to give the best agreement with the observed specific heat. The differences between the values are due to the different forms of the frequency distribution. Thus, in KB, there is no sharp maximum in the lower part of the range, but the distribution increases linearly with ν up to a maximum at ν_m. This accounts for the low value of Θ_t needed to match the specific heat curve.

The constants σ, κ, and ρ affect the specfic heat at temperatures below 100°. In KN, the use of $\sigma=0$ and $\kappa=0$ causes c_v to vary as T^2 at low temperatures, and the theoretical results are much too high below 100°. It is clearly necessary to have $\sigma>0$, and in KB σ is chosen so that the planar and transverse frequency distributions should be exactly similar. But the weak resistance to slipping between the layers suggests that this value is too high; moreover, Brennan (1952) has calculated that the energy difference between the graphite structure and one in which every atom has nearest neighbours in each of the adjacent layers is no more than 0·36 kcal/mole. The value $\sigma=0{\cdot}01$ therefore seems more appropriate. Also the KB approximation permits the law $c_v \propto T^3$, which is to be expected near $T=0$, to appear at too high a temperature, and the theoretical results are too low below 50°. The approximation cannot be improved by changing ρ, because the frequency distribution, which changes rapidly from $\mathscr{D}\nu \propto \nu^2$ to $\mathscr{D}\nu \propto \nu$, implies a rapid change from $c_v \propto T^3$ to $c_v \propto T^2$, while the empirical law derived from the observed results

is $cv \propto T^{\epsilon}$, where ϵ varies from 2·0 at 40° to 2·4 at 1·5°. This slow transition can be realized by choosing κ small, and it is found that the calculated specific heat below 20° is very sensitive to the value of κ. It seems likely that the ultimate T^3 region is never reached, because at such low temperatures the electronic component, which is proportional to T, would become dominant.

§ 6. Discussion of the Transverse Vibrations

Objections (see KB) have been raised to the KN calculation because it is based on the assumption that each layer plane vibrates in the same manner as a uniform elastic plate whose thickness is small compared with the extent, but large compared with the atomic distances, and this is said to lead to certain physical inconsistencies. Despite the artificiality of the model, it gives a frequency distribution closely resembling that which would be obtained from the atomic model with $\kappa=0$; that is, the model corresponds to the force constants having certain critical values. In fact, the correct force constants seem to be very nearly critical, and consequently the KN model provides an approximation which is better than one might expect.

There is considerable theoretical justification for choosing κ very small. In eqn. (1), the function V_1 corresponds to a model in which the atoms in the layer are joined by tightly stretched strings, the constants α and β being the tensions per unit length in the strings connecting first and second neighbours. However, the flatness of the layer is maintained not by tensile forces, but by energy changes involved in the distortion of the orbitals of the binding electrons. The four valence electrons of the carbon atom in the trivalent state occupy hybridized orbitals, three σ-orbitals symmetrically directed at mutual angles of 120 in one plane, and one π-orbital normal to the plane. The stability of the graphite layer is due primarily to the interactions between σ-electrons belonging to nearest neighbours, and it is these electrons in the directed orbitals which determine the crystalline configuration. This is confirmed by the fact that the angles are constant over a whole group of molecules.

We may therefore expect the angles between the bonds to be the chief factors in the force constants for transverse vibrations, and central forces between second neighbours to be relatively unimportant. A suitable measure of the angular distortion of the orbitals at atom 1 (see fig. 1), due to transverse displacements, is the length h of the perpendicular from 1 to the plane 234. If we assume that the potential energy of the single layer is a quadratic form in variables such as h, we find that, in our approximation, $\beta=-\frac{1}{6}\alpha$, that is $\kappa=0$. The same result is obtained using any suitable angle between lines joining two atoms and planes containing three atoms. It implies that the tensions in the strings in the model may be negative, and it is equivalent to the condition that the model as a whole is subject to zero stress when all the transverse displacements are zero. Thus the type of binding involved leads us to expect a very small value for κ. In § 8 this point is considered generally.

The comments and conclusions in this section and the previous one confirm suggestions made by Newell (1955) in his comprehensive qualitative survey of the problem.

§ 7. The Elastic Constants

It should be possible to correlate the various parameters in this calculation with the elastic constants of the graphite crystal. Only the bulk modulus is known reliably. Bridgman (1945) has studied the compressibility of graphite at high pressures. Extrapolation of the results to zero pressure produces the value $3{\cdot}36\times10^{11}$ dynes/cm. It has been observed by Brennan (1952) that since the binding energy between layers is much smaller than that of atoms in the layers, the bulk modulus should be almost equal to the Young's modulus E for compression in the direction perpendicular to the planes. It can therefore be derived from ρ and Θ_t, and its value is

$$E=\frac{4\rho c\pi^2k^2m}{3\sqrt{3}(3+\rho)a^2h^2}\Theta_t{}^2=10{\cdot}5\times10^{11}\text{ dynes/cm.}$$

Here ρ and Θ_t have been chosen to give the best fit with the experimental specific heat data. The discrepancy between this and the observed modulus may be due to our neglect of interactions between atoms which are neither first nor second neighbours, or to the approximation adopted for the distribution of the planar modes, or perhaps to the neglect of coupling between the planar and transverse vibrations. All these considerations may have effect at low temperatures, where the specific heat is sensitive to ρ. Another possibility is that the compressibility measurements may not apply to a perfect single crystal, and consequently strain may be produced in the material partly by slipping of the layers on each other. Such slipping occurring only to a slight exent would appreciably lower the bulk modulus, as is exemplified by the work of Faris *et al.* (1951) on artificial polycrystalline graphite samples, in which values as low as $4{\cdot}7\times10^{10}$ dynes/cm are obtained. On this account it seems likely that the value of E for a single crystal may be higher than that inferred from Bridgman's results.

§ 8. Critical Potential Functions

In § 2 it is observed that $\kappa=0$ is a critical value in the sense that the frequency distribution $\mathscr{D}\nu$ for the transverse vibrations of a single layer is non-zero at $\nu=0$ instead of being proportional to ν. In general the potential energy function of the transverse displacements of the atoms of a plane layer will be termed critical if it leads to such an anomaly in the behaviour of $\mathscr{D}\nu$ at the origin. We now determine the conditions for a potential function to be critical.

Consider a two-dimensional crystal containing n atoms of mass m_j ($j=1, 2, \ldots n$) in each unit cell. Let the position vector of the jth atom in the cell whose lattice vector is $\mathbf{r}$ be $\mathbf{r}+\mathbf{a}_j+w_{j\mathbf{r}}\mathbf{c}$, where $\mathbf{c}$ is a unit vector

perpendicular to a fixed plane containing all the constant vectors $\mathbf{r}$ and $\mathbf{a}_j$, and $w_{j\mathbf{r}}$ is small compared with the interatomic distances. The potential energy of the transverse displacements is assumed to be a quadratic form in the variables $w_{j\mathbf{r}}$ in which the coefficient of $w_{j\mathbf{r}}\, w_{k,\mathbf{r}+\mathbf{s}}$ is $\alpha_{jk\mathbf{s}}$. By the symmetry of the lattice

$$\alpha_{jk,-\mathbf{s}}=\alpha_{kj\mathbf{s}}. \quad . \quad . \quad . \quad . \quad . \quad . \quad . \quad . \quad . \quad . \quad (2)$$

It will be assumed that $\alpha_{jk\mathbf{s}}$ is zero whenever $|\mathbf{s}|>R$, where R is small compared with the size of the crystal.

The equations of motion are

$$-m_j\ddot{w}_{j\mathbf{r}}=\partial V/\partial w_{j\mathbf{r}}=2\alpha_{jj0}w_{j\mathbf{r}}+\sum_{k=1}^{n}\sum_{\mathbf{s}}\alpha_{jk\mathbf{s}}w_{k,\mathbf{r}+\mathbf{s}} \qquad (j=1, 2, \ldots n).$$

In this and all succeeding expressions the terms involving coefficients of the form α_{jj0} are understood to be omitted from the summations.

Since V and its partial derivatives must be unaltered by a uniform transverse displacement of the whole crystal,

$$2\alpha_{jj0}=-\sum_{k=1}^{n}\sum_{\mathbf{s}}\alpha_{jk\mathbf{s}}, \quad (j=1, 2, \ldots n). \quad . \quad . \quad . \quad (3)$$

The solutions of the equations of motion are plane waves of the form

$$w_{j\mathbf{r}}=W_j \exp\{2\pi i[\boldsymbol{\kappa} \,.\, (\mathbf{r}+\mathbf{a}_j)-\nu t]\},$$

in which the frequency ν and the wave-vector $\boldsymbol{\kappa}$ are connected by the equation

$$\Delta(\nu, \boldsymbol{\kappa})=0, \quad . \quad . \quad . \quad . \quad . \quad . \quad . \quad . \quad . \quad (4)$$

where Δ is a $n\times n$ determinant whose elements are

$$\Delta_{jk}(\nu, \boldsymbol{\kappa})=\sum_{\mathbf{s}}\alpha_{jk\mathbf{s}} \exp\{2\pi i\boldsymbol{\kappa} \,.\, (\mathbf{s}+\mathbf{a}_k-\mathbf{a}_j)\}, \qquad (j\neq k)$$

$$\Delta_{jj}(\nu, \boldsymbol{\kappa})=-\sum_{k=1}^{n}\sum_{\mathbf{s}}\alpha_{jk\mathbf{s}}+\sum_{\mathbf{s}}\alpha_{jk\mathbf{s}} \exp(2\pi i\boldsymbol{\kappa} \,.\, \mathbf{s})-4\pi^2 m_j\nu^2.$$

To examine the spectrum in the neighbourhood of $\nu=0$ we expand $\Delta_{jk}(0, \boldsymbol{\kappa})$ in powers of the components κ_x and κ_y of $\boldsymbol{\kappa}$, discarding cubic and higher terms. Write

$$\Delta_{jk}(0, \boldsymbol{\kappa})=A_{jk}+B_{jk}(\boldsymbol{\kappa})+C_{jk}(\boldsymbol{\kappa}), \quad (j, k=1, 2, \ldots n)$$

where

$$A_{jk}=\Delta_{jk}(0, 0),$$

$$B_{jk}(\boldsymbol{\kappa})=2\pi i\sum_{\mathbf{s}}\alpha_{jk\mathbf{s}}\,\boldsymbol{\kappa} \,.\, (\mathbf{s}+\mathbf{a}_k-\mathbf{a}_j),$$

and

$$C_{jk}(\boldsymbol{\kappa})=-2\pi^2\sum_{\mathbf{s}}\alpha_{jk\mathbf{s}}\{\boldsymbol{\kappa} \,.\, (\mathbf{s}+\mathbf{a}_k-\mathbf{a}_j)\}^2.$$

By (3) the determinant Δ (0, 0), whose elements are A_{jk}, is zero, and all its signed minors of order $n-1$ are equal to the same quantity D. By (2) the linear terms in κ_x and κ_y in the expansion of Δ $(0, \boldsymbol{\kappa})$ vanish, so that eqn. (4) will in general give ν^2 proportional to a quadratic expression in κ_x and κ_y, and hence $\mathscr{D}\nu\propto\nu$, since by the cyclic boundary condition the points (κ_x, κ_y) are uniformly distributed in the reciprocal lattice space.

The condition for the potential energy to be critical is therefore that, for an arbitrary vector $\boldsymbol{\kappa}$, the quadratic terms in κ_x and κ_y should vanish

in the expansion of $\Delta(0, \boldsymbol{\varkappa})$. Let the determinant obtained from $\Delta(0, 0)$ by replacing A_{jk} by B_{jk} and $A_{j'k}$ by $B_{j'k}$ $(k=1, 2, \ldots n)$ be $E(j, j', \boldsymbol{\varkappa})$. Then the quadratic terms amount to the left hand side of the equation

$$\sum_{j=1}^{n}\sum_{j'=1}^{n} E(j, j', \boldsymbol{\varkappa})+D\sum_{j=1}^{n}\sum_{k=1}^{n} C_{jk}(\boldsymbol{\varkappa})=0, \quad \ldots \quad (5)$$

which is the condition for the potential energy to be critical. If it is satisfied eqn. (4) gives ν^2 proportional to a quartic expression in κ_x and κ_y, and so the expansion of $\mathscr{D}\nu$ at $\nu=0$ begins with a constant term.

We now show that the potential energy is critical if its density is unaltered by rotation of the crystal about any line.

Because of (3) the potential energy may be written

$$V=-\tfrac{1}{4}\sum_{\mathbf{r}}\sum_{j=1}^{n}\sum_{k=1}^{n}\sum_{\mathbf{s}}{}'\alpha_{jk\mathbf{s}}\,(w_{j\mathbf{r}}-w_{k,\,\mathbf{r}+\mathbf{s}})^2.$$

Here the summation with respect to $\mathbf{r}$ extends over all the cells of the crystal, and the summation Σ' extends over all values for which the cell $\mathbf{r}+\mathbf{s}$ is occupied. This restriction takes effect only when the cell $\mathbf{r}$ is within a distance R of the boundary, and the proportion of such cells will be regarded as a small quantity.

The increase in $w_{j\mathbf{r}}$ caused by a small rotation about an arbitrary line through the origin may be written $\boldsymbol{\lambda}\,.\,(\mathbf{r}+\mathbf{a}_j)$, where $\boldsymbol{\lambda}$ is an arbitrary vector in the plane of the vectors $\mathbf{r}$ and $\mathbf{a}_j$. The potential energy after such a rotation is

$$V'=-\tfrac{1}{4}\sum_{\mathbf{r}}\sum_{j=1}^{n}\sum_{k=1}^{n}\sum_{\mathbf{s}}{}'\alpha_{jk\mathbf{s}}\{w_{j\mathbf{r}}-w_{k,\,\mathbf{r}+\mathbf{s}}-\boldsymbol{\lambda}\,.\,(\mathbf{s}+\mathbf{a}_k-\mathbf{a}_j)\}^2.$$

We require that $(V'-V)/N$, where N is the total number of cells in the crystal, should be zero for all $w_{j\mathbf{r}}$ and $\boldsymbol{\lambda}$. Since the proportion of cells within a distance R of the boundary is small, we may replace $\sum_{\mathbf{s}}'$ by $\sum_{\mathbf{s}}$, and the coefficient of $w_{j\mathbf{r}}$ in $(V'-V)/N$ is

$$\sum_{k=1}^{n}\sum_{\mathbf{s}}\alpha_{jk\mathbf{s}}\,\boldsymbol{\lambda}\,.\,(\mathbf{s}+\mathbf{a}_k-\mathbf{a}_j)=(2\pi i)^{-1}\sum_{k=1}^{n} B_{jk}(\boldsymbol{\lambda}).$$

The term independent of all the $w_{j\mathbf{r}}$'s in $(V'-V)/N$ is

$$-\tfrac{1}{4}\sum_{j=1}^{n}\sum_{k=1}^{n}\sum_{\mathbf{s}}\alpha_{jk\mathbf{s}}\{\boldsymbol{\lambda}\,.\,(\mathbf{s}+\mathbf{a}_k-\mathbf{a}_j)\}^2=\tfrac{1}{8}\pi^{-2}\sum_{j=1}^{n}\sum_{k=1}^{n} C_{jk}(\boldsymbol{\lambda}).$$

The conditions for the invariance of the energy density with respect to rotation are therefore

$$\sum_{k=1}^{n} B_{jk}(\boldsymbol{\lambda})=0 \quad (j=1, 2, \ldots n) \quad \ldots \quad (6)$$

and

$$\sum_{j=1}^{n}\sum_{k=1}^{n} C_{jk}(\boldsymbol{\lambda})=0 \quad \ldots \quad (7)$$

for an arbitrary vector $\boldsymbol{\lambda}$.

Now from (3) $$\sum_{k=1}^{n} A_{jk}=0, \quad (j=1, 2, \ldots n)$$

and so (6) implies that

$$E(j, j', \boldsymbol{\varkappa})=0, \quad (j, j'=1, 2, \ldots n). \quad . \quad . \quad . \quad . \quad (8)$$

Since (7) and (8) are true for arbitrary $\boldsymbol{\lambda}$, condition (5) is satisfied and the potential energy is critical.

Condition (5) being weaker than the combined requirements (6) and (7), the converse is not true, and a potential function may be critical without being invariant under rotation.

References

Bacon, G. E., 1951, *Acta Crystallographica Camb.*, **4,** 558.

Bergenlid, U., Hill, R. W., Webb, F. J., and Wilks, J., 1954, *Phil. Mag.*, **45,** 851.

Brennan, R. O., 1952, *J. Chem. Phys.*, **20,** 40.

Bridgman, P. W., 1945, *Proc. Amer. Acad. Arts Sci.*, **76,** 9.

de Sorbo, W., and Tyler, W. W., 1953, *J. Chem. Phys.*, **21,** 1660.

Faris, F. E., Green, L., and Smith, C. A., *J. App. Phys.*, **23,** 89.

Komatsu, K., and Nagamiya, T., 1951, *J. Phys. Soc. Japan*, **6,** 438.

Krumhansl, J., and Brooks, H., 1953, *J. Chem. Phys.*, **21,** 1663.

Newell, G. F., 1955, *J. Chem. Phys.*, **23,** 2431.

Rosenstock, H. B., 1953, *J. Chem. Phys.*, **21,** 2064.

Spencer, H. M., 1948, *J. Ind. Eng. Chem.*, **40,** 2152.

Wallace, P. R., 1947, *Phys. Rev.*, **71,** 622.

LXXXII. *Etchpits and Dislocations in Zinc Single Crystals*

By A. H. A. Méléka†
The British Iron and Steel Research Association, Sheffield‡

[Received February 6, 1956]

Summary

The object of this work was to obtain information on the possibility of indexing dislocations by the presence of etchpits. High-purity zinc single crystals have been etched in 0·1% iodine in alcohol and the distribution of the etchpits was studied. This agreed with the theoretical calculations based on the interaction of dislocations, provided every etchpit is taken to represent the site of a single dislocation of unit strength.

§ 1. Introduction

It is now generally accepted that dislocations are responsible for the plastic behaviour of crystals. The theories that have been put forward, from Taylor to Mott, are mainly observational in nature, i.e. they lay emphasis on certain features of dislocation grouping which seem to be suggested by experimental facts. This approach had to be taken since it was not possible to observe or locate dislocations. It has been recently shown, however, that single dislocations can be located by the presence of etchpits under suitable etching conditions.

The present paper describes the results of an attempt to use this technique in revealing dislocation configurations in deformed single crystals of high-purity zinc.

Zinc is a suitable metal for the present investigation. There are two reasons : Firstly, slip occurs on the basal plane only and the dislocation configurations are therefore not of a complicated nature. Secondly, the density of the dislocations that exist inside the deformed crystal is not very high. This makes the observation of single dislocations easier than, say, in the case of a cubic crystal where the density is understood to be rather high.

§ 2. Indexing a Dislocation

2.1. *Dislocations and Growth Spirals*

Single dislocations were first located in crystals by the appearance of growth spirals. This follows from the ideas put forward by Frank (1952)

† This paper is a summary of part of a Ph.D thesis presented to the University of London in May, 1954. The work was carried out at the Sir John Cass College, London.

‡ Communicated by the Author.

in his original theory of crystal growth, and from the extensive study of growth spirals, e.g. Verma (1953). The fundamental point is that a step must always be raised on a surface of a crystal if a dislocation emerges with a component of its Burgers vector normal to that surface. Conversely, every termination of a step must mark the seat of a dislocation. Thus the property of producing spiral growth patterns offers a direct means for locating dislocations. This method, however, is limited to crystals that develop these patterns. Again elaborate optical techniques are usually necessary for these observations, and a good surface is required. In the case of large metal crystals grown from the melt, which crystals are generally used in experiments on plastic deformation, the above conditions are not fulfilled. The search for dislocations must therefore rely on a property other than that of producing growth spirals.

2.2. *Dislocations and Etchpits*

Horn (1952) working on silicon carbide crystals was the first to demonstrate that, because of their chemical properties, dislocations can be located by the presence of etchpits in the surface of crystals. Forty (1954) and Gevers (1953) obtained similar results on other crystals.

The experiments of Vogel *et al.* (1953) on lineage boundaries in germanium crystals provide convincing evidence that single edge dislocations of unit strength can be accurately located by the presence of etchpits.

This etching technique for indexing dislocations is independent of high surface quality and does not require very refined microscopic techniques. It, therefore, offers a simple and convenient way of locating dislocations in crystals.

The first attempt to apply this technique to the study of the phenomenon of slip is reported by Amelinckx (1953). By etching a deformed electrolytically polished aluminium specimen made up of large crystals, he found that etchpits grouped themselves along slip lines and certain grain boundaries together with a random distribution.

Sets of etch channels have been observed by means of the electron microscope on the (111) faces of a ZnS crystal by Dekeyser *et al.* (1953). The channels were made up of individual pits while the rest of the surface was free of them. As the lines coincide crystallographically with expected slip lines, these authors argue that the pits represent sites of dislocations along slip lines.

The present author (Abdou 1954) in some preliminary experiments has reported the grouping along slip lines of etchpits in zinc single crystals, revealed by etching in 20% chromic acid and by natural corrosion. Later a systematic study was undertaken under standard conditions, the results of which are reported below.

§ 3. Experimental

Throughout the investigation 99·997% pure zinc was used. The crystals were grown from the melt in a gradient furnace. They were polished electrolytically in 20% chromic acid at a current density of 2·5 amp/cm². This gave a well-polished surface suitable for microscopic observations.

3.1. *Choice of Etching Reagent*

The two main conditions to be fulfilled by the reagent are :—

(*a*) The etchpits it produces should not be large compared with the average distance between them, otherwise they would run into each other forming channels and thus make a detailed study of the behaviour of the pits rather difficult.

(*b*) The etching should not result in a random distribution of etchpits due to a general attack on the surface.

Several etching reagents have been tried to find out the most suitable for the present investigation. The one decided upon and used throughout the work was 0·1% iodine in alcohol. Weaker solutions gave very fine pits which were difficult to detect. This reagent rapidly developed etchpits and a standard time of two seconds was decided upon.

' Atmospheric etching ' proved to satisfy the above conditions but was not systematically adopted because of the relatively long periods of etching and the difficulty in standardization.

§ 4. Results

(1) A crystal was deformed in tension at room temperature. Only a small number of fine slip lines appeared on the surface. Upon etching the crystal under standard conditions etchpits developed along the slip lines, a typical appearance is shown in fig. 1 (*a*). The same area is shown in figs. 1 (*b–e*) after successive etching of the crystal for the total times indicated. The fine etchpits that first appeared enlarge and deepen by increasing the etching time. The main observation is that the number of the pits along the slip lines remained constant. This behaviour was typical of all the groups of pits along other slip lines.

(2) Several crystals were deformed in tension at various temperatures and then polished electrolytically to obliterate the slip lines. The thickness of the removed layer ranged from about 0·05 mm to 0·25 mm as determined by the difference in diameter before and after polishing. The crystals were then etched under standard conditions. In no case did any etchpits develop even after increasing the etching time to 20 minutes.

Some of the above mentioned crystals were further deformed in tension and slip lines appeared on the surface. Standard etching produced grouping of etchpits along slip lines as in (1).

(3) To investigate whether the method of producing slip lines influenced the development of etchpits, some crystals were deformed by bending. The slip lines that appeared resembled those produced by tensile deformation, and etchpits developed along them in the same manner as mentioned in (1).

A fine scratch by a steel needle on the polished surface of a zinc single crystal produces fine short slip lines along both sides of the scratch. The essential difference between these lines and those produced by tension or bending is that the former do not run completely round the crystal surface while the latter always do. Figure 2 shows the result of etching scratch-produced slip lines. Two observations are noted here. Firstly, etchpits appeared *only* along the limited length of the slip line. Secondly, the pits showed a tendency to group together in clusters of two or three pits ; this usually occurred at the end of the slip line which was far from the scratch.

(4) To investigate the effect of the slip displacement on the number and grouping of etchpits, crystals were deformed in tension and lines with different shear were observed. The slip displacement of a number of lines was measured by means of multiple-beam interferometry. Upon etching the crystal under standard conditions etchpits developed along the lines in the usual way. Figure 3 shows a typical field of view.

The conclusion reached from this study was that the density of etchpits generally increased along lines with larger shear. (Compare lines 1 and 2 on the micrograph.) This, however, was not always the case. Another important factor was the spacing between the lines ; closely-spaced lines of small shear may have more pits along them than widely-spaced ones with larger shear. Lines 3 and 4 for example have almost the same amount of slip, but the pits are more crowded along 3 which has got a number of slip lines in its immediate neighbourhood.

(5) To investigate the effect of additional deformation on the grouping of etchpits, a crystal was deformed at an applied resolved stress of $\sim$50 g/mm^2 and then etched. A typical field of view is shown in fig. 4 (*a*). The crystal was further deformed with the stress increased to $\sim$85 g/mm^2 and again etched under standard conditions. The same field of view is shown in fig. 4 (*b*). The number of etchpits increased on one line from 4 to 11, while the minimum spacing of pits decreased from 9 μ to 1 μ. This general behaviour was typical of other slip lines on the surface of the crystal.

(6) The configuration of the etchpits in some crystals exhibited some geometrical regularities. Consider fig. 5. On each of the two slip lines indicated there is a group of etch pits which shows a tendency to pile up, but the striking feature is that each pit on one slip line is situated midway between two pits on the other slip line. This is clearly seen in the region shown enlarged in the corner of the micrograph.

(7) In a heavily deformed crystal, though the whole crystal was covered with well-defined lines, etchpits developed along some of them only, as shown in fig. 6. The striking feature was that the pits persisted along the preferred lines, all round the crystal. It was noticed that the favoured lines were not necessarily those with larger shear.

(8) Undeformed crystals developed no etchpits with the standard etching solution, even after increasing the etching time to 20 minutes.

§ 5. Discussion

The appearance of slip lines on the surface of a deformed crystal indicates that a large number of dislocation rings have swept across the whole of the slip plane and escaped to the surface. There are, however, other dislocations that are trapped inside the deformed crystal. This is substantiated by microscopical evidence, besides the indirect evidence of the hardening of the slip plane. X-ray reflection studies of cold worked metals further support the conception of trapped dislocations. This evidence, however, gives no indication as to how these dislocations are distributed, or where they are situated. It has been suggested (Brown 1952) that trapped dislocations in cubic crystals exist not only on the slipped planes but also in the glide packets between them. In a hexagonal crystal, however, there is no need to assume that, since the hardening is slow. The number of retained dislocations is not very large, and the slipped planes can accommodate them.

It is not surprising, therefore, to find that etchpits in all the deformed zinc single crystals examined group themselves along slip lines only. Because of their stress fields, more dislocations are trapped on closely-spaced slip planes than on widely-spaced ones. This was found to be the behaviour of etchpits as shown in fig. 3. As deformation proceeds the slip planes become harder and harder ; more dislocations are, therefore, expected to be retained in the slipped plane. This is clearly seen to be the behaviour of etchpits as in fig. 4.

5.1. *Distribution of the Etchpits*

If every etchpit represents the location of a single dislocation, the distribution of the pits should agree with the dislocation configurations based on the interaction of dislocations. How far the above results agree with theoretical calculations will now be discussed. Three cases will be considered.

(i) *Equi-distant dislocations*

The simple case of two dislocations of the same sign on the same slip plane, will be considered first. These dislocations will repel but can be kept at an equilibrium distance d apart if a sufficient stress σ is applied. This distance is given by :

$$d=\frac{Gb}{2\pi k\sigma} \qquad \text{(Kuhlmann 1951)}$$

where G is the shear modulus, b the lattice constant, and k is unity for a screw dislocation, and $(1-\nu)$ for an edge dislocation. (ν is Poisson's ratio.)

Figure 4 (a) shows a set of equi-distant etchpits. The mean distance is

$$d=9\times10^{-4}\text{ cm.}$$

The stress that developed the slip lines was $\sigma=5\times10^{3}$ g/cm^2. Substituting the constants for zinc, the above expression gives

$$d=5{\cdot}3\times10^{-4}\text{ cm.}$$

The distance between the etchpits is, therefore, of the same order as the equilibrium distance between like edge dislocations under the corresponding applied stress.

(ii) *Piled-up groups of dislocations*

Consider a section of a slip plane of length L between a source and a barrier. The source will generate a number of like dislocations under an applied stress σ, which will drive them towards the barrier. This case has been discussed by Cottrell (1953) and treated in more detail by Eshelby *et al.* (1951). Under equilibrium conditions n dislocations will be packed along the slip plane under the applied stress σ. From Cottrell's calculations $n=2L\sigma/Gb$.

Fig. 7

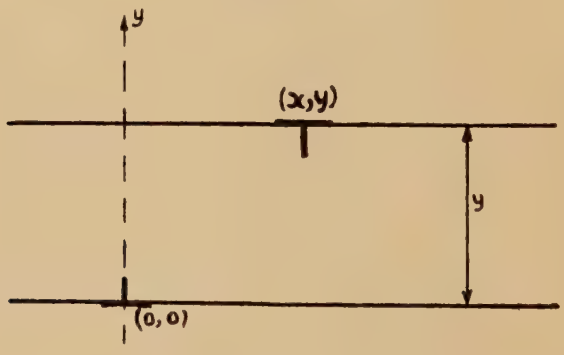

Stable-equilibrium Configuration of two Dislocations.

Now consider fig. 1 (a). The distance between the pits is not constant but shows the appearance of a piled-up group. The spacing decreases as we move from pit P_1 to pit P_2. This section of the slip plane is of length $L=4{\cdot}4\times10^{-3}$ cm. The applied stress at this stage $\sigma=1{\cdot}5\times10^{4}$ g/cm^2. Substituting these values, the above expression gives $n=13{\cdot}8$.

We should, therefore, expect to find 14 dislocations piled up in this section of the slip plane. The number of etchpits actually observed is $n=11$.

(iii) *Regular arrays of dislocations*

In his theory of work hardening Taylor (1934) introduced the model of a regular array of dislocations in a work hardened crystal. Consider the simple case of fig. 7 where two parallel edge dislocations in parallel slip

planes try to pass each other under the action of an applied stress σ. This case has been considered by Cottrell (1949). Because of their stress fields these dislocations will interact and there are two equilibrium positions. The $x=0$ position is one of unstable equilibrium, while the $x=\pm y$ positions are of stable equilibrium. Under the applied stress σ the two dislocations can lock into a stable configuration, σ being given by

$$\sigma=\frac{Gb}{8\pi(1-\nu)y}$$

where y is the distance between the two slip planes.

Now consider fig. 5. The $x=\pm y$ condition for stable equilibrium is very closely satisfied in the enlarged region.

If the dislocations have passed each other to reach this stable configuration, the above equation can be applied. Substituting the constant for zinc and 5×10^3 g/cm^2 for the applied shear stress along the slip planes, we get the distance

$$y=1{\cdot}14\times10^{-4}\text{ cm}.$$

Fig. 8 (*a*) Fig. 8 (*b*)

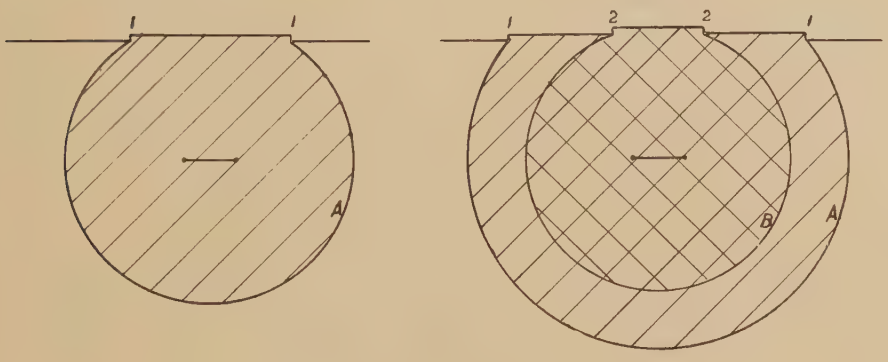

Trapped Dislocations.

Now the observed distance between the two slip lines is $1{\cdot}5\times10^{-4}$ cm, and the angle χ between the crystal axis and the slip plane is $\chi=56°$. Thus the distance between the two slip planes

$$y=1{\cdot}24\times10^{-4}\text{ cm}$$

which agrees very closely with the theoretical value.

The above calculations show a quantitative agreement between the observed manner in which the etchpits group themselves and the theoretical configurations based on the interaction of dislocations, on the assumption that each etchpit locates a single dislocation of unit strength.

5.2. *Trapped Dislocations and Etchpits*

Consider a double-pivoted Frank–Read source, in the slip plane, just below the surface of the crystal. Figure 8 (*a*) shows the first dislocation

loop A to be generated under the applied stress. A limited length of a unit slip line is developed between the two points 1–1 where the loop meets the free surface. The slipped region is shown shaded in the illustration.

As the first loop expands under the applied stress the unit slip line 1–1 extends in length. The source generates a second loop B, as shown in fig. 8 (b), which meets the surface at points 2,2 giving a further unit rise in the slip displacement. This expands under the applied stress and the stepped line widens sideways. The process is repeated each time a new loop is generated. Those which expand right through the slip plane and escape to the surface will each give rise to an overall unit slip, superimposed by stepped regions due to those loops that remain in the interior. These steps are of atomic dimensions and cannot be detected on the crystal surface. It is points such as 1,1, 2,2, ... etc. that are located by the appearance of etchpits.

§ 6. Conclusion

Because of their chemical properties, dislocations can be located by the appearance of etchpits. With the proper choice of etching reagent, a simple and convenient technique can be used to locate dislocations.

The quantitative agreement between the manner in which etchpits group themselves and the theoretical configurations based on the interaction of dislocations illustrates the potentialities of this technique. A new tool is, therefore, available which can be used in tackling the problems of work hardening in terms of the theory of dislocations.

Note added in proof.—The author's attention has been drawn to a lecture delivered by Professor Mott in November, 1954 (see References). In dealing with work hardening Professor Mott introduced a model for 'dislocation doublets' and 'unpaired dislocations' on two parallel adjacent slip planes. On each slip plane a source is situated, giving out dislocations under an applied stress which is sufficient to push pairs of dislocations past each other. When the stress is taken off doublets are formed under their mutual attraction. If, on the other hand, one source produces an excess of dislocations, an unpaired group is formed.

The configuration in fig. 5 of the present paper shows five unpaired etchpits on the extreme right of slip line 1, followed by eight pits forming doublets with corresponding ones on slip line 2. The following table compares the distribution of etchpits on both lines. The distances, in microns, are measured from the first doublet following the unpaired group. The exactness of doubling is closely confirmed.

Slip line 1	1·1	2·7	9·4	13·1	17·8	23·8	33·6
Slip line 2	1·3	2·8	11·0	14·7	17·9	23·7	31·3

References

Abdou, A. H., 1954, *Phil. Mag.*, **45,** 105.

Amelinckx, S., 1953, *Phil. Mag.*, **44,** 1048.

Brown, A. F., 1952, *Advances in Physics*, **1,** 427.

Cottrell, A. H., 1949, *Progress in Metal Physics*, Vol. 1 (ed. B. Chalmers) (London : Butterworths Scientific Publications) ; 1953, *Dislocations and Plastic Flow in Crystals* (Oxford : University Press).

Dekeyser, W., Amelinckx, S., Votava, E., and Vandermeerssche, G., 1953, *Phil. Mag.*, **44,** 1142.

Eshelby, J. D., Frank, F. C., and Nabarro, F. R. N., 1951, *Phil. Mag.*, **42,** 351.

Forty, A. J., 1954, *Advances in Physics*, **3,** 1.

Frank, F. C., 1952, *Advances in Physics*, **1,** 91.

Gevers, R., 1953, *Nature, Lond.*, **171,** 171.

Horn, F. H., 1952, *Phil. Mag.*, **43,** 1210.

Kuhlmann, D., 1951, *Proc. Phys. Soc.* A, **64,** 140.

Mott, N. F., 1955, *Nature, Lond.*, **175,** 365.

Taylor, G. I., 1934, *Proc. Roy. Soc.*, **145,** 362, 388.

Verma, A. R., 1953, *Crystal Growth and Dislocations* (London : Butterworths Scientific Publications).

Vogel, F. L., Pfann, W. G., Corey, H. E., and Thomas, E. E., 1953, *Phys Rev.*, **90,** 489.

LXXXIII. *Quenching Vacancies in Platinum*

By F. J. Bradshaw and S. Pearson
Metallurgy Department, Royal Aircraft Establishment, Farnborough, Hants †

[Received February 22, 1956 ; and in revised form March 12, 1956]

Abstract

The electrical resistance of platinum wires was measured in liquid nitrogen before and after heating to high temperatures and quenching to room temperatures. It was found that the resistance after quenching was greater than its original value but that the increase could be removed by annealing at temperatures in the region of 400°c. This annealable increase is interpreted as being due to lattice vacancies. The whole annealing process was governed by an activation energy of 1·1 ev and this energy is considered to be that for movement of a single vacancy. It is deduced that a vacancy made on average 10^9 jumps before disappearing.

The annealing results are used to show that in certain cases quenching was fast enough to retain the high temperature equilibrium concentration of vacancies. Hence the variation of increase of resistance on quenching with initial temperature is used to deduce an energy of 1·4 ev for forming a vacancy. The entropy factor required does not disagree with theory.

§ 1. Introduction

It is currently assumed that in a metal at a temperature T there is an equilibrium concentration of vacancies n, given by :

$$n = A \exp(-\Delta H_1/kT),$$

where ΔH_1 is the heat of formation per vacancy and A the entropy factor whose value is probably between 1 and 10 (Le Claire 1953). Both are usually assumed invariant with temperature.

Quenching the metal from a high temperature might be expected to retain the vacancies provided that the quenching is quick enough. Since the vacancies should contribute to the electrical resistance of a specimen, changes in resistance following quenching and annealing can be interpreted in terms of vacancies.

Kauffman and Koehler (1952, 1955) investigated gold in this manner and deduced (1955) ΔH_1 to be $1{\cdot}28 \pm 0{\cdot}03$ ev. By studying the temperature variation of annealing rates of the excess resistance due to vacancies they also found that the activation energy for vacancy movement, ΔH_2, in gold was $0{\cdot}68 \pm 0{\cdot}03$ ev.

We have carried out a similar investigation on platinum and this paper gives the results.

† Communicated by the Authors.

During the course of the work Larazev and Ovcharenko (1955) published figures for ΔH_1 and ΔH_2 in both gold and platinum. These were respectively Au, 0·79 ev and 0·52 ev; Pt, 1·18 ev and 1·08 ev. Pending full publication of the Kauffmann and Koehler work it is only possible to speculate on the reasons for the markedly different results for gold. However, we believe that Lazarev and Ovcharenko's quenching rates were inadequate in platinum and probably even more so in gold so that their values of ΔH_1 may be in error.

§ 2. Method

Platinum wires of 99·999% purity (Johnson, Matthey & Co. 'Thermopure') of 0·2, 0·1 and 0·05 mm dia were mounted for heating by d.c. with potential leads 0·02 mm dia welded on to them ~2·5 cm apart. The resistance of the section between the potential leads was determined by a vernier potentiometer. The wires were heated in air to temperatures between 950°C and 1700°C and with the current still on, plunged into water at ~4°C. They were transferred to liquid nitrogen and their resistances were measured. On removal from the nitrogen the wires were heated to ~1000°C for a short time, slowly cooled, and their resistances in nitrogen again measured.

The temperature of the wire just before quenching was determined from its resistance using the parabolic law resistance–temperature data provided by the Johnson Matthey Co., and values for the increases in resistance due to quenching, ΔR, were obtained for different temperatures. The temperature–time curves during a quench were obtained from oscillograph camera records of potential in the usual way. To see how ΔR annealed out, wires were held at fixed temperatures in the region of 400°C and periodically, after given times, immersed in liquid nitrogen for measurement.

In addition 0·02 mm dia wires were quenched simply by switching off currents through them, the surrounding atmosphere being air or argon (no difference between these gases was observed). The quenching times were estimated to be of the order of 10 m sec. As no potential leads could usefully be welded on there were errors due to temperature gradients near the supports. Also the temperature had to be measured optically involving substantial emissivity corrections. However, we have given the results to show that they do not disagree with the data from the water quenched wires and demonstrate that a different atmosphere and quenching method did not produce totally different answers. The decay of ΔR on annealing the 0·02 mm wires was studied by placing the whole assembly in a furnace for given times and the results agreed reasonably with anneals on water quenched wires.

Apart from those needed for preliminary experiments, twelve specimens in all were used and each was quenched many times. As a typical example one of the 0·1 mm wires, after initial annealing at ~1600°C, was quenched 32 times from temperatures within the range 900°C to 1400°C, this range being covered twice for increasing and decreasing temperatures.

§ 3. Results

3.1. *Quenching Rates*

The general form of the temperature–time curves for water quenching was similar to that shown in fig. 1 for all three wire sizes. The difference between wires of different size could be characterized by an initial slope and a total time to reach water temperature. For the 0·2 mm wire these were 30°c/m sec and 20 m sec respectively ; for the 0·1 mm wire, 100°c/m sec and 6·5 m sec ; for the 0·05 mm wire 210°c/m sec and 3·4 m sec. The initial quenching rates did not vary significantly with initial temperature : the total times for the highest or lowest initial temperatures were roughly 20% longer or shorter than the mean times given here.

3.2. *Quenching*

The increases in resistivity, $\Delta\rho$, obtained by quenching are plotted for all wires in fig. 2. In view of the large number of observations only the 95% probability zones are drawn. The results of the 0·02 mm air-quenched wire can be seen to be below the water-quenched results ; the errors mentioned above having apparently caused a simple displacement of the curve.

With the 0·2 mm wires at all temperatures the resistance after an anneal was the same within the limits of error as that before quenching. But the thinner wires when quenched from high temperatures did not always fully recover on annealing. This could have been due to pick up of impurity or to a permanent extension of the wire. To distinguish between these effects the resistance at 0°c was measured and Matthiessen's rule was assumed to apply to the resistance due to impurity. It was found that the fall in the ratio of resistance at 0°c to that in liquid nitrogen in the case of the 0·2 mm wire over the whole life of any specimen was not more than $\frac{1}{5}$%. For the thinner wires the total drift was finally about $\frac{3}{4}$%. A $\frac{3}{4}$% change would imply that the resistance ratio $R_{100°c}/R_{0°c}$ had dropped from say, 1·3920 to 1·3914. Since $\frac{3}{4}$% is comparable with the ΔR's quenched in from the lower temperatures one specimen was allowed to drift to $1\frac{1}{2}$%, but no changes in the ΔR's obtained were observed over its whole life. The remaining non-recoverable increase in resistance in the thin wires was obviously due to change in dimensions when being held at high temperatures (substantial changes occurred during initial annealing). Because the wires were fixed at both ends plastic extensions might possibly have occurred during cooling. However, from experiments on wires extended 10% at room temperature we estimate that to produce an annealable increase in resistivity of 0·0005 μohm cm it would require an extension of about 1%. This is considerably more than the maximum extension which occurred in any quench. So even if all the permanent increase in resistance were due to cold work it would not have produced a measurable annealable increase. Similarly radial temperature variations in the wire could cause thermal stresses, but calculation shows these to be negligible also ; the wire cooled virtually isothermally.

Fig. 2

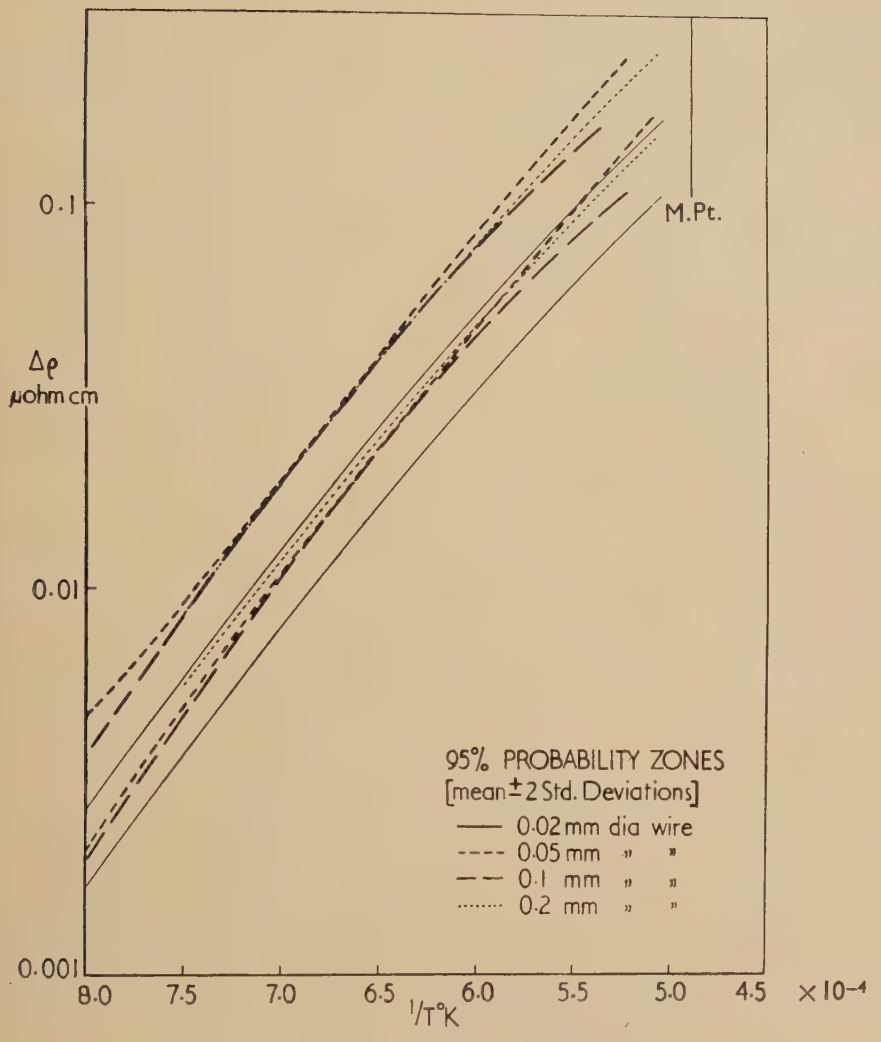

Increase of Resistivity by Quenching.

0·2, 0·1 and 0·05 mm dia wires quenched in water ; 0·02 mm dia wire quenched in air; $\Delta\rho$ is low for the 0·02 mm wire because the ends of the wire were at a lower temperature than the measured temperature of the central portion.

3.3. *Annealing*

Wires quenched from different temperatures were used for annealing, but the manner in which the fractional decay rates varied with time did not appear to depend on the ΔR quenched in. Figure 3 is a good example of the way in which the decays occurred. They were obviously not exponential, but there was no question of the annealing taking place in more than one stage as occurs in cold work experiments (Manintveld 1954).

If there were any second stage to the decay curves then it only involved the last $\sim 5\%$ of ΔR. The range of annealing temperatures used was 380° to 460°C.

If the decay of ΔR at a given temperature is interpreted in terms of a loss of vacancies of concentration v and the possibility of vacancies agglomerating is ignored (see later) then we assume

$$-\frac{1}{v}\frac{dv}{dt} = n\nu_D B \exp(-\Delta H_2/kT), \quad \ldots\ldots \quad (1)$$

where n is the probability per jump that a vacancy is lost, ν_D is the Debye

Fig. 3

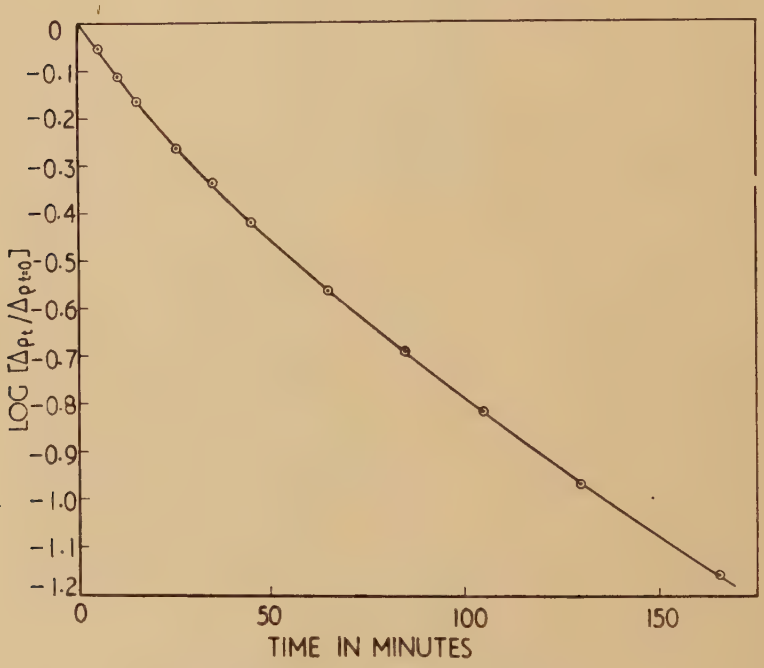

Annealing Curve for 0·05 mm dia wire.
Annealing temperature 653°K.
Quenching temperature 1687°K.

frequency, B is the entropy factor for movement (again probably in the region of 1 to 10) and ΔH_2 the heat of activation per vacancy. From anneals at different temperatures the values of ΔH_2 and nB (assuming $\nu_D = 10^{13}$) were obtained when various amounts of ΔR remained.

The mean values of ΔH_2 and nB are given in the table in which is also included values of τ, the mean time constant for decay of ΔR at 426°C. Although the annealing curves did not all have exactly the same shape their initial slopes were usually about twice those at the end of the anneal, indicating that nB must have altered by this much during the anneal. However, this variation is far smaller than our uncertainty in the absolute value of nB.

Table

Wire diameter (mm)	ΔH_2 (ev)	nB	τ (mins)	nB (1·1 ev)
0·2	1·04	$0{\cdot}9\times10^{-9}$	50	$1{\cdot}6\times10^{-9}$
0·1	1·25	40×10^{-9}	35	$2{\cdot}3\times10^{-9}$
0·05	0·94	$0{\cdot}6\times10^{-9}$	20	4×10^{-9}
0·02	1·09	10×10^{-9}	8	10×10^{-9}

It was found that if before quenching the wires were heated to near the melting point the ΔR subsequently quenched in from high temperatures was increased ; similarly to a lesser extent the ΔR quenched from lower temperatures was increased. In addition the annealing rates became slower. For example an 0·2 mm dia specimen already heated to remove most of the effects of cold work during assembly on the rig was further heated ; as a result the ΔR quenched in from 1450°C increased by 5% and the annealing rate was halved. We interpret this effect as being due to a reduction in the number of sinks available for vacancies. An obviously necessary but not sufficient condition to trap all the vacancies on quenching was to anneal the wire at temperatures near to its melting point long enough for any subsequent measurements of ΔR quenched from any temperature to be stable and repeatable. In practice, before quenching or annealing measurements were made, all wires were held at temperatures near to the melting point so as to stabilise ΔR.

§ 4. Discussion

4.1. *Annealing*

Considering the annealing results further we conclude that the process has a mean activation energy of 1·1 ev. It is obvious from the table that although the absolute values of nB are not well known, they should vary from one wire size to the next in the manner required by the measured variation of τ. Accordingly better values of nB could be obtained by assuming the same mean activation energy for all wires and making nB consistent with this and the τ values. The last column of the table gives such corrected figures.

Assuming that the concentration of vacancies near a sink is nearly the same as that elsewhere, n will be equal to the concentration of sinks. But it is obvious that any value of n obtained from nB (1·1 ev) in the table will only be an order of magnitude estimate and also n would be expected to vary along the length of a wire and from wire to wire depending on its history. In view of the small size of the specimens it might be expected that their surfaces would be sinks for vacancies in competition with the internal sinks such as dislocations. The increase in τ with wire size supports the view.

Decay by diffusion to a sink in the form of a cylindrical surface becomes effectively exponential when half the diffusant has vanished. The surface

then behaves like a random distribution of point sinks of concentration $n' \simeq a^2/r^2$ where a is the distance between atoms and r is the radius of the cylinder. Grain boundaries also acting as sinks modify this for the 0·2 mm and 0·1 mm wires (the grain boundaries in the 0·05 and 0·02 mm wires were few enough to be ignored) and allowing for this, n' is estimated to be for the 0·2, 0·1, 0·05, 0·02 mm wires $1{\cdot}6\times10^{-11}$, $1{\cdot}5\times10^{-10}$, $1{\cdot}2\times10^{-10}$, and $7{\cdot}5\times10^{-19}$. If B lies between 1 and 10 then this suggests that surface sinks might possibly have been important in all but the 0·2 mm wire. However, if they had been predominant the slopes of the initial parts of the annealing curves would have been much steeper than that in fig. 3 which is typical for all wire sizes. Also as can be seen the decay is not exponential even when only 10% of the vacancies remain. However, the decay could be explained by an internal sink concentration varying down the length of the wire ; two distributions, one about four times the concentration of the other would suffice.

Summarizing, if B lies between 1 and 10, we think that there were internal sinks at a concentration of order 10^{-9}.

With such a low sink concentration it is appropriate here to mention impurity effects and vacancy agglomeration. Although impurities were no doubt present to a concentration greater than 10^{-9} we will only say that we did not notice any significant change in annealing rates as the resistance ratio of a wire dropped, i.e. as impurities were picked up. With regard to agglomeration and/or the formation of vacancy pairs, the results do not appear to suggest any such mechanisms. Since (see below) we suggest that vacancy concentrations of 10^{-4} to 10^{-5} were being annealed, the value of $n=10^{-9}$ is incompatible with the idea of even pair formation. In addition the shape of the annealing curve does not appear to be that of a bimolecular reaction and quenching in varying amounts of ΔR did not affect annealing rates.

4.2. *Quenching*

Before deducing a value for ΔH_1 it is necessary to decide whether at the temperatures used the quenching rate was adequate to trap all the vacancies.

Following Lomer (1954) we may estimate the transition temperature T_L below which most of the vacancies are frozen in. The rate of disappearance is assumed to be as in eqn. (1).

T_L is the temperature where the rate of fall of the equilibirum concentration of vacancies becomes greater than the rate at which the vacancies can vanish, i.e. is given by

$$d/dt\,[A\exp(-\Delta H_1/kT)]=A\exp(-\Delta H_1/kT)n\nu_D B\exp(-\Delta H_2/kT)$$

whence $$dT/dt\,.\,\Delta H_1/kT_L^2=-n\nu_D B\exp(-\Delta H_2/kT_L) \quad . \; . \; . \; . \quad (2)$$

where dT/dt is the quenching rate.

To determine how sharp the transition is from adequate to inadequate quenching, i.e. to get the theoretical number of vacancies retained on

quenching from all temperatures, the equation giving the rate of loss of vacancies at any temperature

$$dv/dt = -n\gamma_D B \exp(-\Delta H_2/kT)[v - A \exp(-\Delta H_1/kT)] \quad . \quad (3)$$

must be solved. This can only be done numerically and allowance must be made for the variations in n which will spread the transition zone over a wider range. However, some solutions of (3) show that for the values of ΔH_1, ΔH_2 and T_L in which we are interested, and for a single value of n, the transition occurs over the range $1/\tau \simeq 1/\tau_L \pm 1 \times 10^{-4}$. Thus for $1/\tau_L = 6 \times 10^{-4}$, the slope of the logarithmic quenching curve at temperatures below $1/T = 7 \times 10^{-4}$ will be within $\sim 5\%$ of the value $\Delta H_1/k$.

Assuming for the moment that fig. 3 does represent the trapping of all the vacancies at low temperatures we have $\Delta H_1 = 1{\cdot}4$ ev (in any case T_L is not very sensitive to changes in ΔH_1). Putting $\Delta H_2 = 1{\cdot}1$ ev and taking a value of $nB = 10^{-7}$ to give a lower limit for T_L it is found that for the 0·2, 0·1 and 0·05 mm wires, $1/T_L$ is $6{\cdot}6 \times 10^{-4}$ (1240°C), $5{\cdot}8 \times 10^{-4}$ (1450°C) and $5{\cdot}4 \times 10^{-4}$ (1580°C). These figures show that at least for the 0·05 mm wire all the vacancies at the lower temperatures were trapped.

The values of T_L are probably pessimistic in that although the quenching conditions for the 0·1 and 0·2 mm wires were less good, the resulting curves lie virtually on those for the 0·05 mm wire. From the annealing decay times it may be seen that the sink densities were respectively 1/1·6 and 1/2·5 that of the 0·05 mm wire but the quenching rates were 2·1 and 7·3 times slower.

Thus from fig. 3 $\Delta\rho = 1400 \exp(-1{\cdot}4/kT)\,\mu$ ohm cm, kT being expressed in electron-volts.

Calculations for the effect of vacancies on the resistivity of platinum are not available. It might be expected that platinum being a transition metal the scattering effects in it will not be less than those in Cu, Ag and Au for which Jongenburger (1953) has deduced 1·3, 1·5 and 1·5 μ ohm cm per atomic % of vacancies. Alternatively, if equal amounts of cold work produce the same amount of disorder in copper as in platinum, Manintveld's (1954) cold work experiments, showing the different resistivity changes found in these two metals, may be used to obtain a figure for the effect on resistivity of a vacancy in platinum. This is $\sim 4\,\mu$ ohm cm per atomic % (using the Ag or Au data it would be ~ 8 or $7\,\mu$ ohm cm). whence $v = 3 \exp(-1{\cdot}4/kT)$.

The estimate of $A = 3$ may be out by a factor ~ 3 in either direction due to experimental errors, with further errors arising from our sketchy conversion of resistivity to vacancy concentration. Accordingly, all that may be said is that the value of A arrived at does not disagree with theoretical predictions.

ΔH_1 has $\sim 0{\cdot}1$ ev experimental error, with that for ΔH_2 the same or slightly more. ΔH_1 which may be the more susceptible to systematic errors, cannot vary too widely without producing rather too improbable values of A. With the above interpretations the activation energy for self diffusion is predicted to be 2·5 ev and the concentration of vacancies

at the melting point is predicted to be $\sim 10^{-3}$, taking the same conversion factor as above.

Assuming that dislocation lines are providing the sinks, whatever their mechanism is for absorbing vacancies, a reasonable density of dislocations ($\gtrsim 10^8$ lines/cm^2) will imply that in absorbing 10^{-3} vacancies there must be a big reshuffle in the dislocation network— perhaps of the order of the network spacing.

The energy of 1·1 ev for the annealing process agrees well with that given by Lazarev and Ovcharenko (1955). We do not propose to identify it with any similar processes observed in cold work or irradiation except to point out that although Dugdale's (1952) result of 1·2 ev for annealing platinum, cold worked or irradiated at room temperature, lies within our error limits, the value of n in his experiments is much larger (10^{-1} to 10^{-2}). Similarly Manintveldt's figure of $0{\cdot}99 \pm 0{\cdot}09$ ev for annealing platinum cold worked in liquid nitrogen could agree, but again demands a higher value of n(~unity).

§ 5. Conclusions

Assuming that the observed resistance increases have been correctly interpreted as being due to single vacancies, the energy of vacancy formation was found to be 1·4 ev ; the entropy of formation appeared to be of the right order. The energy of movement was found to be 1·1 ev and on average a vacancy made 10^9 jumps before disappearing.

This number of jumps is inconsistent with clustering and may be considered surprisingly high. Also the predicted value of 2·5 ev for self diffusion may be thought to be low, but with the interpretation given these conclusions seem to be inescapable.

Acknowledgments

We are grateful to Dr. W. M. Lomer for valuable consultations during the course of the work, to Dr. N. J. Wadsworth, several of those suggestions on the interpretation have been incorporated and to Mr. L. G. Carpenter for advice and encouragement throughout.

References

Dugdale, R. A., 1952, *Phil. Mag.*, **43**, 912.
Jongenburger, P., 1953, *Appl. Sci. Res.* B, **3**, 237
Kauffmann, J. W., and Koe. ler, J. S., 1952, *Phys. Rev.*, **88**, 149 ; 1955, *Ibid.*, **97**, 555.
Lazarev, B. G., and Ovcharenko, O. N., 1955, *Dokl. Akad. Nauk. S.S.S.R.*, **100**, 875.
Le Claire, A. D., 1953, *Acta. Met.*, **1**, 438.
Lomer, W. M., 1954, *A.E.R.E. Report*, T/R 1540.
Manintveld, J. A., 1954, *Delft* : Technische Hogeschool.

LXXXIV. *The Elastic Scattering of Protons by Light Elements*

By G. Dearnaley
Cavendish Laboratory, Cambridge †

[Received February 1, 1956]

Summary

The elastic scattering of protons by ^{19}F, ^{9}Be and ^{23}Na has been studied over a range of angles and energies between 0·5 and 2·6 Mev. The anomalies observed in the scattering cross section curve at resonances excited in the compound nucleus have been analysed using dispersion theory. Resonance energies, widths and partial widths are deduced, and conclusions are given as to spins and parities of various states in ^{20}Ne, ^{10}B and ^{24}Mg based on this and other evidence.

§ 1. Introduction

Around 1948, Wigner drew attention to the desirability of experimental evidence on elastic scattering, for which the dispersion theory (Wigner and Eisenbud 1947) of nuclear resonance predicts a variation from Rutherford scattering near a resonance, in form similar to the optical dispersion near an absorption band. Protons which suffer Rutherford scattering interfere coherently with those scattered by short range forces without change of spin. Protons with spins reversed give incoherent scattering. The result is an anomaly in the curve of the scattering cross section variation with energy, which may be fitted by a suitable choice of the resonance energy, width, and partial width, together with the angular momenta of the incident proton and of the compound nucleus. The method has been used previously for the investigation of a number of light nuclei (Laubenstein and Laubenstein 1951, Jackson and Galonsky 1951, Mooring *et al.* 1951, Thomas *et al.* 1949) for which the level width is large enough to allow a convenient target thickness. This paper describes the application of the method to several elements which have been studied by other means in this laboratory.

§ 2. Experimental Method

The thin target technique was used in these investigations, using a 90° magnetic analyser to separate the protons scattered from nuclei of different atomic weight in the target and backing. The magnet used has been described previously (Burcham and Freeman 1949), but has been mounted on a turntable so as to receive particles at $22\frac{1}{2}°$ to the horizontal from a target chamber, the upper and lower plates of which can rotate on vacuum seals about the turntable axis. The beam enters

† Communicated by E. S. Shire.

through cooled, adjustable collimating slits to strike the target at the centre of the chamber. A long tube serves to catch the beam passing through thin targets, and is also the pumping tube, insulated for beam integration. The target holder is designed so that targets can be changed without breaking the vacuum in the chamber, and also to allow the target no rapid changes in pressure, which would easily destroy a thin foil. Scattered particles enter a wave guide bent through 90° between the magnet poles, and pass through defining slits into a thin-windowed proportional counter. The target box and beam tubes are of thick steel to minimize unwanted deflections due to the stray field of the magnet, and the magnet box is insulated to allow application of a bias voltage to suppress secondary electrons. The magnet current is stabilized electronically to 0·1%, and control is by an amplidyne generator.

For the measurement of the scattering cross sections, accurate current integration is necessary. An integrator was constructed consisting of a galvanometer-photocell d. c. amplifier to amplify the input current, after which it is integrated by polystyrene-film condensers. Two of these are used, the current being switched from one to the other when the voltage reaches that of a neon reference, the switching being electronic so that the loss during changing over is negligible. Accuracy and linearity are better than 1%.

The target backing used must be as thin and as pure as possible, and be of low atomic weight, to reduce the scattering. Thin films of spectroscopically pure carbon were used, prepared by evaporation from an arc *in vacuo* on to glass slides coated with detergent. The target material was then evaporated on to the carbon, the film floated off on water, and picked up on a wire frame. Alternatively, the evaporation may be made on to the framed carbon film. Films of the order of 500 Å can be produced, and are relatively robust. The method is adapted from a technique in electron microscopy (Bradley 1954).

§ 3. Method of Analysis

The theory of resonant elastic scattering has been given previously in various forms (Cohen 1949, Blatt and Biedenharn 1952, Baranger 1955), and a graphical method of analysis developed by Laubenstein and Laubenstein (1951) for spinless target nuclei. The coherent scattering amplitudes and phases are represented by vectors in the complex plane, and the resultant found. Extending the method for the general case of the scattering of particles of spin i from a target of spin I, at a resonance for the formation of a state of spin J_0, then, using the notation of Blatt and Biedenharn we have for S-wave scattering the vectors :

Rutherford : $f_C(\theta)\lambda = -\frac{1}{2}\eta \operatorname{cosec}^2(\frac{1}{2}\theta) \exp[-2i\eta \log_e \sin(\frac{1}{2}\theta)]$.

Resonant : $f_R(\theta)/\lambda = (\Gamma_{\alpha l}/\Gamma) \cos\beta \exp i(2\psi_l + 2\phi_l + \beta_l + \frac{1}{2}\pi) P_l(\cos\theta)$.

Hard-sphere : $f_{CH}(\theta)/\lambda = \sum_{l'=0}^{\infty}(2l'+1) \sin\phi_{l'} \exp i(2\psi_{l'} + \phi_{l'}) P_{l'}(\cos\theta)$.

Then : $d\sigma/d\Omega = \lambda^2 [|f_C(\theta) + f_{CH}(\theta)|^2 (1 - [2J_0+1]/[2I+1][2i+1]) + |f_C(\theta) + f_{CH}(\theta) + f_R(\theta)|^2 (2J_0+1)/(2I+1)(2i+1)]$.

The method used is to add these vectors graphically in the complex plane, square the magnitude of the resultant, introduce the weighting factors, and multiply by λ^2, which gives the scattering cross section. The locus of the end of the resonant vector is a circle passing through the origin. The hard-sphere scattering contribution is quite small in the low energy region used. There is also a small incoherent contribution :

$$\sum_{L=0}^{L\,\max.} R_L(\alpha,\alpha)\,P_L(\cos\theta)/(2I+1)\,(2i+1)$$

$$-(\Gamma_{\alpha l}/\Gamma)^2\cos^2\beta\sum_{L=0}^{2l}(ll00/llL0)^2\,P_L(\cos\theta)\,[2J_0+1]^2/[(2i+1)\,(2I+1)]^2.$$

The largest contribution to the anomaly, the interference between nuclear and coulomb scattering, varies as $P_l(\cos\theta)$. Thus by observing at the series of angles for which the low order Legendre polynomials disappear, it is possible to pick out the angular momentum l involved. When two or more levels are involved, there are several resonant vectors to consider, and the incoherent contribution also has an interference term.

§ 4. Scattering of Protons by ^{19}F

Thus has been studied at the four angles between 90° and 160° for which Legendre polynomials of order 1, 2, 3 and 4 are zero, and for energies from 0·5 to 2·1 Mev. A beam of protons, monoenergetic to 1 kev and defined to 2 mm by 3 mm was provided by the Cavendish Electrostatic Generator. The target used was 3 kev LiF evaporated on to a carbon backing of some 5 kev thickness and the momentum spectrum taken with the magnetic analyser showed protons scattered from ^{6}Li, ^{7}Li, ^{12}C and ^{19}F as well resolved peaks. These were flattened at the top by setting the receiving aperture of the counter to be larger than the image of the target spot focused by the magnet. This ensured that all the protons scattered into the solid angle of acceptance of the magnet were counted, and the target thickness must be less than the energy range defined by the magnet resolution, which is of the order of 20 kev.

The scattering cross section was obtained by running until a certain charge was recorded by the current integrator, when the scaler counting the scattered protons was automatically stopped. At each setting of the energy of the incident protons it was necessary to locate the top of the peak of the momentum spectrum. The energy of the incident protons was increased in steps of 10 kev, with smaller intervals over the resonance regions. At the same time, the gamma ray excitation function was taken using a Geiger counter ; the gammas were practically all from the strong ^{19}F(p, γ) and ^{19}F(p, γ) reactions, and since the resonance energies are well known (Chao *et al.* 1950, Willard *et al.* 1952, Barnes 1955) serve as an energy calibration of the machine.

Figure 1 shows the differential scattering cross section curves obtained at 90°, 125·3°, 140·8° and 159·8° in the centre of mass system.

Fig. 1

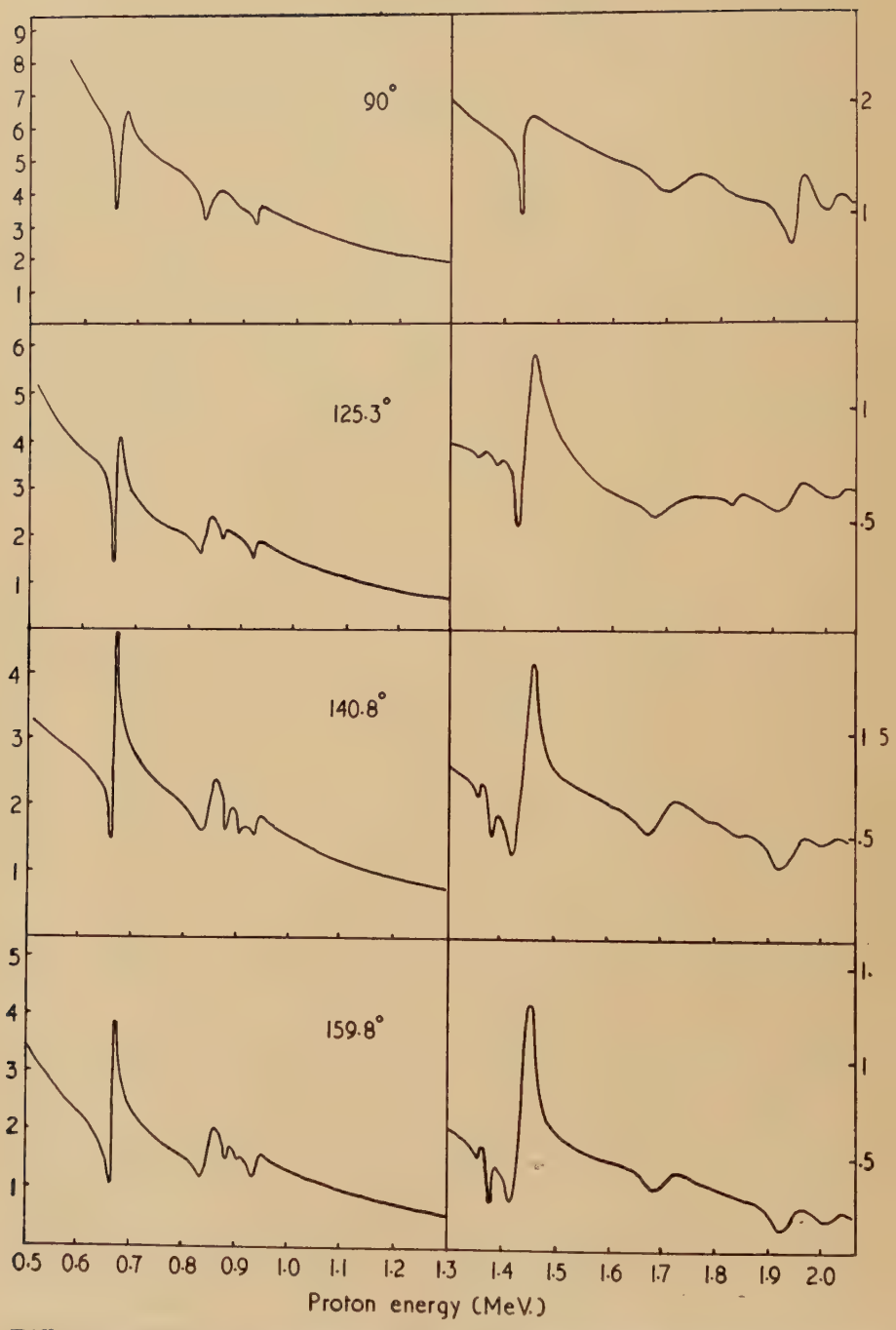

Differential $^{19}F(p, p)$ cross section. The ordinates represent the cross section in laboratory coordinates, measured in units of 0·1 barns/steradian.

The relative accuracy of the points which make up the curves is around 2%, being made up of integrator inaccuracy (0·5%), the slope of the top of the scattered proton peak (1%), statistical fluctuation in the number of counts (1%), and estimated target thickness variation (1%). The target thickness did not appear to alter by more than 1% over a run, as repeated points lay well on the curve. The absolute cross section was obtained by comparison with the scattering from ^{7}Li (Warters *et al.* 1953), assuming the target to be LiF ; the values are probably accurate to 10%. The cross sections given are for the laboratory system of coordinates.

§ 5. Excited States of ^{20}Ne

Scattering anomalies were observed corresponding to known resonances in ^{19}F(p, $\alpha\gamma$) at 669, 874, 935, 1346, 1372, 1690, 1940 and 2030 kev, the ^{19}F(p, γ) resonance at 1422 kev and the ^{19}F(p, $\alpha\pi$) resonance at 842 kev.

The anomaly at 669 kev has been fitted, as stated in the preliminary account of this work (Dearnaley 1954), taking the partial proton width Γ_p equal to 0·98 Γ, the larger of its two possible values (Chao 1950) where the resonance width Γ=7·5 kev. The residual 0·02 Γ is mainly due to alpha emission. Figure 2 shows the fit obtained at the four angles, taking incident S-wave protons, and J=(1,+) (Seed and French 1952). Account was taken of the variation of the Rutherford scattering across the resonance, and a non-resonant background vector added to allow for the effect of other resonances. The amplitude and phase of this were adjusted to fit the results. Figure 3 shows the vector diagram used, with the *loci* of endpoints.

The anomaly at 935 kev is also present at all four angles, indicating S-wave formation, and confirming the assignment (1,+) (Seed and French 1952). However, the proton width must take its smaller value of 0·1 Γ, as the observed anomaly is quite small.

At 842 kev there is a resonance in ^{19}F (p, $\alpha\pi$) leading to the first excited pair-emitting state of ^{16}O, which must be (0,+). The resonance is isotropic, involving S-wave protons, so that the state in ^{20}Ne must also be (0,+). Taking the larger value of Γ_p=0·99 Γ, a fit has been made for this assignment at 90°, where the overlapping 874 kev anomaly disappears. Figure 4 shows the agreement, taking Γ=23 kev.

The 669 kev level differs from the other (1,+) resonances at 340, 935 kev in that some 2% of the transitions from it occur by gamma emission to the first excited level of ^{20}Ne (Devons and Hereward 1948, Rae *et al.* 1950, Carver and Wilkinson 1951). Sinclair (1954) has observed three other resonances for ^{19}F(p,γ)^{20}Ne at 1092, 1324, and 1422 kev. The first corresponds to a resonance in ^{19}F(p,$\alpha\gamma$)^{16}O, whereas the last two do not. No appreciable variations in the proton scattering cross section occur at the first two of these levels, but at the third, there is a large isotropic anomaly. This level is therefore formed by S-wave protons, allowing assignment (0,+) or (1,+), but not (0,−) as suggested by Sinclair.

Fig. 2

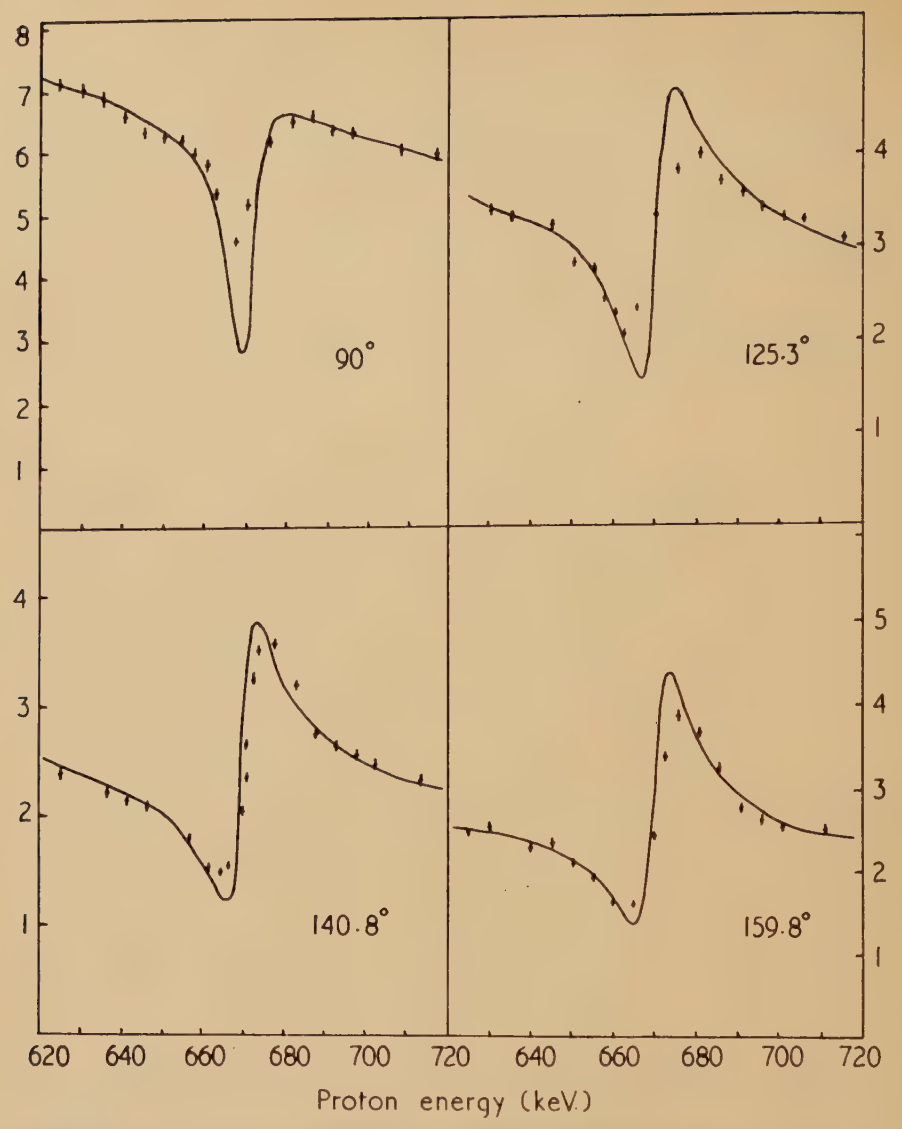

Experimental points and theoretical curves at 669 kev resonance, for $J=1$, $\Gamma=7{\cdot}5$ kev, $\Gamma_p=0{\cdot}98\ \Gamma$.

Fig. 3

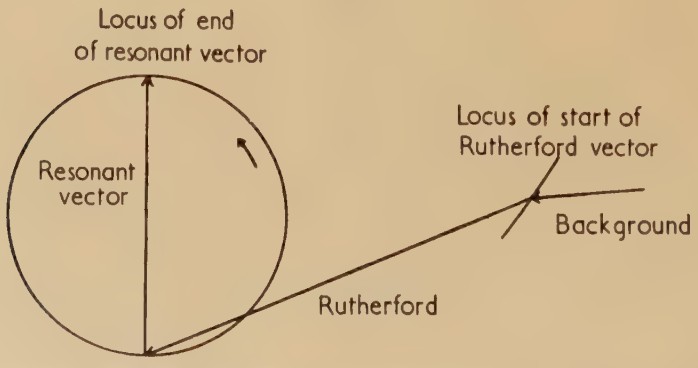

Vector diagram used at 669 kev. The vectors are drawn at resonance, for a scattering angle of 125°.

No alpha emission is observed to levels in ^{16}O of even spin and parity, and the anomaly is too large to allow $(0,+)$ but has been fitted taking $J=(1,+)$, $\Gamma_p=0{\cdot}85\ \Gamma$, $\Gamma=15$ kev (fig. 5). The vector diagram used is shown in fig. 6, with again a non-resonant background added.

For the levels formed at 874, 1346 and 1372 kev, the anomalies disappear at 90°, and become more marked as the scattering angle increases, showing formation by p-wave protons. This agrees with the assignments $(2,-)$ at 874 kev (Seed and French 1952), 1346 kev (Peterson *et al.* (1954), and 1372 kev (Sanders 1953), and the proton width is small in all these cases, supporting the argument of Wilkinson and Clegg (1953) at 847 kev, based on the radiative width. Similarly at 598 kev, no appreciable anomaly occurs, again indicating that Γ_p takes the smaller of the two possible values.

Fig. 4

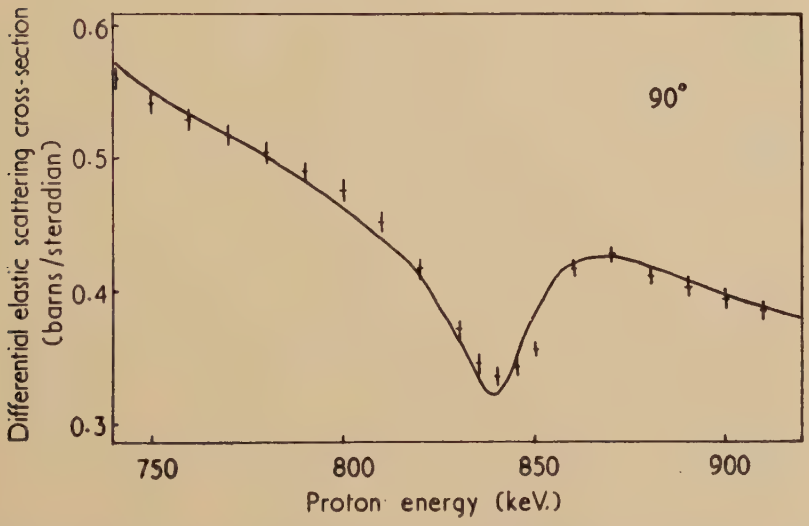

Experimental points and theoretical fit at 842 kev resonance for 90° using $J=(0,+)$, $\Gamma=23$ kev, $\Gamma_p=0{\cdot}99\ \Gamma$.

At 1940 kev, the resonance is probably due to S-wave protons, with a small partial width. The remaining anomalies are too small for reliable analysis.

Since this experiment was completed, measurements have also been made at the California Institute of Technology by Webb *et al.* (1955) and analysed by Baranger (1955). They used a thick target technique, and extended the work to forward angles. The results and analysis are in agreement in all cases, confirming the measured stopping cross section of fluorine, and I am indebted to Mr. T. S. Webb and Professor W. A. Fowler for discussions of the results before publication.

Fig. 5

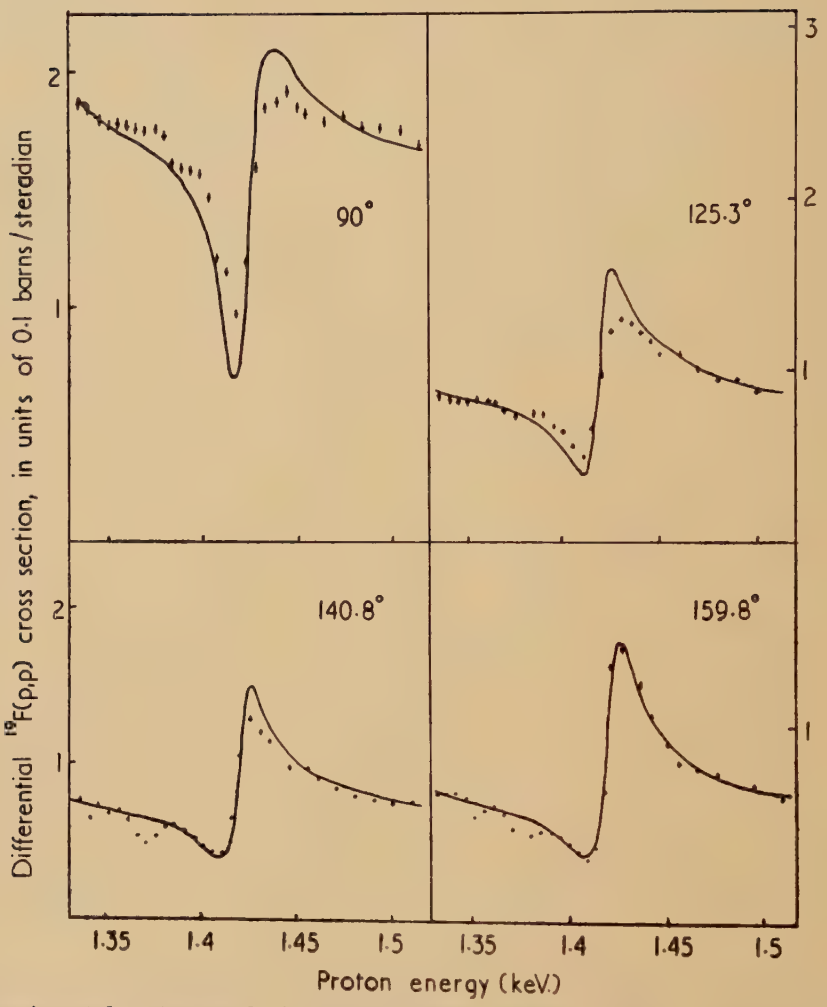

Experimental points and theoretical curves at the 1422 kev resonance for $J=1$, $\Gamma=15$ kev, $\Gamma_p=0{\cdot}85\ \Gamma$. The resonances at 1346, 1372 kev are not fitted in this analysis.

Fig. 6

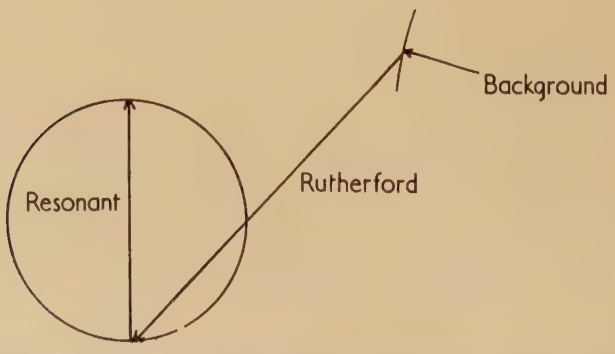

Vector diagram used at 1422 kev. The vectors are drawn at resonance for a scattering angle of 90°.

§ 6. Scattering of Protons by ^{9}Be

At the same four angles, in the centre of mass system, the elastic scattering of protons by ^{9}Be has been studied from 0·8 to 2·6 Mev by means of the Cavendish Electrostatic Generator. The target for this work was of beryllium metal evaporated from a tungsten spiral coated with BeO on to a backing film of carbon. Oxygen was present in the target due to oxidation of the beryllium, but the scattered peaks from ^{9}Be, ^{12}C and ^{16}O, were well separated in the momentum spectrum. The target thickness was about 5 kev Be on 5 kev carbon.

Figure 7 shows the differential cross section curves at the four angles over the energy range studied. The results at 140·8° agree with those obtained at 143° by Thomas *et al.* (1949), who worked up to 1·3 Mev. The accuracy of the points which make up the curves is around 2%.

§ 7. Excited States of ^{10}B

There are four apparent scattering anomalies in the region studied, associated with known resonances in ^{9}Be(p, γ) at 0·998, 1·087 and 2·565 Mev (Fowler and Lauritsen 1949, Hahn *et al.* 1952) and a very broad resonance in ^{9}Be(p, d) at 1·35 Mev.

The present work shows that the anomaly at 998 kev is isotropic involving S-wave protons, and confirming the assignment (2,−) to the 7·483 Mev level in ^{10}B (Cohen 1949). The fit obtained, shown in fig. 7 was made with Γ=90 kev, and Γ_p=0·7 Γ as an adjustable parameter. There may be some admixture of d-wave formation, as indicated by the ^{9}Be(p, γ) distribution (Devons and Hine 1949). This angular distribution of $1+0{\cdot}09\sin^2\theta$ suggests predominant S-wave formation, and the assignment (2,−) would make the main γ-transition to the (3,+) ground state electric dipole.

The narrow level at 1·087 kev produces an anomaly which increases from 90° to 160°, indicating P-wave formation of the 7·56 Mev level in ^{10}B. The resonance is too narrow (4 kev) to allow detailed analysis, owing to the lack of resolution due to target thickness, etc., and so has not been fitted in fig. 7. The assignment (0,+) for this level is then consistent with the absence of gamma transitions to the (0,+) state at 1·74 Mev, and also the lack of alpha or deuteron emission to the ground states or ^{6}Li or ^{8}Be (Cohen 1949). The decay is mainly to the 0·7 Mev state, and these gammas, and the cascade to the ground state are both isotropic to 5%, indicating J=0 (Paul and Gove 1953).

A very broad isotropic anomaly occurs at 1·35±0·05 Mev, probably associated with the broad resonance since observed by S. A. Durrani (private communication) in the reaction ^{9}Be (p, d) with a width of the order of 500 kev. The theoretical curve in fig. 7 was obtained using the assignment J=(2,−) at 1·34 Mev, Γ=0·5 Mev, Γ=0·8 Γ. S-wave protons allow assignment (1,−) or (2,−), but the anomaly is too large for J=1.

Fig. 7

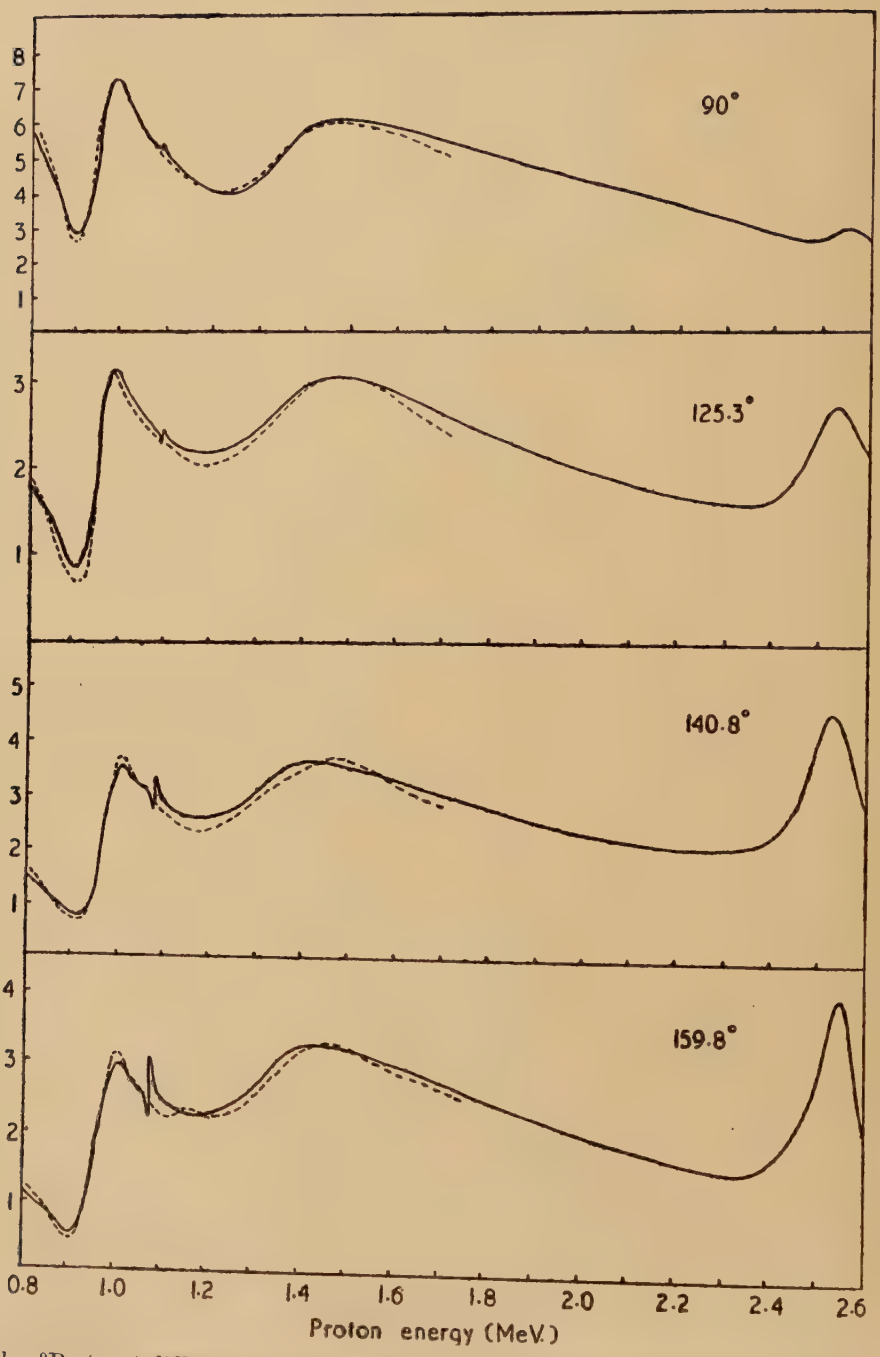

The ^{9}Be (p, p) differential cross section. The dotted curve is the fit obtained with the parameters given in fig. 8.

The angular distribution of the scattering around 1·1 Mev is not accounted for by the resonances so far considered, and the increase in cross section towards higher angles necessitates a broad $L=1$ structure. In order to fit the results, P-wave resonance at 1·1 Mev, $\Gamma=200$ kev is postulated, with Γ_p/Γ depending upon J, but rather small. This broad even parity level would explain the anisotropy of the (p, α) and (p, d) distributions near 1 Mev (Thomas *et al.* 1949), which does not appear to be due to any level below 1 Mev. There are several levels in ^{10}Be in the corresponding region (Adair 1952).

Figure 8 shows the vector diagram used, with a background vector of slowly-varying amplitude chosen empirically to take account of other broad resonances. The phase shift ψ_1, for the P-wave resonance was obtained from the experimental shape of the 1·087 Mev anomaly, and is close to $\pi/2$.

Fig. 8

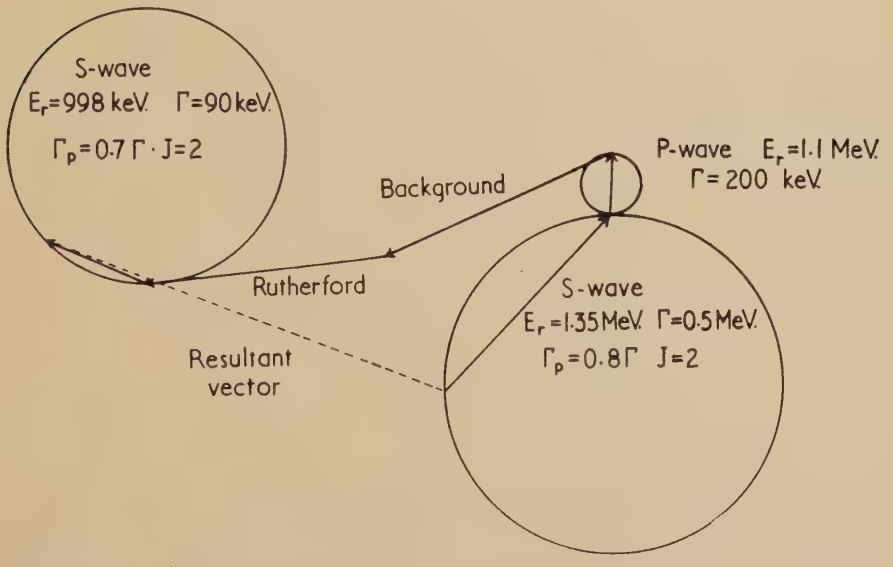

Vector diagram used to obtain fit shown in fig. 7. The circles represent the end-points of the resonant vectors, which are drawn for a proton energy of 1·1 Mev, and scattering angle of 125·3°.

A careful search was made in the region of the ^{9}Be (p, n) threshold at 2·06 Mev for a cusp in the scattering curve similar to the one reported by Bashkin and Richards (1951) in ^{7}Li (p, p) at the neutron threshold. This effect may be due to a ^{7}Li (p, n) resonance near the threshold (Newson and Gibbons 1954) as predicted by Breit and Bloch (1948). No such variation in the ^{9}Be cross section was observed.

At the 2·56 Mev resonance there is a scattering anomaly which increases from being quite small at 90° to very large at 160°, indicating P-wave formation of the 8·894 Mev level in ^{10}B. Assignments (0,+), (1,+), (2,+) or (3,+) are possible. Alphas to the (1,+) ground state and

Fig. 9

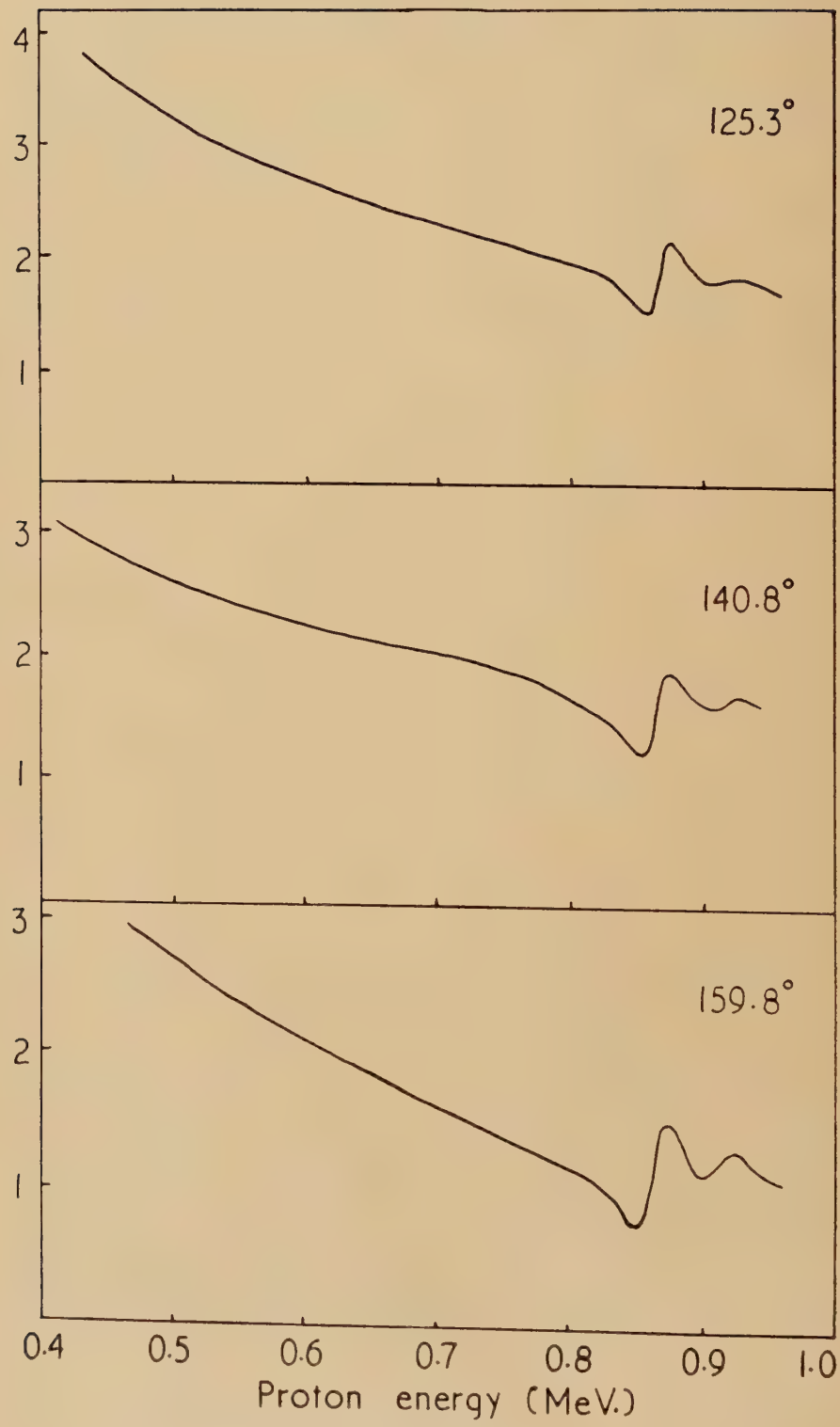

Differential ^{23}Na (p, p) elastic scattering cross section.

(3,+) state at 2·18 MEV in ^{6}Li are not observed, so that (1,+) and (3,+) are unlikely. Also, the large resonant (p,γ) cross section of 0·11 barns indicates $J \geqslant 2$ (Mackin 1954). Since $J=3$ leads to a very large alpha reduced width, the level is probably (2,+). The gamma radiation is predominantly to the 0·7 MEV state ; with this assignment the transition to the 1·74 MEV state would be electric quadrupole. A sufficient energy range of the curve could not be covered in order to fit the complete resonance in detail, but the large size of the anomaly indicates $J \geqslant 2$, with a large proton width.

The proton scattering is also being studied by F. Mozer (private communication) using a thick target technique, and measurements extended to lower energies and forward angles.

§ 8. Elastic Scattering of Protons by Sodium

The differential scattering cross section of ^{23}Na has been measured using the 1 MEV Cockcroft–Walton Generator, from 0·4 to 1·0 MEV at the three angles 125·3°, 140·8°, and 159·8°. Measurements were not possible at 90° owing to insufficient resolution in the magnet analyser.

A target of sodium metal evaporated on to a carbon backing film was used, and the oxygen taken up by the metal produced scattered protons which were difficult to separate from those from the sodium, at low angles. Figure 9 shows the results obtained.

§ 9. Excited States of ^{24}Mg

Only one marked anomaly is observed, at 860 kev, the other resonances in ^{23}Na+p apparently having too small a width or partial proton width to be observable. The anomaly at 860 kev is isotropic, so that the level in ^{24}Mg may have assignment (1,+) or (2,+). From a study of the gamma ray transitions in ^{24}Mg, Newton (1954) concludes that the spin is 1, leaving the possibility (1,+). There is also evidence of a small anomaly around 920 kev, which may have $l_p=1$ or 2.

It is hoped to extend this work to higher energies, using the Electrostatic Generator.

Acknowledgments

I am indebted to Dr. A. P. French for suggesting these problems, to Mr. E. S. Shire for permitting the use of the electrostatic generator, and to the Department of Scientific and Industrial Research for a grant.

References

Adair, R. K., 1952, *Phys. Rev.*, **87,** 1041.
Baranger, E. U., 1955, *Phys. Rev.*, **99,** 145.
Barnes, C. A., 1955, *Phys. Rev.*, **97,** 1226.
Bashkin, S., and Richards, H. T., 1951, *Phys. Rev.*, **84,** 1124.
Blatt, J. M., and Biedenharn, L. C., 1952, *Rev. Mod. Phys.*, **24,** 258.
Bradley, D. E., 1954, *Brit. J. Appl. Phys.*, **5,** 65.
Breit, G., and Bloch, I., 1948, *Phys., Rev.*, **74,** 397.

Burcham, W. E., and Freeman, J. M., 1949, *Phil. Mag.*, **40,** 807.
Carver, J. H., and Wilkinson, D. H., 1951, *Proc. Phys. Soc.* A, **64,** 199.
Chao, C. Y., 1950, *Phys. Rev.*, **80,** 1035.
Chao, C. Y., Tollestrup, A. V., Fowler, W. A., and Lauritsen, C. C., 1950, *Phys. Rev.*, **79,** 108.
Cohen, E. R., 1949, *Thesis*, California Institute of Technology.
Dearnaley, G., 1954, *Phil. Mag.*, **45,** 1213.
Devons, S., and Hereward, H. G., 1948, *Nature, Lond.*, **162,** 331.
Devons, S., and Hine, M. G. N., 1949, *Proc. Roy. Soc.* A, **199,** 56.
Fowler, W. A., and Lauritsen, C. C., 1949, *Phys. Rev.*, **76,** 314.
Hahn, T. M., Snyder, C. W., Willard, H. B., Bair, J. K., Klema, E. D., Kington, J. D., and Green, F. P., 1952, *Phys. Rev.*, **85,** 934.
Jackson, H. L., and Galonsky, A. I., 1951, *Phys. Rev.*, **84,** 401.
Laubenstein, R. A., and Laubenstein, M. J. W., 1951, *Phys. Rev.*, **84,** 18.
Mackin, R., 1954, *Phys. Rev.*, **94,** 948.
Mooring, F. P., Koester, L. J., Goldberg, E., Saxon, D., and Kaufmann, S. G., 1951, *Phys. Rev.*, **84,** 703.
Newson, H. W., and Gibbons, J. H., 1954, *Bull. Amer. Phys. Soc.*
Newton, J. O., 1954, *Phys. Rev.*, **96,** 241.
Paul, E. B., and Gove, H. E., 1953, *Proc. Roy. Soc. Canada*, **47,** 145.
Peterson, R. W., Fowler, W. A., and Lauritsen, C. C., 1953, *Phys. Rev.*, **92,** 1085.
Rae, E. R., Rutherglen, J. G., and Smith, R. D., 1950, *Proc. Phys. Soc.* A, **63,** 775.
Sanders, J. E., 1953, *Phil. Mag.*, **44,** 1302.
Seed, J., and French, A. P., 1952, *Phys. Rev.*, **88,** 1007.
Sinclair, R. M., 1954, *Phys. Rev.*, **93,** 1082.
Thomas, R. G., Rubin, S., Fowler, W. A., and Lauritsen, C. C., 1949, *Phys. Rev.*, **75,** 1612.
Webb, T. S., Hagedorn, F. B., Fowler, W. A., and Lauritsen, C. C., 1955, *Phys. Rev.*, **99,** 138.
Wigner, E. P., and Eisenbud, L., 1947, *Phys. Rev.*, **72,** 29.
Wilkinson, D. H., and Clegg, A. B., 1953, *Phil. Mag.*, **44,** 1322.
Willard, H. B., Bair, J. K., Kington, J. D., Hahn, T. M., Snyder, C. W., and Green, F. P., 1952, *Phys. Rev.*, **85,** 849.

LXXXV. *The Mechanism of Work Softening in Aluminium*

By Anthony Kelly†
Department of Physical Metallurgy, The University, Birmingham‡

[Received April 30, 1956]

Summary

The appearance of slip lines on polished surfaces of aluminium crystals has been studied under the optical microscope as a function of plastic extension at 90°K and at room temperature. Measurements have been made of the lengths of the slip traces produced by the emergence of screw and edge dislocation segments. During deformation at both temperatures the first slip lines produced are long and straight. Further deformation at 90°K results in the appearance of shorter slip traces whilst at room temperature cross slip is observed. Crystals strained at one temperature and subsequently deformed at a higher temperature show a yield point (work softening) ; this is accompanied by an increase in the amount of cross slip and in the intensity of cross slip traces. The result is discussed in terms of dislocation movements.

§ 1. Introduction

Work softening is the name given to the yield point characteristics observed in metal single crystals strained at a certain temperature after prestrain at a lower temperature. The phenomenon has been extensively studied by Stokes and Cottrell (1954), Cottrell and Stokes (1955) in aluminium and by Adams and Cottrell (1955) in copper. These workers concluded that the effect is due to the collapse of piled up groups of dislocations formed at the lower temperature, when the crystal is further strained at a higher temperature. The piled up groups are thought to be formed at sessile dislocations which become glissile due to the joint action of stress and temperature, thus releasing suddenly large numbers of dislocations into the glide plane. This explanation has also been advanced independently by Friedel (1955).

To test this hypothesis it was decided to examine the slip lines appearing on the surface of aluminium crystals during deformation at 90°K and at room temperature and also during work softening. It is to be expected that observations of the slip lines formed during work softening will give information on the mechanism of the breakdown of the piled up groups.

† Now at Metallurgy Department, Northwestern University, Illinois.
‡ Communicated by the Author.

§ 2. Experimental Procedure

Flat tensile specimens of aluminium of 99·992% purity, presented by the British Aluminium Co., were grown into single crystals by the strain–anneal method. The orientation of the crystals was determined from x-ray Laue photographs and is shown in fig. 1. The gauge dimensions of the specimens were $2 \times 0{\cdot}3 \times 0{\cdot}1$ in. and those crystals were selected for a detailed investigation of the slip lines which were oriented such that the slip direction lay most nearly in a plane normal to the width of the specimen and containing the direction of tension. Under these conditions the dislocations emerging through the top surface of the crystal are of predominantly edge character and those emerging via the side faces are of predominantly screw character.

Fig. 1

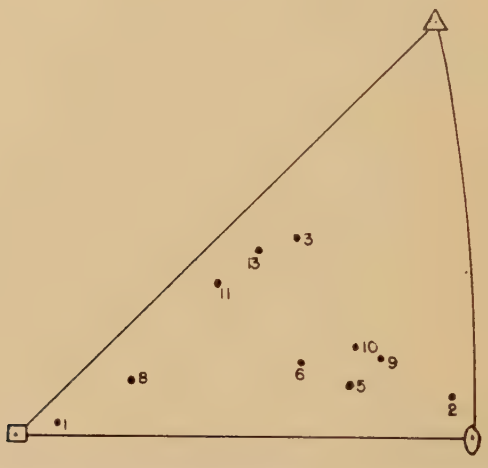

Initial orientations of the tensile axes of the specimens examined.

The specimens were deformed in tension with the hard beam machine of the Polanyi type used by Stokes and Cottrell at a strain rate of 5×10^{-5} sec^{-1}. For deformation at 90°K the specimen was surrounded by liquid oxygen and for deformation at 453°K by a silicone oil bath controlled to ± 1°C. Room temperature (289–293°K) was measured with a mercury in glass thermometer.

The procedure for examination of the slip lines was as follows. Specimens were polished electrolytically in a bath of 95% glacial acetic acid and 5% perchloric acid cooled in ice, and were then strained a few per cent at the desired temperature, unloaded, removed from the specimen grips and examined. The specimens were then remounted, further extended some 5–10%, unloaded and repolished so that a thickness of about 50 microns was removed from each surface of the specimen. The specimen was then further extended a few per cent, unloaded and examined. This procedure was repeated until sufficient deformation

had been produced. The specimen was then deformed about 1%, the temperature raised, and the specimen further deformed so that a Luders Band (cf., Cottrell and Stokes 1955) passed about half way down the gauge length. Crystals strained originally at 90°K were work softened at room temperature and those deformed at room temperature were further strained at 180°C. On unloading and examining the specimen the change in the appearance of the slip lines during the deformation through the yield point could be observed.

Fig. 2

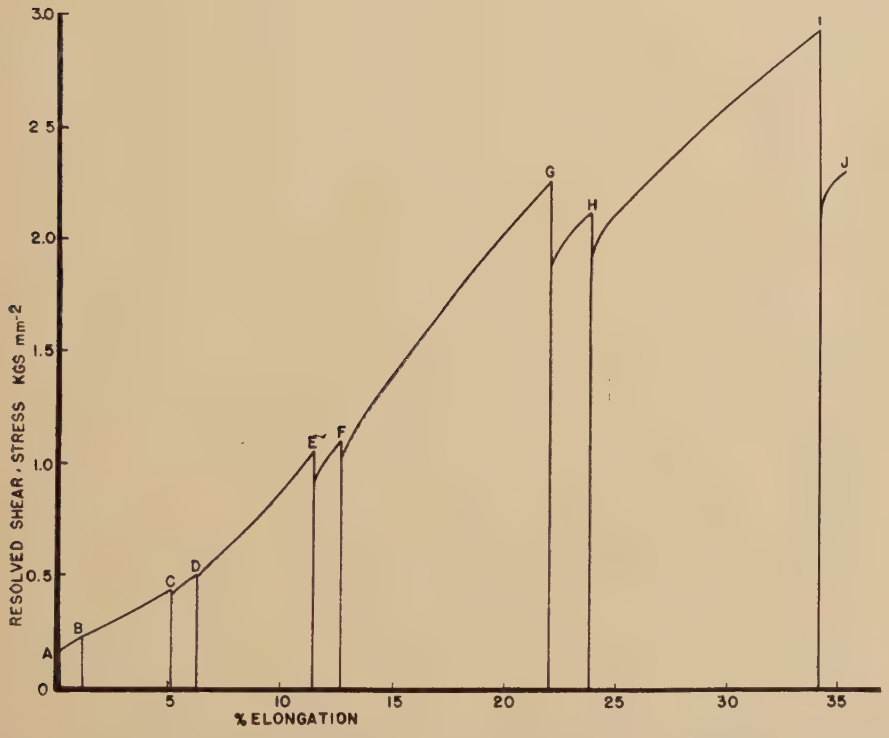

Stress elongation curve of crystal 2, deformed at 90°K. Polishing operations were carried out at points A, C, E, G, I. Slip line examinations were made at points B, D, F, H, J.

The slip lines produced during deformation at room temperature were easily observed using bright field illumination and the lengths of the traces on the top and side surfaces measured using a calibrated and graduated eyepiece. Slip lines formed during deformation at 90°K were often difficult to see, especially after small total deformations. Dark field illumination and phase contrast microscopy were both tried, but eventually the clearest resolution and most consistent measures of slip trace length were obtained using bright field illumination but with the lamp iris of the microscope partially closed.

§ 3. Results

3.1. *Deformation at* 90°K

The interrupted stress–elongation curve for crystal 2, deformed at 90°K, is shown in fig. 2. A definite recovery of the flow stress occurred at room temperature only after the curve had become concave to the elongation axis. A larger amount of recovery occurred when the specimens were polished than when the surface was not removed—the stress values are of course corrected for the change in area on polishing.

Fig. 3

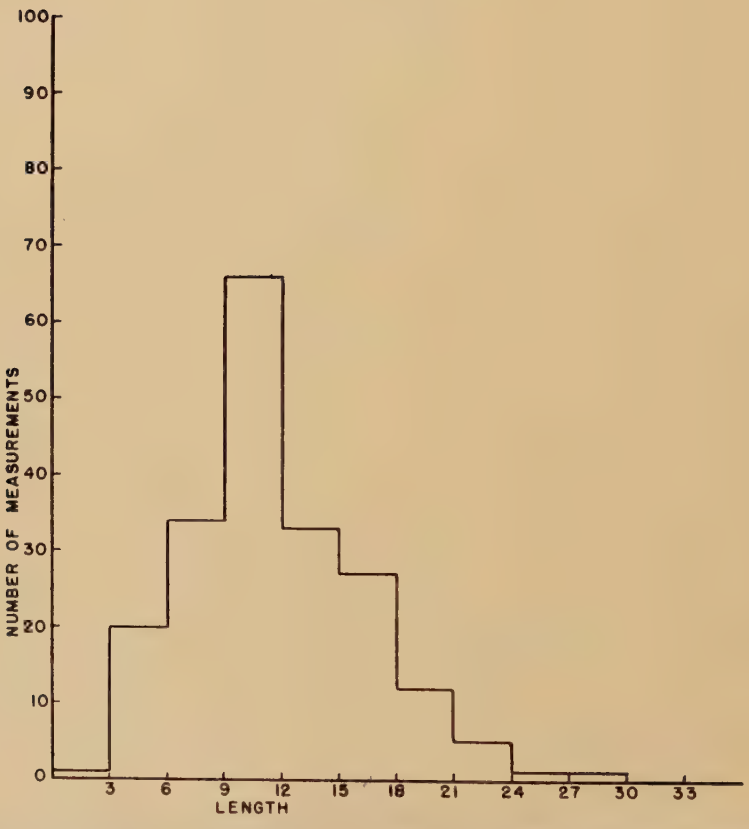

Histogram showing the distribution in length of the slip traces measured on the top surface of crystal 2 after a shear strain of 46·4%. The increment of shear strain was 3·1%, points G to H in fig. 2. The abcissae are in arbitrary units. Mean slip trace length : 29·6 μ.

The slip lines first observed on the top surface of the specimens were long and straight, often being a millimetre in length, and were very difficult to see, presumably because of the small amount of slip on each

plane. As the deformation increased the slip traces were a little easier to see and were shorter in length. After each incremental deformation following polishing, the length of between 200 and 300 individual slip traces, chosen at random on the top surface of the specimen, was measured.

Fig. 5

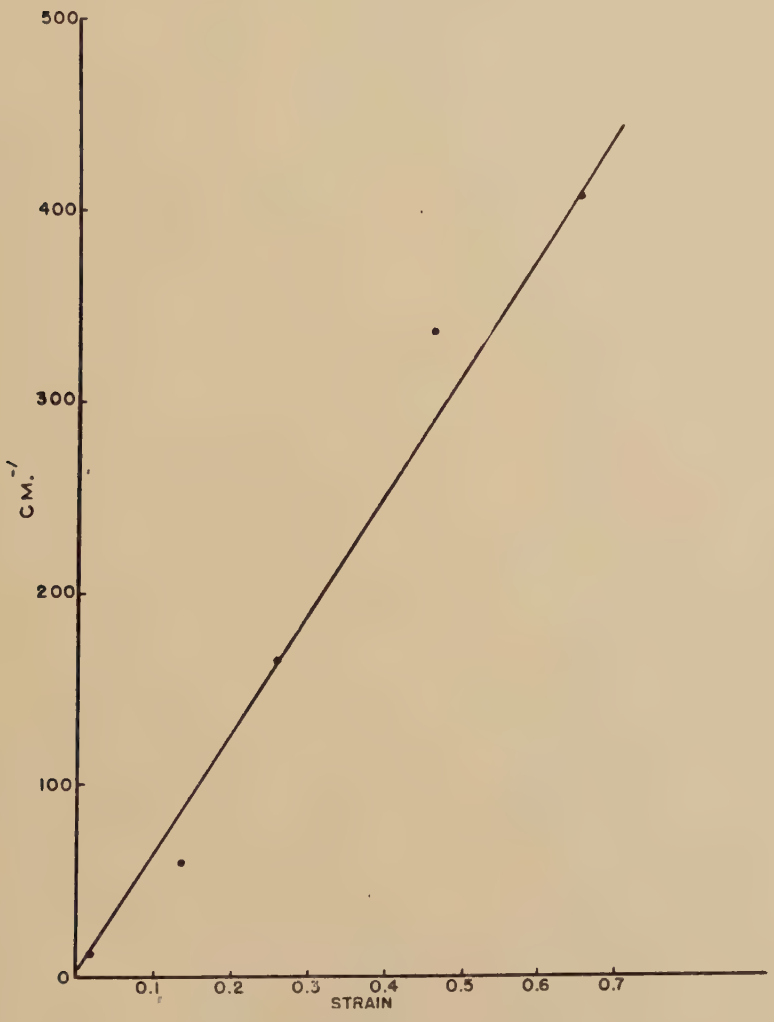

Plot of reciprocal of mean slip trace length against shear strain. Crystal 2 deformed at 90°K.

A histogram showing the distribution in length obtained from one of these sets of measurements is shown in fig. 3. The distribution is skew, the distribution function being steeper for lengths less than the peak value. In general longer slip lines were more prominent and easier to resolve.

If the shorter slip traces are less easily observed and furthermore, their lengths are measured less accurately, the skew character of the distribution may be accounted for. Both factors tend to make the average slip trace length an overestimate.

Figures 4 (*a*) and (*b*) show the appearance of the top surface of crystal 2 after 25·8 and 46·4% shear strain, while fig. 5 is a plot of the reciprocal of the average slip trace length against shear strain. The relationship appears to be approximately linear. Crystals 3 and 6 gave similar values to 2 at comparable strains, within a factor of two.

Deformation bands were observed to form on the side surfaces of the specimens. These became more obvious with increasing deformation and were much more readily observed after the large incremental deformations between polishing operations than they were when few slip lines were present on a polished surface. The slip lines observed on the side surfaces generally terminated in deformation bands and did not generally stop in between, though a decrease in the distance between deformation bands certainly occurred with increasing deformation. Measurements of the separation of deformation bands were generally larger than the average slip trace length by a factor of about two.

The appearance of the top surface of a specimen deformed at 90°K and then at room temperature so that a yield point and Luders deformation is observed, shows a marked change. This is illustrated in figs. 6 (*a*) and (*b*). Two types of slip line are visible. The short straight lines were produced at 90°K prior to deformation at room temperature. The thick, wavy lines were produced on deforming at room temperature. It is difficult to focus clearly on the room temperature slip lines whilst using a magnification that shows the low temperature traces nicely. This is due to the large step height on the surface produced by the former. The high temperature traces consist of segments of slip occurring on the main slip system, joined by jagged lines ; this cross slip does not occur on a single crystallographic plane. The high temperature slip lines extend over very large distances on the crystal surface, allowing for their jogging from plane to plane of the main slip system, and can often be followed completely across the top surface of the crystal.

During work softening the appearance of the slip traces on the side surfaces of the crystals showed a change only in the prominence of the lines. The lines remained sharp and straight but those within the Luders band showed a larger step height, indicating more slip on each plane.

An attempt was made to measure the average length of the straight portions of the high temperature lines on the top face which were parallel to the low temperature traces. This was difficult since the meaning of ' straight portion ' is somewhat arbitrary. For crystal 3 the average slip trace length on the top surface after a total deformation of 64·7% and an incremental strain of 1·8%, was 17 μ and the average length of the straight segments of the slip lines, produced after additional strain at

room temperature, immediately following the low temperature strain, was 18 μ. Similar agreement was found for crystal 6.

3.2. *Deformation at Room Temperature*

The interrupted stress elongation curve for crystal 13 is shown in fig. 7. Again it is noticeable that a larger amount of recovery occurs when the specimen surface is removed by polishing. No recovery occurred at room temperature, after straining at room temperature, until the curve had become concave to the elongation axis.

The slip lines first noticed on the top face after 2·19% shear strain were long and straight and similar to those observed at 90°K. Many of them traversed distances of a millimetre or more on the crystal face, fig. 8 (*a*). As deformation proceeded the slip lines became more prominent but remained sharp and straight. At the same time deformation bands could be observed on the side face and their separation was greater

Fig. 7

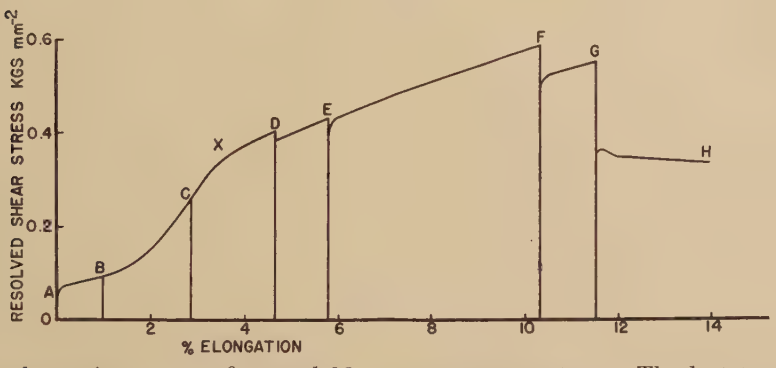

Stress elongation curve of crystal 13 at room temperature. The last test was made at 453°K. Polishing operations were carried out at the points, A, D, F. Slip line examinations were made at the points B, C, E, G, H.

than the average slip trace length on the top face. When the stress–elongation curve passed the point X, fig. 7, i.e., it became markedly concave to the elongation axis, cross slip was observed to link the ends of adjacent traces on the top face, fig. 8 (*b*). In this paper the term cross slip means the short, wavy and often indistinct traces joining together the ends of two prominent slip bands. It has been studied by Cahn (1951) in aluminium and has been called ' overlap ' by Chen and Pond (1952). When first observed this did not occur at the end of every trace and length measurements of the slip traces could still be made. After further deformation the slip traces were found to be shorter and all were linked by cross slips to adjacent traces. This continued until it was impossible to distinguish straight segments of the slip traces and the surfaces resembled those shown by Cahn (1951). A plot of average slip trace length against shear strain was similar to that obtained from crystals

deformed at 90°K. There was no noticeable change in the appearance of the side surface of the specimen when the stress elongation curve became concave to the elongation axis.

Specimens 10 and 13 were subsequently deformed at 453°K after deformation at room temperature. Work softening occurred as shown in fig. 7 (Stokes and Cottrell 1954). Figure 8 (*c*) is a photograph of the top surface of crystal 13 taken within the Luders Band; two types of slip line can be observed. The very marked lines weaving across the surface occurred only in those parts of the specimen which had extended at 453°K. These are more prominent than the slip lines formed at room temperature and also the cross slip jumps are much longer. No obvious change occurred in the appearance of the side surface of the specimens on work softening at 453°K with the exception of an increase in prominence of the slip steps within the Luders Band.

Fig. 9

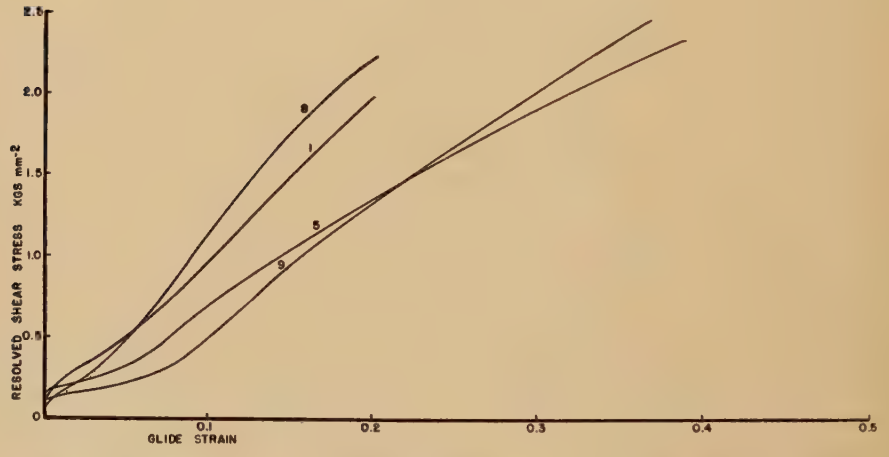

Stress strain curves of four crystals deformed at 90°K. The data for crystal 9 are replotted from measurements by R. J. Stokes.

3.3. *The Occurrence of Cross Slip*

No cross slip was observed in specimens deformed solely at 90°K. This may be due to the lack of resolution of the optical microscope. At room temperature cross slip was observed when the stress–strain curve became markedly concave to the strain axis. To see if an obvious bend occurred in the uninterrupted low temperature stress–strain curves three crystals were deformed continuously at 90°K. These curves are shown in fig. 9 together with one obtained by Stokes (1953) and replotted here as resolved shear stress against shear strain. No marked bend is noticed in the curves after the initial upward swing at the termination of easy glide. The curves all show a slight and continuous curvature.

In specimens deformed at 90°K, subsequently extended at room temperature until work hardening just recommenced, and then re-extended at 90°K the slip lines formed were still short traces of a definite length but were not so straight as those appearing on specimens deformed solely at 90°K. These lines were very carefully examined at $\times 1300$ but in no instance was a cross slip trace positively identified. The waviness of slip lines formed at 90°K under these conditions was observed in two specimens so it may be that the dislocation arrangement produced during deformation at room temperature is affecting subsequent deformation processes at 90°K.

§ 4. Discussion

At 90°K and at room temperature the distance between deformation bands exceeds the length of the slip traces formed on the top surface of the specimen by a factor of about two. If it is equally easy for edge and screw dislocations to pass out of the crystal then we conclude that edge dislocations can travel farther than screws at each of these temperatures. A similar result has been obtained by Muller and Leibfried (1955) for deformation at room temperature and Seeger (1955) has given theoretical reasons for this effect.

It appears that pure screw dislocations are piled up behind one another at the ends of the slip traces seen on the top surfaces of the crystals. The evidence that these dislocations are *pure* screws is that climb occurs immediately on straining at room temperature over distances of 10^{-3} cm. If the dislocations contained an edge component then this would be a diffusion controlled process and would be expected to take place much more slowly than is observed. Since the length of slip traces observed decreases with increasing deformation, the screw dislocations produced later in the deformation process move smaller distances in the crystal.

The actual process of the joining together of the ends of the traces as observed during work softening at room temperature, after prestrain at 90°K, and during deformation at room temperature and above (Cahn 1951), seems to be the mutual annihilation of screw dislocations of opposite sign (Mott 1951). It might be argued that the process is similar to that proposed originally by Koehler (1952) and by Diehl *et al.* (1955) to explain the clustering of slip traces observed under the electron microscope. However, if the latter explanation is the case and a loop of screw dislocation is acting as a Frank–Read source in a neighbouring and parallel slip plane, one would expect to observe slip lines as shown schematically in fig. 10 (*a*), since positive and negative dislocation segments would both be produced. Further, a single screw dislocation moving out of its slip plane would produce no observable cross slip trace. All the cross slip traces appear as in fig. 10 (*b*). The waviness and indistinct nature of the cross slip traces, in comparison with the sharp straight traces on the main slip system, does not suggest the operation of Frank–Read sources in the cross slip planes.

The main difference between the deformation process at low temperatures and at room temperature or above seems to be the ease with which piled up groups of screw dislocations of opposite sign interact by cross slip leading to the mutual annihilation of some of the dislocations. This process will be a thermally activated one and will depend on the shear stress at the head of the piled up group (Schoeck and Seeger 1955). These experiments provide then a picture of the process occurring during work softening which leads to the collapse of piled up groups, as suggested by Cottrell and Stokes and by Friedel.

Work softening will occur when a specimen has been deformed sufficiently at a low temperature to provide pile-ups of screw dislocations of sufficient strength to be unstable under stress at a higher temperature. The sudden annihilation of groups of screws of opposite sign presumably leads to a reduction of the back stress on the Frank–Read sources which can then generate more dislocations leading to the observed increase in step height of the slip lines. That it is the pile up of screw dislocations which causes a given source to stop operating is suggested by the fact that the screws move smaller distances than the edge components, in the absence of cross slip.

Fig. 10

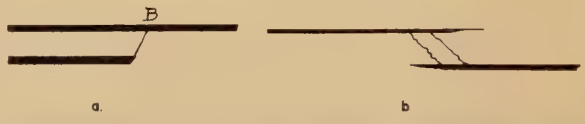

(*a*) Expected appearance of slip lines if point B acts as a Frank–Read source and produces equal numbers of positive and negative dislocation segments.

(*b*) Expected appearance of slip lines if mutual annihilation of screw dislocations of opposite sign occurs.

Cross slip of the type observed in this work becomes frequent at room temperature at stresses of 0·4 kg mm^{-2}, as deduced from the observations on crystals 10 and 13. A crystal having a flow stress of 0·4 kg mm^{-2} at room temperature will have a flow stress of 0·55 kg mm^{-2} at 90°K, according to the measurements of Cottrell and Stokes (1955) of the reversible change of flow stress with temperature. Thus, if a crystal is to show work softening at room temperature after prior strain at 90°K a flow stress of 0·55 kg mm^{-2} must be exceeded at 90°K. This value is in good agreement with that found by Cottrell and Stokes (0·56–0·72 kg mm^{-2}) in an experimental determination of this quantity. Adams and Cottrell (1955) investigated the onset of work softening in copper crystals at 473°K after prestrain at 90°K. A similar prediction can be verified from their results if the stress for the onset of cross slip at 473°K be taken as that stress at which the stress elongation curve becomes concave to the elongation axis. For a given crystal the exact value of the flow stress which must be exceeded at some one temperature in order that work softening can occur at a given higher temperature should then depend on the stress at the higher temperature at which cross slip occurs and hence presumably on the orientation of the crystal.

If this interpretation of the experimental results is correct, then it seems that there must be some process at work in aluminium crystals which can lock pure screw dislocations so that a pile up be formed. Such a process has been suggested for edge dislocations (Lomer 1951, Cottrell 1953) but the formation of sessiles by pure screw dislocations is found by Friedel (1955) to be unlikely.

Similar observations of the variation of slip trace length with strain to those reported here have been made by Blewitt *et al.* (1955) on copper single crystals. These authors noted that ' fragmentation ' occurred of the slip traces produced after deformations of some per cent at room temperature, and that this never occurred at 4·2°K. The fragmentation of the slip traces takes place when the stress strain curve at room temperature deviates from a straight line and becomes concave to the strain axis (Blewitt, private communication). It is suggested that the process of ' fragmentation ' is identical with the cross slip found in the present work. In both aluminium and copper, then, the stress–strain curve deviates markedly from a straight line when cross slip is observed. The cross slip is caused by the mutual annihilation of screw dislocations of opposite sign. This process leads to a reduction in the number of dislocations within the crystal and hence to a reduction in the rate of work hardening.

Acknowledgments

I should like to thank Professor G. V. Raynor in whose laboratory this work was carried out for the generous provision of facilities. It is a pleasure to thank Dr. A. H. Cottrell, F.R.S. for suggesting this investigation and for his encouragement in the course of this work. I am indebted to Drs. A. Seeger and P. Haasen for helpful discussions and to the I.C.I. Fellowship Fund for financial support.

References

Adams, M. A., and Cottrell, A. H., 1955, *Phil. Mag.*, **46**, 1187.
Blewitt, T. H., Coltman, R. R., and Redman, J. K., 1955, *Rep. Conf. Defects in Solids* (London : Physical Society), p. 369.
Cahn, R. W., 1951, *J. Inst. Met.*, **79**, 129.
Chen, N. K., and Pond, R. B., 1952, *J. Metals*, **4**, 1085.
Cottrell, A. H., and Stokes, R. J., 1955, *Proc. Roy. Soc.* A, **323**, 17.
Cottrell, A. H., 1953, *Dislocations and Plastic Flow in Crystals* (Oxford).
Diehl, J., Mader, S., and Seeger, A., 1955, *Z. Metallk.*, **46**, 650.
Friedel, J., 1955, *Phil. Mag.*, **46**, 1169.
Koehler, J. S., 1952, *Phys. Rev.*, **86**, 52.
Lomer, W. M., 1951, *Phil. Mag.*, **42**, 1327.
Mott, N. F., 1951, *Proc. Phys. Soc.* B, **64**, 729.
Muller, H., and Leibfried, G., 1955, *Z. Physik*, **142**, 87.
Schoeck, G., and Seeger, A., 1955, *Rep. Conf. Defects in Solids* (London : Physical Society), p. 340.
Seeger, A., 1955, *Phil. Mag.*, **46**, 1194.
Stokes, R. J., 1953, *M.Sc. Thesis*, Birmingham.
Stokes, R. J., and Cottrell, A. H., 1954, *Acta Met.*, **2**, 341.

LXXXVI. *Electrical and Thermal Magneto-Resistance in Thin Rods of Pure Sodium*

By G. K. White and S. B. Woods
Division of Pure Physics, National Research Council, Ottawa †

[Received December 27, 1955]

Abstract

Measurements are reported on the electrical and thermal resistivity of 130 μ and 350 μ diameter rods of high purity sodium in transverse magnetic fields (0 to 10 000 oersteds) and at temperatures between 2 and 18°K. These indicate that in the thinner specimen at liquid helium temperature the mean free path is limited by the dimensions of the specimen and that relatively small magnetic fields, of magnitude such that the radius of the electron orbit is comparable with that of the rod, decrease the resistance. At higher fields a linear increase in resistance with field is observed, the relative increase being less at higher temperatures where lattice vibration scattering of the electrons is predominant.

§ 1. Introduction

Following earlier work on the electrical resistance of very thin metallic films, Andrew (1949) extended the investigation of the possible geometrical limitation of electron mean free paths to low temperatures by measurements of the electrical resistivity of fine specimens of pure tin and mercury in liquid helium. Shortly afterwards MacDonald (1949) discovered that at liquid helium temperatures the dimensions of very pure sodium specimens 30 μ in diameter limited their electrical conductivity, but that this conductivity could be influenced by a magnetic field. He found that when a magnetic field of strength such that the radius of the electron orbits was comparable with that of the rod was applied the resistivity was reduced toward that of the bulk metal. Theoretical analyses of the influence of a magnetic field on the size variation of electrical conductivity were carried out by Sondheimer (1949) for thin films in a field normal to the surface ; also by MacDonald and Sarginson (1949, 1950) for thin films in a co-planar field and for square-section wires in a longitudinal field. The theory was extended by Chambers (1950) to round wires in a longitudinal field and further experiments on sodium were reported.

† Communicated by Dr. D. K. C. MacDonald.

Such experiments are of particular interest because they yield direct information about the mean free paths of the electrons and we decided to look for a corresponding effect in the thermal conductivity. The correlation of size-effect variations and magnetoresistance measurements for the electrical and thermal conductivity should then yield further information about the mean free paths involved. It might also lead to a better understanding of those processes which furnish the resistive mechanisms at low temperatures—i.e. energy and momentum exchange between electrons and phonons, and between electrons and static impurities.

§ 2. Experimental Method

Two specimens of sodium,† Na3 and Na4, with approximate diameters 130 μ and 350 μ were cast in soft glass tubes with platinum leads attached (see e.g. MacDonald and Mendelssohn 1950, MacDonald and Sarginson 1950 for description of the technique) and their thermal and electrical resistivities, W and ρ respectively, were measured in a cryostat described previously by White and Woods (1955). Detailed measurements of the conductivities of Na3 and other specimens of larger diameter in zero field and over a range of temperatures have been reported elsewhere (Woods 1956, MacDonald, White and Woods 1956). These earlier measurements gave, for Na3, residual electrical and thermal resistivities : $\rho_0 \simeq 1{\cdot}66 \times 10^{-9}$ ohm cm and $W_0 = 0{\cdot}072/T$ cm deg/watt, and ideal resistivities due to scattering of the electrons by thermal vibrations :

$$\rho_i \simeq 8{\cdot}8 \times 10^{-15}\, T^5 \text{ ohm cm } (8^\circ < T < 16^\circ\text{K}),$$

$$\rho_i \simeq 8{\cdot}6 \times 10^{-16}\, T^6 \text{ ohm cm } (T < 8^\circ\text{K}),$$

$$\text{and } W_i \simeq 3{\cdot}5 \times 10^{-4}\, T^2 \text{ cm deg per watt } (T < 20^\circ\text{K}).$$

The low ratio of the residual electrical resistance to that at 295°K ($\rho_0/\rho_{295} \sim 3 \times 10^{-4}$) for these specimens indicates their high purity and suitability for mean free path investigations, apart from the more general consideration that sodium is a relatively ideal free electron metal, which first led us to use it.

For the measurements reported here, the cryostat was placed in a transverse magnetic field produced by an Arthur D. Little electromagnet.

§ 3. Experimental Results

For the finer specimen, Na3, the resistivities were generally found to increase initially with the field for small fields, pass through a maximum and decrease towards the ' bulk ' value, then increase linearly with higher field strengths. With Na4 no marked maximum appeared, but only a slight decrease with increasing low fields and thereafter a linear increase. These linear regions have been extrapolated graphically to zero field to

† We are grateful to Messrs. Phillips (Eindhoven) for supplying this high purity sodium.

give 'bulk' values of the resistivities ρ_x, W_x, which are shown in the table together with the observed zero field resistivities and the calculated mean free paths. The respective mean free paths, l_ρ and l_w, have been calculated from the values of ρ_x and W_x assuming the equations,

$$1/\rho_x = \frac{Ne^2 l_\rho}{mv} \quad . \quad . \quad . \quad . \quad . \quad . \quad . \quad . \quad (1)$$

$$\text{and } 1/w_x = Cvl_w/3, \quad . \quad . \quad . \quad . \quad . \quad . \quad . \quad . \quad (2)$$

where e is the electron charge, m the electron mass, N the number of free electrons per cm^3, v the electron velocity, and C the electronic specific heat. We have assumed one free electron per atom in calculating $N = 2{\cdot}5 \times 10^{22}$ electrons/cm^3 and have used for the electron velocity, $v = (2 \times \text{Fermi energy}/m)^{1/2} = 1{\cdot}07 \times 10^8$ cm/sec. To be consistent with the adoption of a theoretical value for v, C $(=\gamma T)$ has been calculated from the theoretical value for γ, i.e. $\gamma = 2{\cdot}7 \times 10^{-4}$ cal (gm atom)$^{-1}$ deg^{-1}. Chambers's (1950) measurements indicate that $v \simeq 1 \times 10^8$ cm/sec, in reasonable agreement with the free electron value, although the specific heat measurements of Parkinson and Quarrington (1955) yield a higher value for γ and, hence, would give a somewhat lower figure for the Fermi energy or velocity deduced therefrom.

The 'bulk' resistivities, ρ_x and W_x, probably cannot be interpreted directly as the resistivities of an equivalent bulk sample, since strain and impurity, both of which contribute to the residual resistances, may play a significant role in fine specimens at these low temperatures. Nor, in any case, does the theory of magnetoresistance provide an entirely reliable guide for making the extrapolation from the high field measurements to what may be regarded as true bulk values at zero field. However ρ_x and W_x, which cannot be grossly different from the bulk resistivities, provide convenient field independent terms in discussions of magnetoresistance effects.

It should also be noted that the initial increase of the resistivities in transverse magnetic fields, which is due to a diminution of the paths of electrons travelling in certain directions, will not occur in longitudinal fields (see e.g. MacDonald 1949).

In figs. 1, 2 and 3 the experimental values of $\Delta\rho/\rho_x \equiv (\rho - \rho_x)/\rho_x$ and $\Delta W/W_x \equiv (W - W_x)/W_x$ are shown, plotted as functions of the field H. In figs. 1 and 2, for Na3, the top scales show the values of l/r appropriate to the various values of H, where r, the radius of an electron orbit in a field, H, is given by

$$r = mvc/eH = 6{\cdot}09/H, \quad . \quad . \quad . \quad . \quad . \quad . \quad . \quad (3)$$

where H is expressed in oersted and r in cm. In fig. 3 the arrows indicate values of H for which $l/r \simeq 1$, a different value being obtained for each curve because of the different values of ρ_x and W_x.

It may be noted that in each of the experiments l_ρ and l_w differed in value; which we would expect since $l_\rho \equiv l_w$ only in the region where

impurity scattering is dominant for both thermal and electrical resistivity, i.e. when

$$W \simeq W_0,\ \rho \simeq \rho_0$$

$$\text{and } \rho_0/W_0 T \simeq \frac{\pi^2}{3}\left(\frac{k}{e}\right)^2 = 2{\cdot}45 \times 10^{-8} \text{ watt ohm/deg}^2.$$

Unfortunately in the case of Na3 the specimen was so thin that sufficiently accurate measurements of the thermal resistivity could only be obtained at temperatures where the ideal and impurity resistivities were comparable ; and for Na4 the ideal resistivity is still significant even at 2·7°K, due to the high purity of the sodium used. Of course in the electrical case, since ρ_i falls more rapidly than W_i with temperature, $\rho \simeq \rho_0$ for all temperatures below about 5°K.

Fig. 1

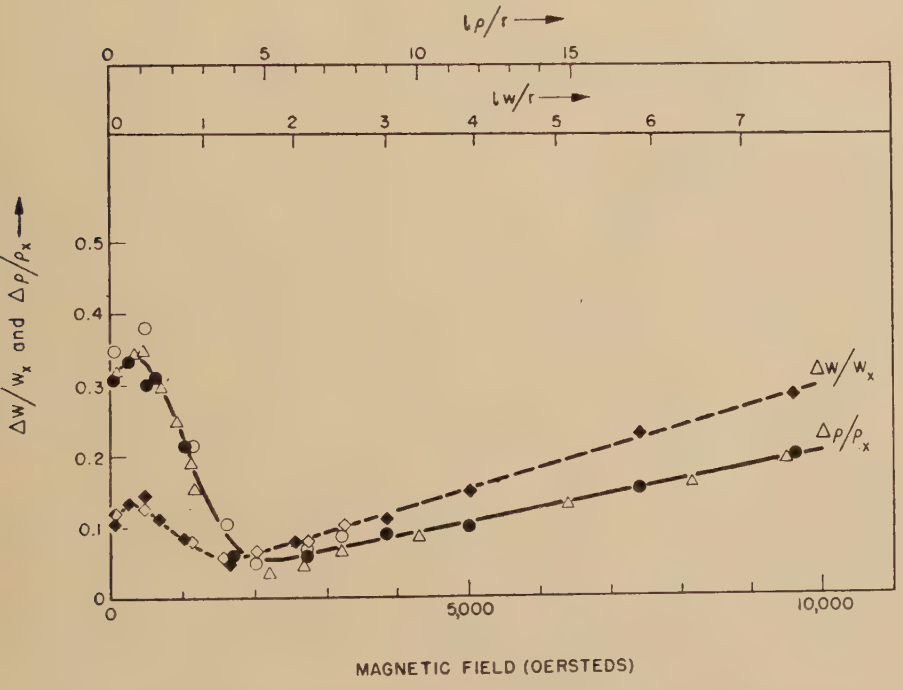

Variation of resistivity with magnetic field for a 130 μ diameter rod of sodium (Na 3)

○ $\Delta\rho/\rho_x$ at 4·2°K (Run 1)
● $\Delta\rho/\rho_x$ at 4·2°K (Run 2)
△ $\Delta\rho/\rho_x$ at 2·8°K
◇ $\Delta W/W_x$ at 4·3°K (Run 1)
◆ $\Delta W/W_x$ at 4·3°K (Run 2)

§ 4. Discussion

The experimental results show first that there is a size limitation on thermal conduction similar to that found in electrical conductivity. In the latter case Dingle (1950) (cf. also MacDonald and Sarginson 1950) has shown that for a rod of diamater a

$$\frac{\rho}{\rho_{\text{bulk}}} = 1 + \frac{3}{4}\frac{l}{a}(1-p)\left(\frac{l}{a} \ll 1\right) \quad . \quad . \quad . \quad . \quad (4)$$
$$= \frac{l}{a}\left(\frac{1-p}{1+p}\right) \quad \left(\frac{l}{a} \gg 1\right).$$

Fig. 2

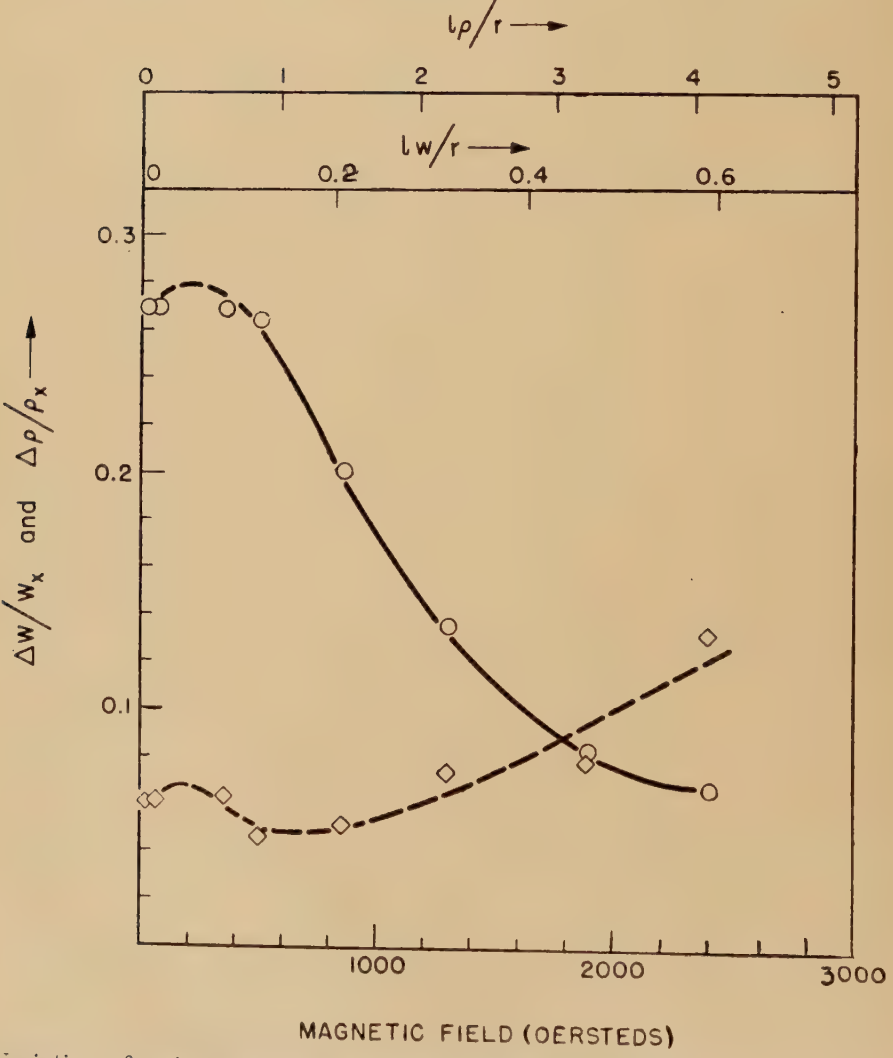

Variation of resistivity with magnetic field for a 130 μ diameter sodium rod (Na 3)

——○—— $\Delta\rho/\rho_x$ at 8·2°K

– – –◇– – – $\Delta W/W_x$ at 8·3°K

where p is the fraction of electrons specularly reflected at the surface. In this expression l is the mean free path for electrical conduction. MacDonald and Sarginson had to assume a degree of elastic reflection to interpret their experimental results on sodium. Andrew (1949) and Chambers (1950) however, found that the assumption of entirely diffuse scattering ($p=0$) was most appropriate for their data on other metals, this work including measurements on the so called 'anomalous skin-effect'. If we compare our results with eqn. (4), setting $l=l_\rho$, $\rho/\rho_{\text{bulk}} = \rho_{H=0}/\rho_x$ and $l=l_w$, $W/W_{\text{bulk}} = W_{H=0}/W_x$ for the electrical

Fig. 3

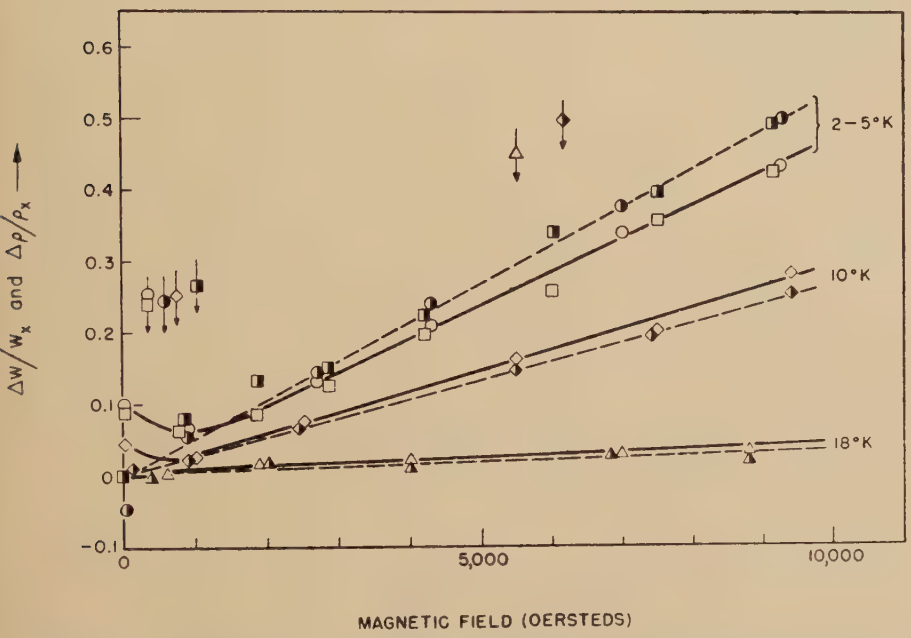

Variation of resistivity of a 0·35 mm diameter rod of sodium (Na 4) with magnetic field

——○—— $\Delta\rho/\rho_x$ at 2·10°K
— — —◑— — — $\Delta W/W_x$ at 2·68°K
——□—— $\Delta\rho/\rho_x$ at 4·21°K
— — —◨— — — $\Delta W/W_x$ at 4·65°K
——◇—— $\Delta\rho/\rho_x$ at 10·0°K
— — —◑— — — $\Delta W/W_x$ at 10·1°K
——△—— $\Delta\rho/\rho_x$ at 18·35°K
— — —◭— — — $\Delta W/W_x$ at 18·6°K

Arrows mark the fields for which $l/r \simeq 1$.

and thermal data respectively, the values of p in the last column of the table result. Our thermal measurements on the thicker specimen were not sufficiently accurate to yield reliable values for p in that case, but it

is interesting to notice that rather uniform values for p (with an average value 0·55) are deduced from the data on Na3, and also that in agreement with MacDonald and Sarginson, the degree of elastic reflection apparently is increased in the thicker specimen.

Electrical and Thermal Resistivity Data, and Calculated Electrical Thermal Mean Free Paths for Pure Sodium Specimens

	T (°K)	$10^9\rho_{H=0}$ ohm cm	$10^9\,\rho_x$ ohm cm	$W_{H=0}$ cm deg watt^{-1}	W_x cm deg watt^{-1}	l_ρ μ	l_w μ	p
Na3	2·8	1·42	1·08			140		0·59
~130 μ								
	4.2 (1)	1·36	1·01			140		0·53
	4·3 (1)			$0{\cdot}022_0$	$0{\cdot}0197_5$		48	0·56
	4·2 (2)	1·40	1·08			140		0·61
	4·3 (2)			$0{\cdot}22_2$	$0{\cdot}020_0$		48	0·60
	8·2	1·72	1·32			115		0·53
	8·25			$0{\cdot}364_4$	0·0345		15	0·43
Na4	2·1	0·930	0·845			180		0·74
~350 μ								
	2·7			0·0145	0·0152		115	—
	4·2	0·920	0·845			180		0·78
	$4{\cdot}6_5$			0·0166	0·0167		60	—
	10·0	1·72	1·64			92		0·75
	10·1			0·0456	0·0454		10	—
	$18{\cdot}3_5$	14·0	14·0			11		—
	18·6			0·134	0·137		~2	—

Turning now to the influence of a magnetic field on the resistivities, we see that, aside from a small initial effect in transverse fields, the resistivity is generally decreased by the application of a small magnetic field, provided that the major limitations on the electron mean free path are the dimensions of the specimen. When bulk impurity scattering or scattering by thermal vibrations is dominant—states of affairs created respectively by increasing the field until $l/r \gg 1$ or increasing the temperature until the ideal resistance is greater than the impurity resistance—the resistivity becomes a linear function of field strength. The relative increase of resistivity with field decreases as the temperature is raised, so that independently of temperature, we may write very approximately

$$\Delta\rho/\rho_x \simeq \text{constant } H/\rho_x$$

$$\text{and } \Delta W/W_x \simeq \text{constant } H/W_x.$$

In the case of electrical magnetoresistance measurements, theory indicates that generally $\Delta\rho/\rho$ will be a function of l_ρ/r ; when size-effects are present the factor l_ρ/a (where a is a dimension of the specimen) will also occur, as in (4). We might then expect that in corresponding thermal

magnetoresistive experiments $\Delta W/W$ should be a similar function of l_w/r.

Our results show that indeed a magnetic field does cause a variation of thermal resistivity somewhat similar to that found in electrical resistivity. However, no simple scaling of the abscissae or ordinates by factors containing l_ρ, l_w, a, or r appears to bring the electrical and thermal data into correspondence and the deduction of further information about electron scattering from the results appears difficult. Perhaps further measurements using a longitudinal magnetic field may give results more amenable to theoretical treatment on the basis of a free electron model.

Acknowledgment

The authors are very grateful to Dr. D. K. C. MacDonald for many interesting discussions on this subject.

References

Andrew, E. R., 1949, *Proc. Phys. Soc.*, **62,** 77.
Chambers, R. G., 1950, *Proc. Roy. Soc.* A, **202,** 378.
Dingle, R. B., 1950, *Proc. Roy. Soc.* A, **201,** 545.
MacDonald, D. K. C., 1949, *Nature, Lond.*, **163,** 673.
MacDonald, D. K. C., and Mendelssohn, K., 1950, *Proc. Roy. Soc.* A, **202,** 103.
MacDonald, D. K. C., and Sarginson, K., 1949, *Nature, Lond.*, **164,** 922; 1950, *Proc. Roy. Soc.* A, **203,** 222.
MacDonald, D. K. C., White, G. K., and Woods, S. B., 1956, *Proc. Roy. Soc.* A, **235,** 358.
Parkinson, D. H., and Quarrington, J. E., 1955, *Proc. Phys. Soc.* A, **68,** 762.
Sondheimer, E. H., 1949, *Nature, Lond.*, **164,** 920.
White, G. K., and Woods, S. B., 1955, *Canad. J. Phys.*, **33,** 58.
Woods, S. B., 1956, *Canad. J. Phys.*, **34,** 223.

LXXXVII. *The Specific Heats of Cadmium and Mercury*†

By P. L. Smith and N. M. Wolcott‡
Clarendon Laboratory, Oxford

[Received February 8, 1956]

Abstract

The specific heat of cadmium has been measured over the range 1·3° K to 20° K. The electronic term is found to be $1{\cdot}5\times10^{-4}T$ cals mole^{-1} deg^{-1} and the Debye θ at 0° K is 188°, in fair agreement with the value calculated from elastic constants. The specific heat of mercury has also been measured over the same range and is shown to be characterized by a sharply changing Debye θ with a minimum at 3° K. The lowest points measured have not reached a T^3 dependence of the lattice specific heat.

§ 1. The Specific Heat of Cadmium

1.1. *Introduction*

The specific heat of cadmium has been studied by Simon and Lange (1928) and by Craig *et al.* (1953) down to liquid hydrogen temperatures, whilst Samoilov (1952) has made measurements below 1° K. Until the present work was undertaken there were no specific heat data in the range 1° K to 12° K. It was therefore felt desirable to cover this range in order to check the value of the electronic specific heat term given by Samoilov and to determine the Debye θ.

The variation of the Debye θ in this temperature range is often of interest. At extremely low temperatures, below about $\theta/50$, all lattice specific heats vary as T^3, and may thus be expressed in terms of one θ. The value of θ in this region is independent of the lattice structure since only those frequencies are present in the vibration spectrum whose wavelengths are much greater than the interatomic spacing. Under these conditions. the relation between the frequency and the number of modes $f(\nu)d\nu$ having a frequency in the range ν to $\nu+d\nu$ is accurately $f(\nu)d\nu=BV\nu^2d\nu$, where B is a constant and V is the volume of the solid (Born and von Karman 1912). B is found from the elastic constants and a method for its evaluation in the case of an anisotropic solid is given by Hopf and Lechner (1914).

At higher temperatures, above about $\theta/10$, it is found for many regular solids that θ varies relatively little with temperature, the initial success

† Communicated by the Authors.
‡ Now at the Naval Research Laboratories, Washington.

of the Debye theory being of course due to this. Even for more anisotropic solids, the change in θ with temperature is relatively small. The reason for this is that the apparent Debye θ is not sensitive to the shape of the frequency spectrum, and hence to the lattice structure, since it is the integral of the frequency distribution which enters into the calculation.

The shape of the θ–T curve between these two regions, however, is intimately connected with the form of the frequency distribution curve and hence with the lattice structure. The temperature range containing this region of changing θ is nearly always the neglected range 4° to 15° K, and for this reason measurements were made to cover it.

The θ–T curve for zinc shows a very sharp fall between 4° and 20° K, and since the lattices of the two metals are so very similar, its comparison with the same curve for cadmium should be of interest.

1.2. *Experimental*

A cylindrical block of cadmium was supplied by Johnson, Matthey and Co., who machined the metal so that it would fit the calorimeter. The sample weighed about 250 gm and its purity was given as better than 99·99%.

The method of measurement was that described by Parkinson *et al.* (1951), but several improvements in calorimetric technique have been introduced which merit description. These concern both calorimeter design and the problem of thermal isolation and they will be considered separately.

The calorimeter used was a cylindrical copper vessel 2·54 cm in diameter and about 7 cm long. Since it was not required for work above 20° K no radiation shielding was provided for the thermometers and these and the heater were wound directly on to the surface of the calorimeter, using ' Araldite ' as the adhesive. The electrical leads were also bonded to the body of the calorimeter before they reached the thermometers. A phosphor-bronze wire was used as resistance thermometer in the liquid helium range and constantan above these temperatures.

The calorimeter lid carried a small dome of about 1 cm^3 capacity which served as a condensation chamber. Placing this chamber on the lid has the advantage over the type of calorimeter described by Hill (1953) that the removal and replacement of a sample is much easier. Instead of unsoldering one or more tubes, the only joint to be broken is that around the lid. The complete calorimeter is shown in fig. 1.

The calorimeter was brought to about 1·3° K by pumping on liquid helium which had been condensed into the condensation chamber. Measurements were made as soon as this helium was evaporated, but an undesirably large temperature drift was often present. In fact, with the surroundings at 4° K, the heat leak to the calorimeter is largest at the moment when its heat capacity is smallest. To improve upon this

situation, a 1 cm^3 copper pot was suspended from the Simon expansion vessel on a piece of 1 mm german silver tubing. A flange on the copper pot was soldered to the two tubes leading to the calorimeter at about two-thirds of their lengths from the calorimeter. Liquid helium was introduced into this pot and pumped to a temperature of about 1·8° K at the beginning of the measurements. It thus acted as a heat sink and greatly reduced the heat leak to the calorimeter at the temperature at which the calorimeter's heat capacity was least.

Fig. 1

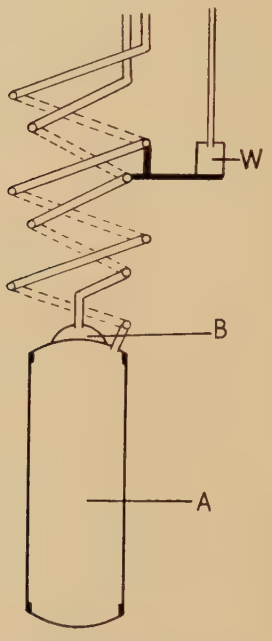

Calorimeter assembly. A is the sample space, B the condensation chamber and W the ' heat sink '. The electrical leads are not shown.

As the calorimeter temperature was raised above 1·8° K, heat flowed away from it at an increasing rate. Since, however, the heat capacity of the calorimeter increased with temperature much more rapidly than the heat leak, the seriousness of the heat leak was much reduced. Using this method, temperature drifts only a few per cent of the heating rate employed in taking a specific heat point are achieved.

1.3. *Results*

The values of the specific heat of cadmium found in this work agree with those of Craig *et al.* in the hydrogen range but are about 10% higher than those of Simon and Lange. The experimental points are shown

in fig. 2. Figure 3 shows a plot of C/T against T^2 from which an electronic contribution of $1{\cdot}5\times10^{-4}T$ cals mol^{-1} deg^{-1} is found. This is in fair agreement with the value of $1{\cdot}7\times10^{-4}T$ given by Samoilov. The value of θ derived from fig. 3 is 188°, considerably lower than Samoilov's tentative figure of 300°. At 1° K, however, the lattice specific heat is

Fig. 2

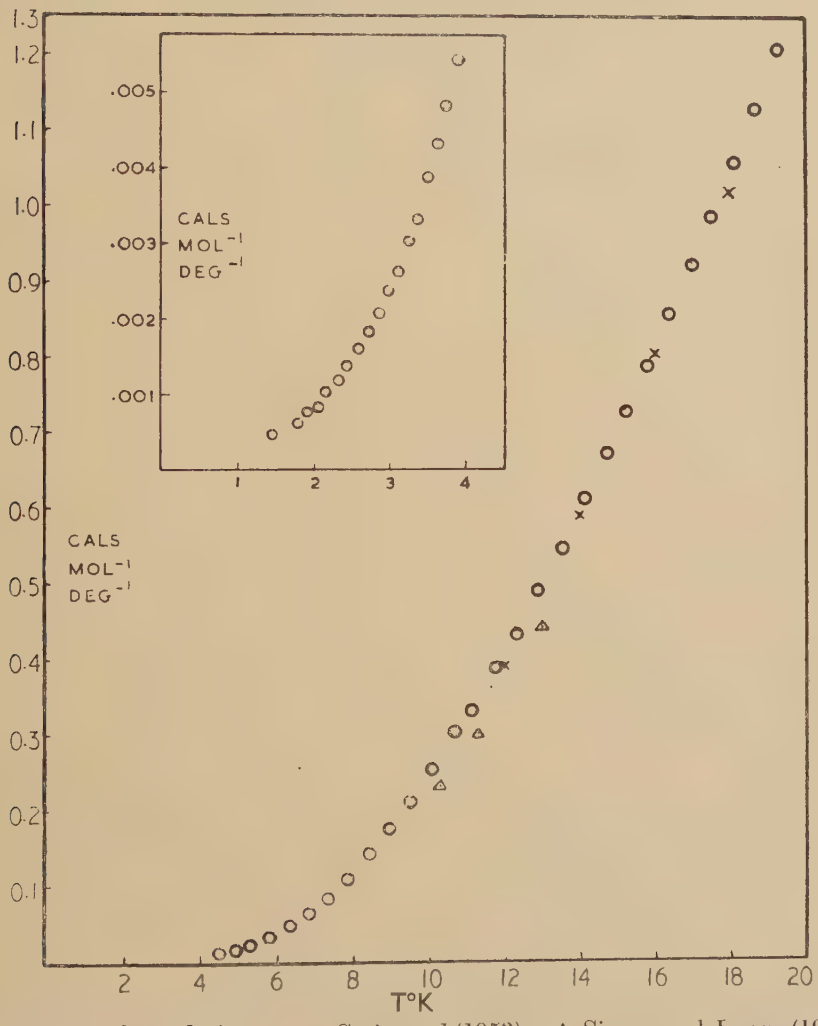

C_p against T for cadmium. × Craig *et al* (1953); △ Simon and Lange (1928)

only half the electronic term, so that it is clear that measurements taken between 0·3° and 0·9° K can only give an uncertain value of θ.

The standard entropy of cadmium given by Craig *et al.* is not affected by the present measurements since their estimate of $S_{12}-S_0$ agrees with our measured value.

1.4. *Discussion*

(*a*) *The Lattice Specific Heat*

The hexagonal cadmium lattice has an axial ratio of 1·866 and is therefore far removed from the ideal ratio of 1·633 corresponding to closest packing. The lattice properties are thus strongly anisotropic and large changes in the Debye θ may be expected, since the Debye theory applies to an isotropic continuum. Figure 4 gives the Debye θ of cadmium as a function of temperature, the values above 20° K being derived from

Fig. 3

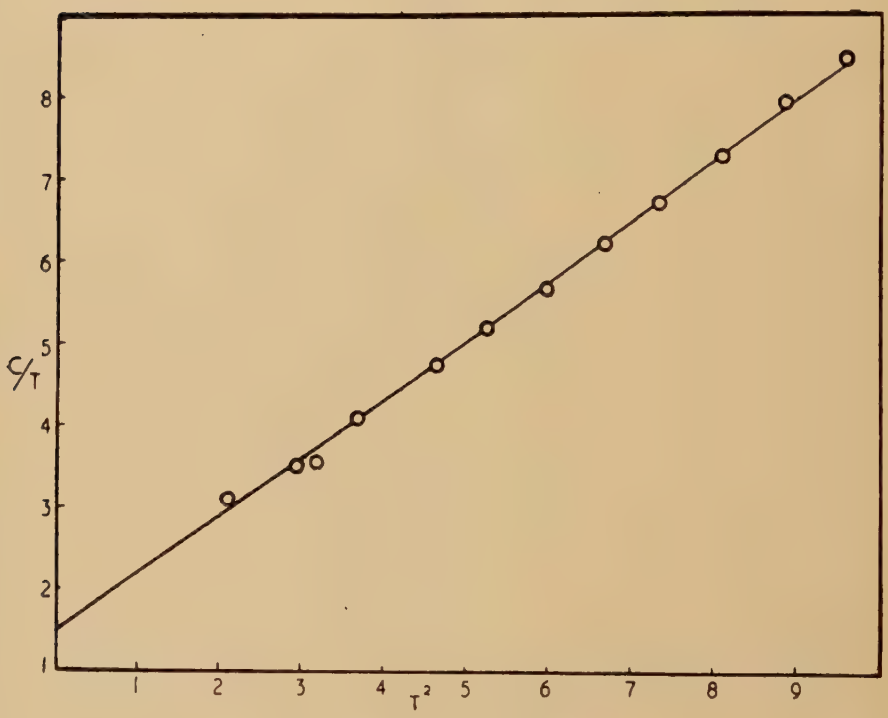

C_p/T against T^2 for cadmium.

Craig's work. It is seen that the lattice specific heat cannot be represented by a single Debye θ at any temperature above 3° K.

Since the axial ratio of the zinc lattice is very close to that of the cadmium lattice, it is not unreasonable to expect similarities in the behaviour of the two Debye θ's. Figure 4 also gives the θ–T relation for zinc, using the data of Clusius and Harteck (1928) and Smith (1955).† At low temperatures the similarity is quite pronounced, for the ratio of

† Corrigendum—In this paper the θ values given for zinc at 125° K and 150° K are incorrect. They should be as in fig. 4.

the θ values at 0° K is the same as the ratio of the minimum values—1·6. In addition, both minima occur at a temperature of about θ(min.)10.

At higher temperatures the curves continue to resemble each other, but it must be borne in mind that the Debye θ is an extremely sensitive parameter in the region of $T=\theta$ and that small inaccuracies in the measurements or in the determination of the C_p–C_v correction, will have a large effect on the value of θ which is derived.

Fig. 4

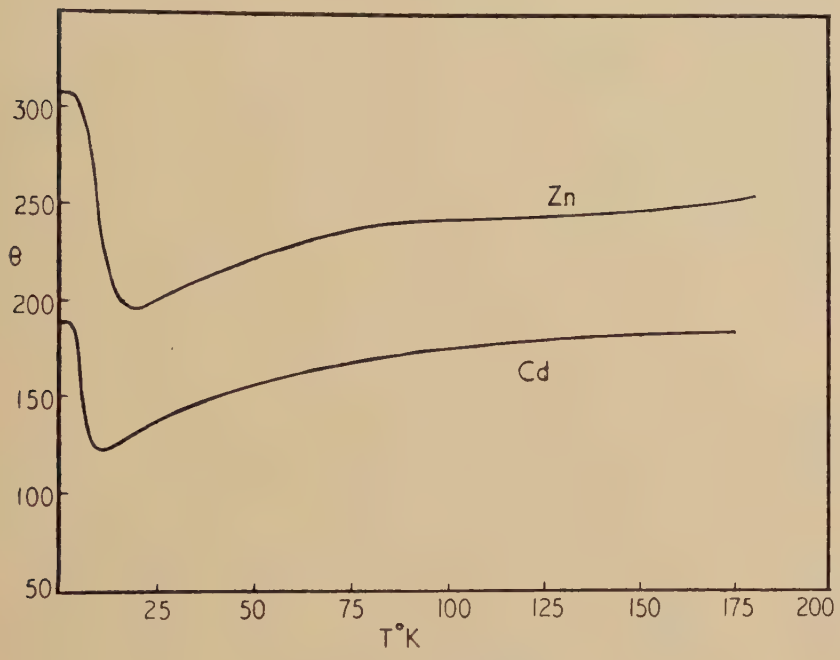

The Debye θ for cadmium.

Honnefelder (1933) has used the method of Hopf and Lechner to calculate the specific heat of cadmium from the elastic constants. Only room temperature elastic constants were available, but the agreement with experiment is not unreasonable. Honnefelder gives a value for C_v/T^3 of $8{\cdot}59\times10^{-5}$, corresponding to a $\theta(0°\text{ K})$ of 175°. Using elastic constants extrapolated to low temperatures, Fowler and Guggenheim (1939) give a $\theta(0°\text{ K})$ of 200°. The present experimental value of 188° lies just midway between these.

This result thus confirms Blackman's (1935) assertion that the disagreements between the θ values observed calorimetrically and those calculated from the low temperature elastic data are due to the fact that the former did not apply to the 'true T^3 region' but to a false T^3 region around the minimum θ value.

(*b*) *The Electronic Specific Heat*

The temperature coefficient of the electronic specific heat γ is related to the density of the electronic energy states $g(\epsilon)$ by the general relation

$$\gamma = 2/3\pi^2 k^2 g(\epsilon')$$

where ϵ' is the energy of the highest occupied state. If $g(\epsilon)$ is expressed in levels per electron volt per atom and γ in calories mol^{-1} deg^{-2}, the relation becomes

$$g(\epsilon') = 887\gamma.$$

The Brillouin zones for the hexagonal lattice have been calculated by Mott and Jones (1936). Their work shows that for an axial ratio greater than that corresponding to closest packing (1·633) energy overlaps into the second zone occur in such a way that $g(\epsilon)$ varies relatively little with ϵ, at least in the region of ϵ'. This means that the electronic specific heats of both zinc and cadmium should be about the same and should not show the large difference found between the γ's for beryllium and magnesium (whose axial ratios are 1·568 and 1·623 respectively) (Hill and Smith 1953, Smith 1955).

Table 1. Cadmium

T	C_p	θ	T	C_p	θ
1·5	0·000562	188	10·0	0·240	124
2·0	0·000855	188	12·0	0·410	125
3·0	0·00242	188	14·0	0·600	127
4·0	0·00651	177	16·0	0·809	129
5·0	0·0170	151	18·0	1·038	131
6·0	0·0389	138	20·0	1·30	133
8·0	0·114	128			

C_p is in cals mol^{-1} deg^{-1}

Daunt and Silvidi (1952) find the electronic specific heat of zinc to be $1{\cdot}50\times10^{-4}T$ cals mol^{-1} deg^{-1}. Since the value of γ for cadmium is also found to be $1{\cdot}5\times10^{-4}$ cals mol^{-1} deg^{-2}, the theoretical predictions seem to be confirmed in a satisfactory manner.

§ 2. The Specific Heat of Mercury

2.1. *Introduction*

Several sets of published data on the specific heat of mercury exist. Kamerlingh Onnes and Holst (1914) give two points in the liquid helium range ; Simon (1922, 1923) has made measurements from room temperature down to 10° K, and Pickard and Simon (1948) have covered the range

from 3° to 90° K. The most recent data are those of Busey and Giaque (1953) whose measurements extend from room temperature to 16° K.

Simon has shown that the strong anisotropy of mercury leads to an unusual shape of the specific heat curve at low temperatures ; it could be represented by the sum of a 3/4 of a Debye function with a θ of 120° and 1/4 of an Einstein function with $\theta=25°$. Later Pickard and Simon added some values down to liquid helium temperatures. As these, however, seemed abnormally high, a new set of experiments was carried out. The range from 1·2° K to 20° K was covered, and particular attention was paid to the region around 6° K.

2.2. *Experimental*

The mercury was contained in an open glass vessel constructed to fit the calorimeter. Although this vessel could hold about 1·5 moles of mercury, only about 0·6 moles were used since it was already known that the heat capacity of mercury at low temperatures is many times that of other metals. The method of measurement was exactly that given in the first part of this paper.

The mercury was supplied by Johnson, Matthey and Co. and described as ' triple distilled ' and at least 99·999% pure. The heat capacity of the glass vessel was measured in a separate experiment.

2.3. *Results*

Pickard and Simon's values are about 4% lower than the present figures down to 12° K, but below this temperature the curves cross. The agreement with Busey and Giauque's work is good around 20° K but their lowest figures (at 15° K) fall about 2% below ours. From 10° to 14° the agreement with Simon's values is excellent.

The slight hump observed by Pickard and Simon at 6° K was not found, but the shape of the present specific heat curve shown in fig. 5 is still very different from that of most metals. The θ–T curve demonstrates this feature even more clearly. The measured points are given in the graph, and smoothed values in table 2.

Table 2. Mercury

T	C_p	θ	T	C_p	θ
1·2	0·00282	68·5	8·0	0·837	64·0
1·5	0·00612	65·0	10·0	1·125	70·0
2·0	0·0230	55·0	12·0	1·40	76·5
3·0	0·100	50·5	14·0	1·70	81·0
4·0	0·200	52·5	16·0	1·98	85·0
5·0	0·360	53·0	18·0	2·26	89·0
6·0	0·520	57·0	20·2	2·52	92·0

C_p is in cals mol^{-1} deg^{-1}

The entropy at 20° K is found to be 1·840 e.u. compared with the value given by Busey and Giaque of 1·856 e.u., suggesting that their standard entropy of 18·19 e.u. should be reduced by about 0·02 e.u.

Below 4·15° K, the observed specific heat is that of the superconducting state, usually denoted by C_s. To obtain the lattice specific heat, C_s

Fig. 5

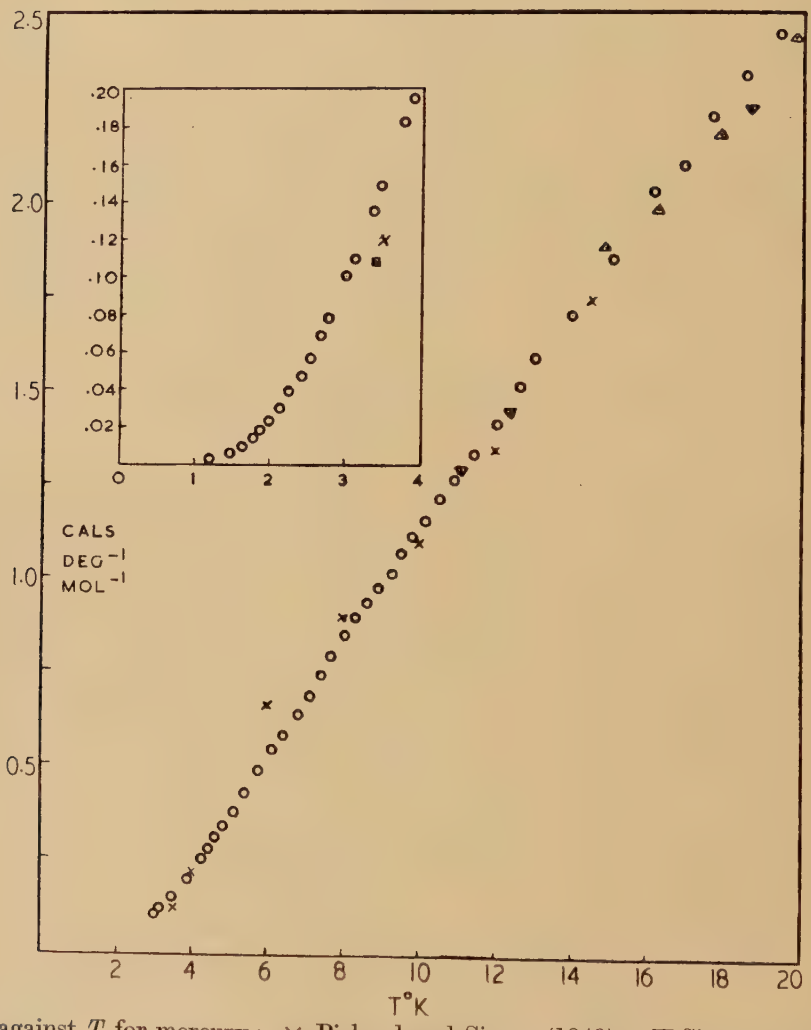

C_p against T for mercury ; × Pickard and Simon (1948) ; ▽ Simon (1955) ; △ Busey and Giaque (1953) ; ⊡ Kamerlingh Onnes and Holst (1914).

must be corrected to C_n, the specific heat in the normal phase and C_n must then be further corrected for the electronic contribution before the true lattice term is found. In principle, C_s–C_n may be found calorimetrically, but in the case of mercury it is only about 1% of the total

specific heat at the transition temperature. The correction is, moreover, a function of temperature so that it is clear that calorimetry is a very inconvenient method for its determination. Fortunately, both C_s–C_n and the electronic contribution are available from magnetic threshold field data. Daunt and Mendelssohn (1937) and Misener (1940) have made magnetic measurements on mercury in the superconducting state and the more recent data of Misener have been used in this paper.

It may be shown quite generally that the value of γ, the temperature coefficient of the electronic specific heat is given by $(\partial \Delta C/\partial T)_{T=0}$, where ΔC is C_s–C_n, provided that C_s contains no term linear in temperature. An analysis of the present data revealed no linear term and the use of Misener's figure of $4{\cdot}5\times10^{-4}$ cal mol^{-1} deg^{-2} for γ is therefore justified. A full discussion of this and related topics is given by Shoenberg (1953).

Below 5° K the specific heat of pyrex glass was found to be represented by

$$C=7{\cdot}5\times10^{-7}T^3 \text{ cals g}^{-1}\text{ deg}^{-1}$$

The smoothed specific heat values up to 20° K are given in table 3.

Table 3. Pyrex Glass

T	$C\times10^4$	T	$C\times10^4$
2	0·060	10	10·0
3	0·20	12	17·7
4	0·48	14	27·1
5	0·93	16	38·6
6	1·80	18	51·4
8	5·0	20	65·5

C in cals gm^{-1} deg^{-1}

2.4. *Discussion*

Like its behaviour for other highly anisotropic lattices, the Debye θ for mercury shows strong variations with temperature. As can be seen in fig. 6, the value of θ falls steadily from 92° at 20° K to a minimum of 50° at 3° K. Below this temperature θ rises again and continues to do so down to the lowest point measured. It is clear that measurements below 1° K are required in order to obtain the electronic specific heat by the usual analyis of the data.

Busey and Giaugue's data have been used to find the Debye θ values above 20° which are shown in fig. 6. Since no value of the compressibility of solid mercury appears in the literature, recourse was made to the approximate relation $C_p-C_v=0{\cdot}0214C_p^2T/T_s$ where T_s is the melting point of the metal, to determine C_v. Even allowing for the empirical

nature of the relation, it is clear that the Debye θ rises markedly with temperature over a wide range. If, for instance the correction were doubled, the θ at 50° K would only be raised from 114° to 119°, whilst if it were not made at all, the θ would fall to 109°.

Gruneisen and Hoyer (1935) have used elastic constants measured at 80° K to calculate the Debye θ. Their value is 68°, which will refer to the θ value in the genuine T^3 region if it is assumed that the elastic constants do not change appreciably between 80° and 0° K.

Fig. 6

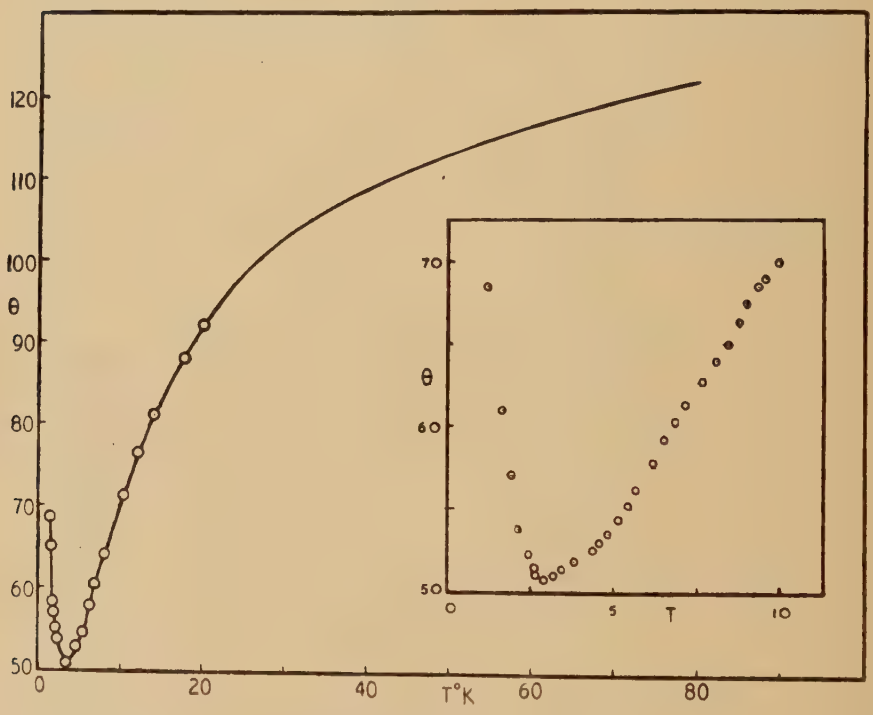

The Debye θ for mercury.

Since this true T^3 region has not been reached in this work, no value for θ (0° K) can be predicted from the θ-T curve. The trend of the curve suggests, however, that the calculated value cannot be in violent disagreement with the calorimetric figure.

Acknowledgments

We should like to express our gratitude to Sir Francis Simon for the great interest he has taken in this work, and to Messrs. Johnson, Matthey for their helpful co-operation in preparing the samples.

References

Blackman, M., 1935, *Proc. Roy. Soc.* A, **149,** 117.

Born, M., and von Karman, 1912, *Z. Phys.*, **13,** 297.

Busey, R. H., and Giauque, W. F., 1953, *J. Amer. Chem. Soc.*, **75,** 806.

Clusius, K., and Harteck, P., 1928, *Z. Phys. Chem.*, **134,** 243.

Craig, R. S., Krier, C. A., Coffer, L. W., Bates, E. A., and Wallace, W. E., 1954, *J. Amer. Chem. Soc.*, **76,** 238.

Daunt, J. G., and Mendelssohn, K., 1937, *Proc. Roy. Soc.* A, **160,** 127.

Daunt, J. G., and Silvidi, A. A., 1950, *Phys. Rev.*, **77,** 125.

Fowler, R. M., and Guggenheim, E. A., 1939, *Statistical Thermodynamics* (Cambridge : University Press), p. 149.

Gruneisen, E., and Hoyer, H., 1935, *Ann. Phys., Lpz.*, **22,** 663.

Hill, R. W., 1953, *J. Sci. Instrum.*, **30,** 331.

Hill, R. W., and Smith, P. L., 1953, *Phil. Mag.*, **44,** 636.

Honnefelder, K., 1933, *Z. Phys. Chem.*, B, **21,** 53.

Hopf, L., and Lechner, G., 1914, *Verh. d. Phys. Ges.*, **16,** 643.

Mott, N. F., and Jones, H., 1936, *The Theory of the Properties of Metals and Alloys* (Oxford : University Press).

Onnes, H. K., and Holst, G., 1914, *Leid. Comm.*, 142 c.

Parkinson, D. H., Simon, F. E., and Spedding, F. H., 1951, *Proc. Roy. Soc.* A, **207,** 137.

Pickard, G. L., and Simon, F. E., 1948, *Proc. Phys. Soc.*, **61,** 1.

Samoilov, B. N., 1952, *Dokl. Akad. Nauk.*, SSSR, **86,** No. 2, 281.

Shoenberg, D., 1952, *Superconductivity* (Cambridge : University Press).

Simon, F. E., 1923, *Z. Phys. Chem.*, **107,** 279 ; 1922, *Ann. Phys., Lpz.*, **68,** 261.

Simon, F. E., and Lange, F., 1928, *Z. Phys. Chem.*, **134,** 374.

Smith, P. L., 1955, *Phil. Mag.*, **46,** 744.

LXXXVIII. *The Stress to Move a Free Dislocation in Alpha Iron*

By J. Heslop † and N. J. Petch

Metallurgy Laboratory, University of Leeds ‡

[Received February 8, 1956]

Abstract

It is shown that the portion of this stress due to interaction with random C and N atoms is temperature-independent. At low temperatures, another, very temperature-dependent portion is dominant, and this is interpreted as evidence of a sizeable Peierls–Nabarro force in α-iron.

§ 1. Introduction

The stress required to move a free dislocation in α-iron during the early stages of deformation has already been studied at room temperature (Cracknell and Petch 1955). This stress is obtained as σ_0 in the relationship

$$\sigma_{\text{l.y.p.}}=\sigma_0+kl^{-1/2}, \quad . \quad . \quad . \quad . \quad . \quad . \quad . \quad . \quad (1)$$

which connects the lower yield point $\sigma_{\text{l.y.p.}}$ of polycrystalline α-iron with the grain diameter l. Here k is a constant.

The form of this relationship is consistent with the propagation of a Lüders band from grain to grain by the stress concentration ahead of an array (piled-up group) of blocked dislocations that is proportional in length to the grain diameter. The constant k is a measure of the stress required ahead of the array to operate dislocation sources, and σ_0 appears as a stress opposing the motion of the dislocations in the array, so that $(\sigma_{\text{l.y.p.}}-\sigma_0)$ is the resultant stress acting on the array.

Equation (1) is particularly useful in the study of α-iron, since it separates the effects on the lower yield point of grain size, of the resistance to the motion of a free dislocation and of impurity locking of the dislocation sources.

The room-temperature measurements have shown that the principal contribution to σ_0 at that temperature arises from interaction between the dislocations and random C and N atoms (Cracknell and Petch 1955). Theoretically and experimentally, this gives a linear relationship between σ_0 and the concentration of C+N in solution. In addition, there is another contribution of about 2 tons/in.^{2} that is independent of the presence of C or N (fig. 1).

The present paper deals with measurements at lower temperatures.

† Now at the Naval Construction Research Establishment, Dunfermline.
‡ Communicated by the Authors.

§ 2. Experimental Measurements of σ.

These followed the procedure already described for the room temperature work (Cracknell and Petch 1955). To obtain σ_0 for any particular

Fig. 1

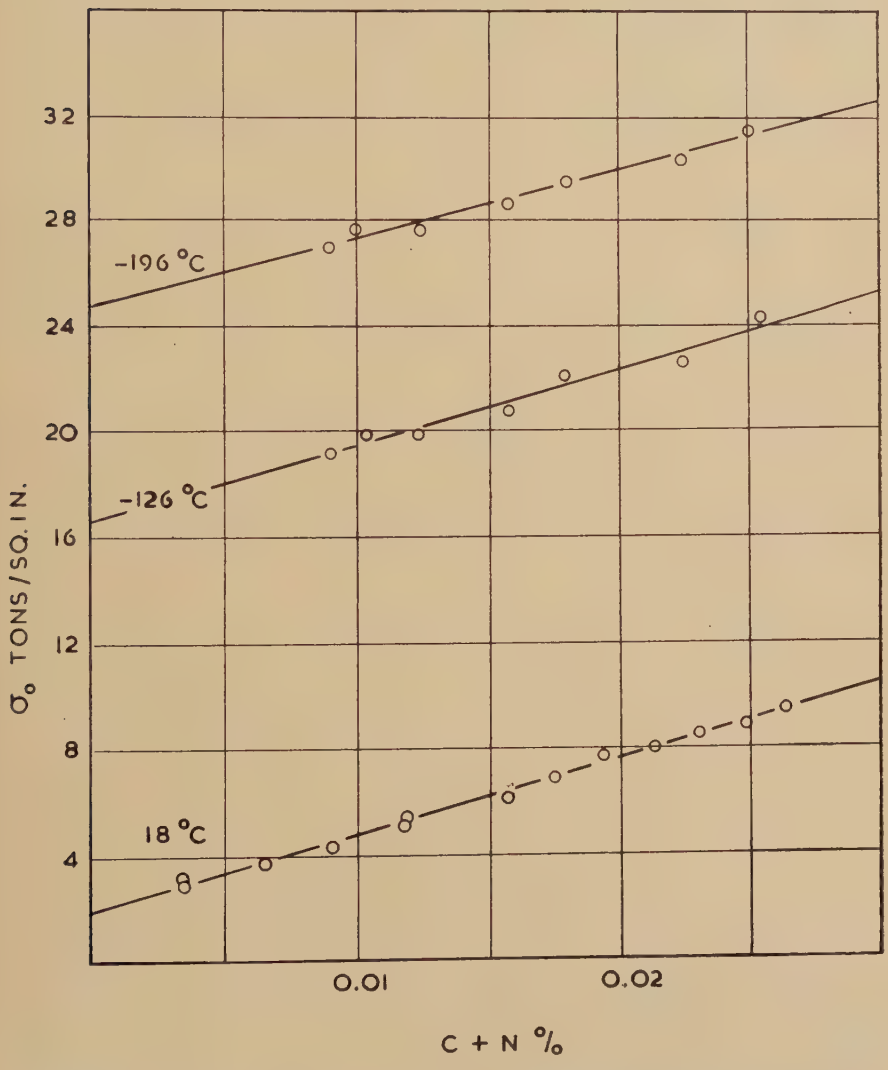

Effect of the concentration of C+N in solution on σ_0 for a mild steel.

condition, measurements of the lower yield point were made over a wide range of grain size, so that (1) could be plotted. The same mild steel was used as before and it gave clear upper and lower yield points down to

the lowest temperature used (−196°C). The composition (weight %) was

C	Si	S	P	Mn	Ni	Cr	N
0·15	0·02	0·05	0·03	0·51	0·08	0·05	0·008

Figure 1 shows the dependence of σ_0 at 18, −126 and −196°C on the concentration of C+N in solution. This concentration was varied by nitriding and by sub-critical quenching as in the previous work.

It is apparent that the portion of σ_0 due to interaction with these solute atoms is temperature-independent. But the other portion of σ_0, not

Fig. 2

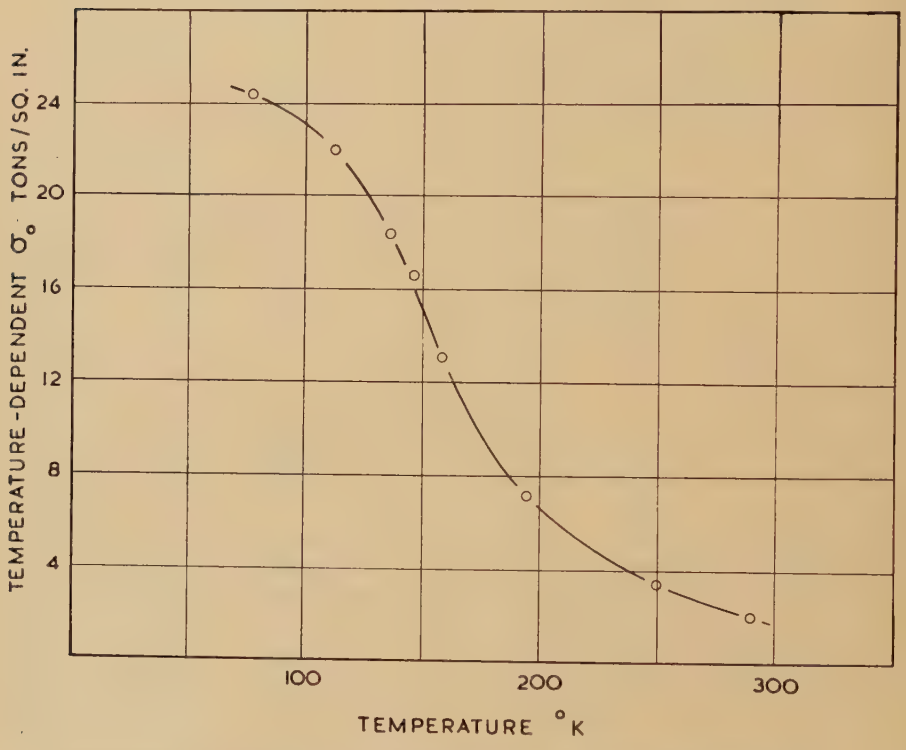

Temperature variation of the temperature-dependent portion of σ_0.

associated with the C+N, is very temperature-dependent and becomes dominant at the lower temperatures.

Figure 2 gives further detail of the temperature variation of the temperature-dependent portion of σ_0.

Figure 3 shows the relationship between $\sigma_{l.y.p.}$ and $l^{-1/2}$ at 18 and −196°C for this steel in the annealed condition and after quenching from 680°C, followed by ageing at 150°C. It is apparent that the resistance to dislocation motion due to the stresses around the fine precipitates produced during ageing is also temperature independent.

§ 3. The Temperature-Independent Part of σ_0

The temperature-independence of the C+N resistance was rather unexpected, so the theoretical dependence has been examined.

A calculation of σ_0 due to interaction with random C and N atoms in solution has already been given using Mott's (1952) modification of the Mott and Nabarro (1948) treatment for the motion of a dislocation against the opposition of very finely dispersed centres of internal stress (Cracknell and Petch 1955). The temperature-dependence in this calculation is readily obtained.

If Λ is the mean separation of the solute atoms, the dislocation is bent by interaction with the nearest-neighbour solute atoms into loops of

Fig. 3

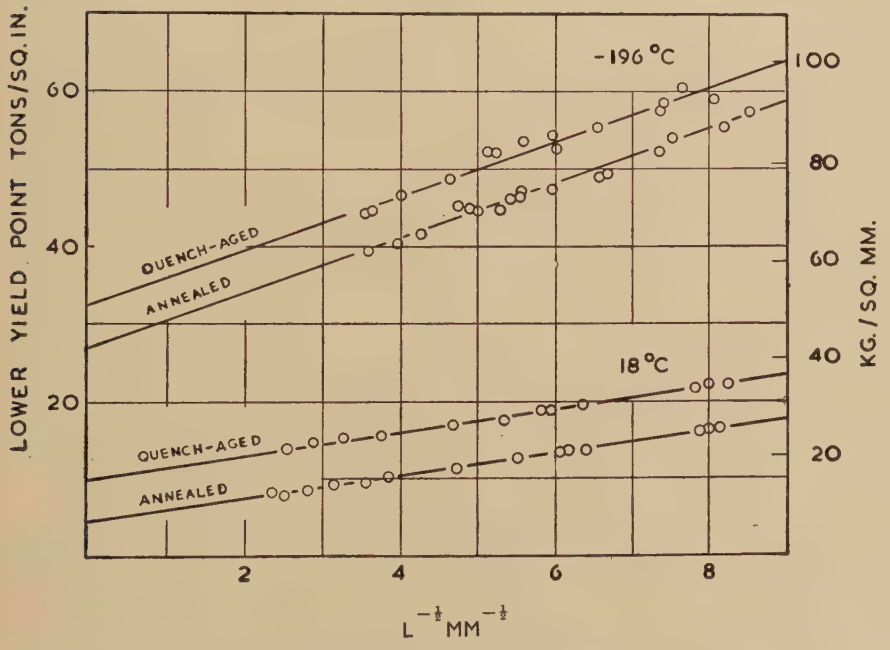

Influence of quench-ageing on σ_0.

average length $\sim\Lambda$. The elementary step in the motion of the dislocation is performed by a compound loop containing n^2 single loops that is able to move from one equilibrium position to the next (fig. 4). This requires that the centre of the compound loop should be able to move through a distance of $\sim 2\Lambda$.

If the force exerted on the dislocation in the glide direction by each nearest-neighbour solute atom is, on average, $\pm F$, the force due to these atoms on the compound loop as it moves is most simply taken as uniformly $\pm nF$. Thus, the work done against this force in an activated jump forward as in fig. 4 is $nF\,\frac{2}{3}\Lambda$.

In moving to the mid-position, the loop shortens, so some energy is recovered.

Thus, the activation energy for a jump is

$$U=\frac{2nF\Lambda}{3}-2\gamma r(\theta-\sin\theta),$$

where γ is the line tension of the dislocation, $r=n^4\Lambda/8$ is the mean radius of curvature of the compound loop and θ is half the mean angle turned along its length. Here $\gamma=\alpha\mu\mathbf{b}^2$, where $\alpha\sim0{\cdot}5$, μ is the rigidity modulus and **b** is the Burgers vector.

Taking the constant in the Cottrell interaction as $1{\cdot}5$–$3{\cdot}0\times10^{-20}$ dyne cm^2 and using the expressions in Cracknell and Petch (1955), $\Lambda=2\times10^{-7}$ cm, $n=9{\cdot}5$–$7{\cdot}5$ and $F=3$–6×10^{-6} dynes for 0·025 weight % C+N in solution. These figures give $U=1{\cdot}5$–$2{\cdot}2$ ev. Practically the same value is obtained throughout the composition range used in the experimental measurements (0·005–0·025% C+N). Thus, the process is on the border line for any appreciable help from thermal activation.

We now estimate the actual effect of temperature. Let τ_i be the shear stress necessary for dislocation movement in the absence of any thermal help. Under an applied stress τ, the compound loop is displaced to the

Fig. 4

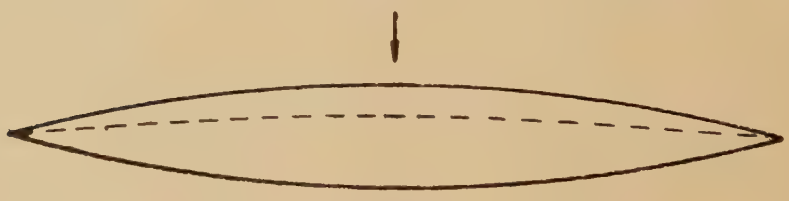

The motion of the compound loop.

dotted position in fig. 4. The amplitude of the loop is then $(\tau_i-\tau)n^4\Lambda^2/8\alpha\mu\mathbf{b}$, the radius of curvature becomes r^1 and the semi-angle turned θ^1.

The activation energy $U(\tau)$ for a jump forward is then

$$U(\tau)=\frac{(\tau_i-\tau)^2n^6\Lambda^3}{12\alpha\mu}-2\gamma r^1(\theta^1-\sin\theta^1).$$

$$\text{With } (\theta^1-\sin\theta^1)\sim\frac{\sin^3\theta^1}{6} \text{ for small } \theta^1,$$

$$U(\tau)=\frac{(\tau_i-\tau)^2n^6\Lambda^3}{24\alpha\mu}.$$

If a is the cross sectional area of the specimen and d is its length, one activated jump will produce an increment of shear strain given by

$$\delta s = \frac{4n^2\Lambda^2\mathbf{b}}{3da}.$$

If L is the total length of the active dislocations, the number of loops available for jumps is $\sim L/n^2\Lambda$.

Thus, at temperature T,

$$\frac{ds}{dt} = \frac{4\Lambda\mathbf{b}L\nu\exp[-U(\tau)/kT]}{3da}$$

where ν is the frequency of vibration of the loops.

Substituting for $U(\tau)$, rearranging and using $\tau_i = F/n\Lambda\mathbf{b}$,

$$\left(1-\frac{\tau}{\tau_i}\right) = \frac{\mathbf{b}}{Fn^2\Lambda^{\frac{1}{2}}}\left(24\alpha\mu kT\ln\frac{4\Lambda\mathbf{b}L\nu}{3da\dot{s}}\right)^{1/2}.$$

At the lower yield point, the deformation is confined to the grains at the edge of an advancing Lüders band. Assuming that only a few Frank–Read sources, producing $\sim 10^3$ dislocations, operate per grain, $L = 10^3 a/l$, where l is the grain diameter.

At room temperature, with $\dot{s} \sim 10^{-3}$ sec^{-1}, $l \sim 10^{-2}$ cm, $d \sim 1$ cm, $\nu \sim 10^9$ sec^{-1}, $F = 6\times 10^{-6}$ dynes and other values appropriate for 0·025% C+N

$$\tau = 0{\cdot}75\,\tau_i.$$

The activation energy is possibly somewhat underestimated in this calculation, but it appears that the stress required to move a dislocation against the interaction with random C and N atoms must be only just temperature-independent.

§ 4. The Temperature-Dependent Part of σ_0

The other impurity atoms in the mild steel cannot explain the temperature-dependent σ_0, since their interaction with dislocations is minor compared to that of C and N.

With the steel in the condition used in the present measurements, the main part of the carbon content is out of solution as pearlite, but this does not explain the temperature-dependent σ_0, since pearlite makes little contribution to σ_0 (Petch 1953).

There may be some dispersion hardening due to fine distributed precipitates, but dispersion hardening only contributes a few tons/in.^{2} to σ_0 even when the conditions are made favourable by quench-ageing, and this contribution is temperature-independent.

The resistance to dislocation motion due to intersecting dislocations and to elastic interaction between dislocations has recently been very fully discussed for the face-centred cubic metals (Adams and Cottrell 1955, Seeger 1955). But, in spite of the dissociation of the dislocations in these metals, the observed, low temperature magnitude of this resistance

(<1 ton/in.^{2}) at the beginning of deformation is very much smaller than the value of σ_0 in α-iron at $-196°$C.

Since these other possibilities do not supply an explanation, and since the high resistance to dislocation motion at low temperatures appears to distinguish α-iron from the close-packed metals, it is now suggested that the temperature-dependent portion of σ_0 may be evidence of a sizeable Peierls–Nabarro force in α–iron.

It is generally recognized that departure from close-packing will favour a narrowing of the dislocations and a considerable increase in the stress required for dislocation motion may then result, since this stress depends exponentially on the width. A proper quantitative treatment still seems far from achievement, so experimental evidence is of particular interest.

The temperature-dependence of the Peierls–Nabarro force will arise from thermal broadening of the dislocation and from the thermally activated jump of sections of the dislocation from one energy minimum to the next.

If there is indeed a sizeable Peierls–Nabarro force in α–iron, it means that throughout consideration of the mechanical properties of non-close packed metals greater attention must be given to this force than is currently the case.

Note added 23rd February, 1956.

Concurrently with the submission of this paper, measurements on iron single crystals appeared (Allen *et al.* 1956). At $-253°$C, these crystals cleave without detectable slip and the shear stress on the glide planes is then considerably higher than in slip at $-196°$C. This is interpreted as an indication of a sharp rise in the stress for the movement of a free dislocation. The present authors feel that a more probable interpretation is a sharp rise in the stress required for the initial unlocking of a dislocation. Consistent with this, it was observed in the present measurements that the slope k, which depends on the dislocation locking, increases rapidly below about $-160°$C.

The single crystal measurements also show that at $-196°$C crystals particularly favourably oriented for conjugate slip cleave without detectable plastic deformation, and the shear stress on the glide planes is then appreciably higher than in slip at other orientations. Obstruction by the formation of some sessile dislocations is the suggested explanation. Such obstruction is probably of importance in the initial stages of the formation of an array (Friedel 1955) rather than in the stage where the array has broken out across the crystal, which is the one of interest in the present measurements on the yield propagation.

Acknowledgment

The authors wish to thank Mr. A. Fillingham for his assistance with the experimental work.

References

Adams, M. A., and Cottrell, A. H., 1955, *Phil. Mag.*, **46**, 1187.
Allen, N. P., Hopkins, B. E., and McLennan, J. E., 1956, *Proc. Roy. Soc.* A, **234**, 221.
Cracknell, A., and Petch, N. J., 1955, *Acta Met.*, **3**, 186.
Friedel, J., 1955, *Phil. Mag.*, **46**, 1169.
Mott, N. F., 1952, *Imperfections in Nearly Perfect Crystals*, ed. W. Shockley (New York : J. Wiley), p. 173.
Mott, N. F., and Nabarro, F. R. N., 1948, *Bristol Conference on the Strength of Solids* (London : Physical Society), p. 1.
Petch, N. J., 1953, *J. Iron Steel Inst.*, **173**, 25.
Seeger, A., 1955, *Phil. Mag.*, **46**, 1194.

LXXXIX. *A Solution of the Diffusion Equation for Isotopic Exchange between a Semi-Infinite Solid and a Well Stirred Solution*

By I. R. Beattie
Department of Chemistry, King's College, London

and

D. R. Davies
Department of Mathematics, The University, Sheffield†

[Received February 24, 1956]

Summary

A theoretical solution of the problem of diffusion of material from a semi-infinite solid of known surface area into a given volume of a well-stirred liquid is derived. The equations developed are based on the assumption that Fick's Law may be applied to the system under consideration.

This paper describes the derivation of an equation enabling the calculation of diffusion coefficients in a solid, from measurements of changes in concentration of a well-stirred finite body of fluid in contact with the solid. The classical solutions of the heat flow equations in many instances may be directly applied to problems involving diffusion in solids (see, for example, Barrer 1941). Self diffusion coefficients in resins have been calculated by Boyd and Soldano (1953), using the equation for the cooling of a sphere in a well-stirred liquid (see for example Carslaw and Jaeger 1947a), together with the approximation suggested by Paterson (1947). However, it must be noted that in general these solutions apply to geometrically exact surfaces or volumes. In practice one is frequently faced with an exchange involving a powder which has been obtained by crushing and sieving the original material. This is particularly the case where diffusion coefficients are low, and hence for exchange to occur in a finite time individual particles must be of a small size.

The geometrical surface of a powder may be relatively accurately measured, using for example a permeability method such as that developed by Carman (1937). The absolute meaning of the measured area may be questioned, since it is well known that gas adsorption measurements and permeability techniques yield widely differing results for the same material. However, it does appear that similar materials may be compared by this means and, further, it is usually possible to carry out a

---

† Communicated by the Authors.

number of exchanges on the same sample in order to evaluate D_0 and E in the equation

$$D=D_0 \exp(-E/RT).$$

A factor of 2 is of little importance in the determination of a diffusion coefficient.

When ion-exchange is being studied, it is possible to maintain the concentration at the liquid–solid interface constant by the use of saturated solutions of two salts containing one of the exchanging ions, in contact with an excess of the solid salts. Clearly this is not possible for isotopic exchange. Therefore the classical equations for the semi-infinite solid cannot be applied. Essentially one is interested in the solution of the Fick's Law equation for the semi-infinite solid in contact with a well-stirred liquid. The result of the calculation can be applied to the case of random particles of known surface area if the diffusion coefficient is low enough, or the time short enough, for the measured surface area to be a reasonably accurate representation of the cross sectional area of the volume into which diffusion has occurred. Unfortunately, the solution of the diffusion problem for a solid in contact with a well-stirred liquid, as given by March and Weaver (1928), is of no value in this instance.

Assuming that normal Fickian diffusion is occurring in the system to be studied, the equation to be solved is given by :

$$\frac{\partial C}{\partial t}=\frac{D\partial^2 C}{\partial x^2} \text{ for } x>0,\ t>0. \quad . \ . \ . \ . \ . \ . \ . \quad (1)$$

The appropriate boundary conditions are :

$$C=C_0,\ t=0,\ x>0, \quad . \ . \ . \ . \ . \ . \ . \ . \ . \quad (2)$$

$$C=0,\ t=0,\ x=0. \quad . \ . \ . \ . \ . \ . \ . \ . \ . \quad (3)$$

Fick's first law (or conservation) also requires that

$$\frac{\partial C}{\partial x}=\frac{V}{DA}\frac{\partial C}{\partial t} \text{ at } x=0, \text{ for all } t. \quad . \ . \ . \ . \ . \quad (4)$$

The symbols used have the following significance: D, Diffusion coefficient in the solid; V, volume of the solution; A, surface area of the solid at the interface; C, concentration (with appropriate suffix); and t, duration of contact between solid and solution.

As these equations are written, it is assumed that the concentration at the surface ($x=0$) is the same in the solution as it is in the solid. It may further be noted that since the solid is infinite while the solution is finite, $C_{(x,t)} \to C_0$ as $t \to \infty$.

Using the method of the Laplace transform (see for example Carslaw and Jaeger 1941) the subsidiary equation is :

$$\frac{D d^2\bar{C}}{dx^2}-p\bar{C}=-C_0,\ x>0, \quad . \ . \ . \ . \ . \ . \ . \ . \quad (5)$$

where $\bar{C}=\int_0^\infty \exp(-pt)C \ . \ dt.$

Also,

$$\frac{d\bar{C}}{dx} = \frac{V}{DA} p\bar{C}, \quad \ldots\ldots\ldots \quad (6)$$

when $x=0$, for all values of t. Solving (5) and (6),

$$\bar{C} = \frac{C_0}{p}\left[1 - \frac{(V/DA)p \exp\left[(-x\sqrt{(p/D)}\right]}{[\sqrt{(p/D)}+(V/DA)p]}\right] \quad \ldots\ldots \quad (7)$$

Equation (7) may be written in the form :

$$\frac{\bar{C}}{C_0} = \frac{1}{p} - \frac{\exp(-qx)}{p} + \frac{h \exp(-qx)}{p(q+h)}. \quad \ldots\ldots \quad (8)$$

where $h=A/V$ and $q=\sqrt{(p/D)}$. Using the table of Laplace Transforms given by Carslaw and Jaeger (1947 b) to solve eqn. (8), the result requires that

$$\frac{C}{C_0} = 1 - \exp(DtA^2/V^2 + Ax/V)\left[1 - \operatorname{erf}\frac{1}{2\sqrt{(DT)}}\left(x + 2Dt \cdot \frac{A}{V}\right)\right] \quad (9)$$

(This equation has also been obtained by using the Calculus of Residues plus the Inversion Theorem). Equation (9) reduces to the expression :

$$C/C_0 = 1 - \exp(DtA^2/V^2)[1 - \operatorname{erf}(A/V)\sqrt{(Dt)}], \text{ at } x=0. \quad . \quad (10)$$

Figure 1 shows the graph obtained when C/C_0 is plotted against β, where

Fig. 1

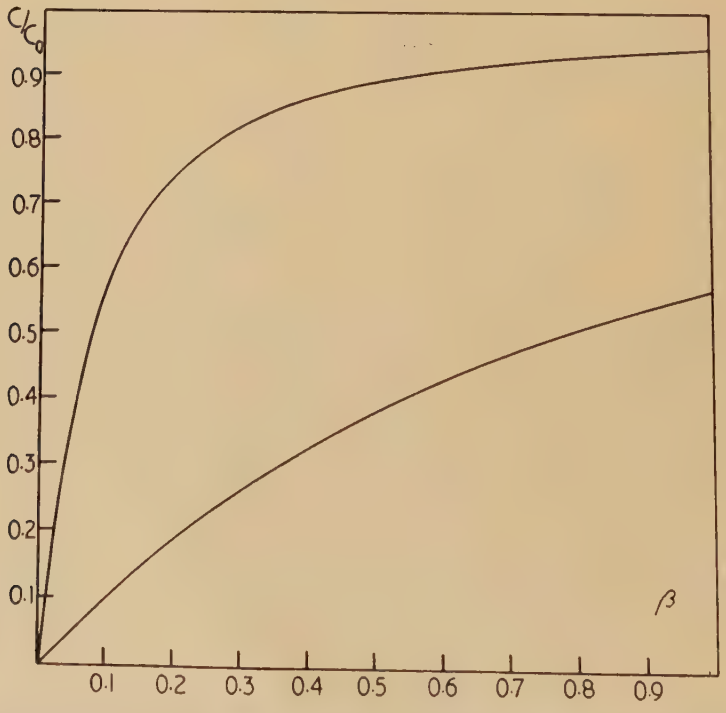

Variation of the ratio C/C_0 with β, where $\beta=(A/V)\sqrt{(Dt)}$. For the upper curve values of β, as given on the abscissa, must be multiplied by ten.

$\beta=(A/V)\sqrt{(Dt)}$. Clearly, for small value of β the approximation $\exp(\beta^2)=1$ and $\operatorname{erf}\beta=2\beta/\sqrt{\pi}$ may be used, giving the equation

$$\frac{C}{C_0}=2\frac{A}{V}\frac{\sqrt{(Dt)}}{\sqrt{\pi}}. \quad . \quad . \quad . \quad . \quad . \quad . \quad . \quad . \quad . \quad (11)$$

Fig. 2

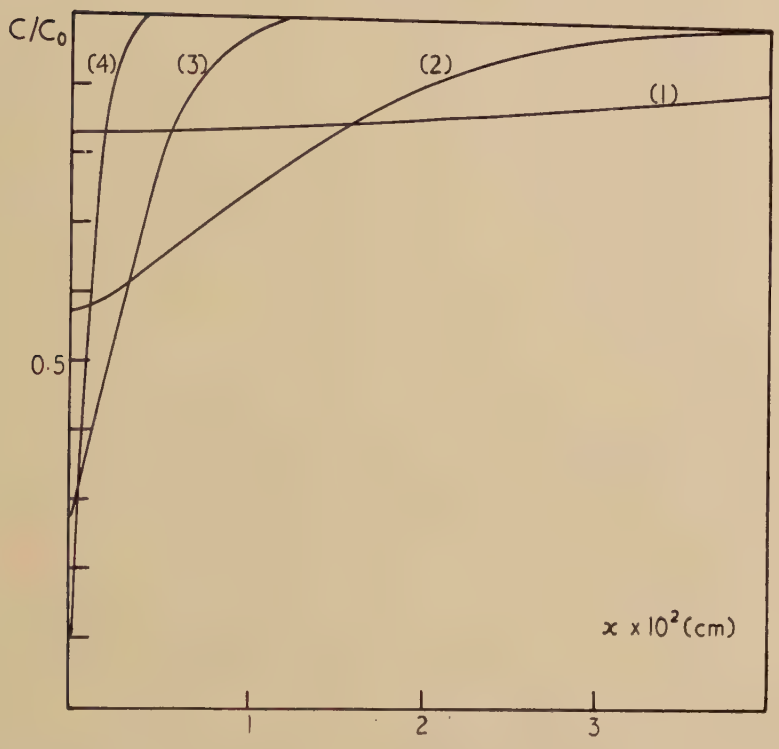

Variation of the ratio C/C_0 with x (in cm) for various values of Dt, at constant A/V equal to 10^2 cm^{-1}.

(1) $Dt=10^{-3}$; (2) $Dt=10^{-4}$; (3) $Dt=10^{-5}$; (4) $Dt=10^{-6}$ cm^2.

This is analogous to the solution for the semi-infinite solid with concentration at the interface constant.

Equation (9) is not likely to be generally necessary to ascertain values of the diffusion coefficient, but it is of considerable importance in assessing to what extent eqn. (10) may be applied to the experimental results. When the depth to which diffusion has occurred is no longer small, eqn. (10) may no longer be used. Figures 2, 3 and 4 indicate the variation of the ratio C/C_0 with x for several values of the surface area to volume ratio, or the product of the diffusion coefficient and the duration of the experiment.

Fig. 3

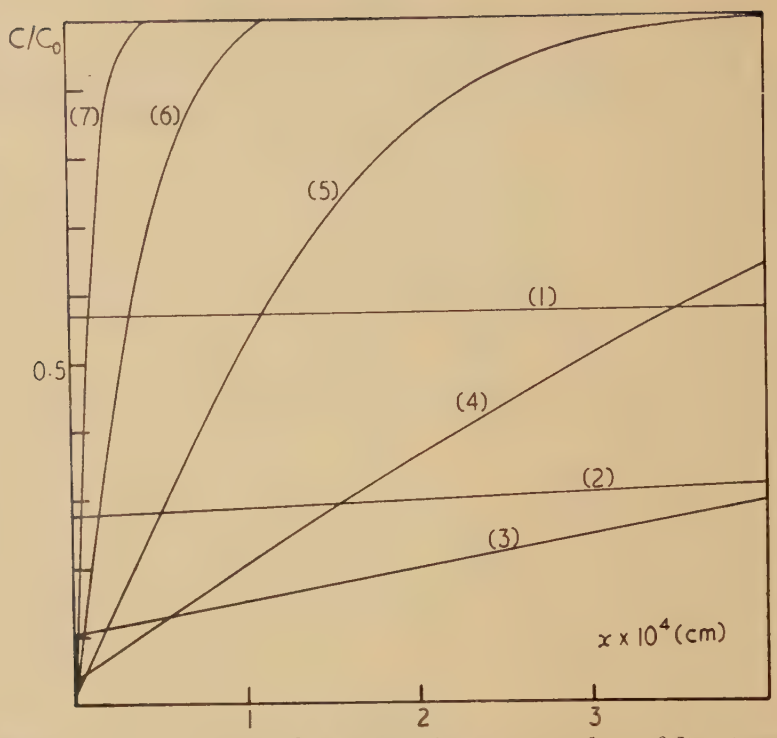

Variation of the ratio C/C_0 with x (in cm) for various values of Dt, at constant A/V equal to 10^2 cm^{-1}.
(1) $Dt=10^{-4}$; (2) $Dt=10^{-5}$; (3) $Dt=10^{-6}$; (4) $Dt=10^{-7}$; (5) $Dt=10^{-8}$; (6) $Dt=10^{-9}$; (7) $Dt=10^{-10}$ cm^2.

Fig. 4

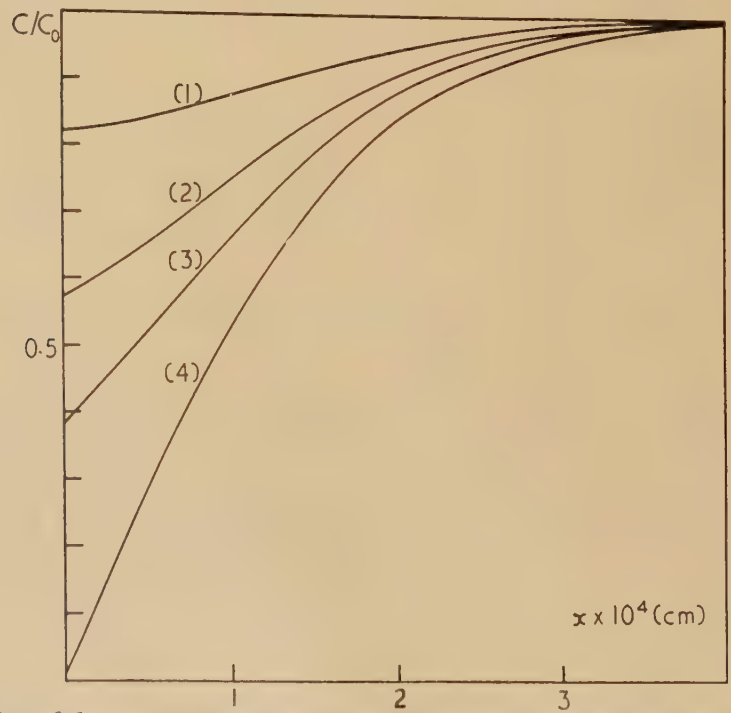

Variation of the ratio C/C_0 with x (in cm) for various values of A/V, at constant Dt equal to 10^{-8} cm^2.
(1) $A/V=3\times10^4$; (2) $A/V=10^4$; (3) $A/V=5\times10^3$; (4) $A/V=10^2$ cm^{-1}.

As a first order approximation one may consider that the equations are applicable providing that the surface area at a distance x inside the solid (where C/C_0 has at no stage during the reaction been less than 0·95) is not less than 95% of the original surface area. For spherical particles this provides that x is less than 0·025 of the radius of the particle.

References

Barrer, R. M., 1941, *Diffusion in and Through Solids* (Cambridge University Press), p. 7.

Boyd, G. E., and Soldano, B. A., 1953, *J. Amer. Chem. Soc.*, **75**, 6092.

Carman, P. C., 1937, *Trans. Inst. Chem. Eng.*, **15**, 50.

Carslaw, H. S., and Jaeger, J. C., 1941, *Operational Methods in Applied Mathematics* (Oxford); 1947 a, *Conduction of Heat in Solids* (Oxford); 1947 b, *Ibid.*, Appendix V, p. 380; formulas 1, 8 and 14.

March, H. W., and Weaver, W., 1928, *Phys. Rev.*, **31**, 1072.

Paterson, S., 1947, *Proc. Phys. Soc.*, **59**, 50.

XC. CORRESPONDENCE

The Effect of Prior Extension on the Annealing Rate of Lattice Vacancies in Platinum

By S. Pearson and F. J. Bradshaw

Royal Aircraft Establishment, Farnborough

[Received May 10, 1956]

Recent experiments have been reported (Kauffman and Koehler 1952, 1955, Lazarev and Ovcharenko 1955, Bradshaw and Pearson 1956) in which an annealable excess resistance introduced in gold and platinum wires by quenching them from high temperatures is interpreted in terms of lattice vacancies. In the paper by the present authors the decay of quenched-in resistance (ΔR) at a given temperature was interpreted in terms of the relation

$$-(1/v)\,dv/dt = n\nu_D B \exp(-\Delta H_2/RT)$$

where v is the concentration of vacancies, n is the probability per jump that a vacancy is lost, ν_D is the Debye frequency, B is the entropy factor for movement (probably in the region 1 to 10) and ΔH_2 is the heat of activation for vacancy movement.

By annealing wires at different temperatures in the region of 400°c it was estimated that for platinum ΔH_2 was 1·1 ev and for thoroughly annealed material a vacancy makes on average 10^9 jumps before it disappears at an internal sink. On the assumption that dislocation lines are providing the sinks for the vacancies it would be expected that the effect of increasing the dislocation density by stretching the quenched wire would be to increase the rate at which the vacancies anneal out. The experiments reported here support this view.

'Thermopure' platinum wires of 0·2 mm diameter were used and the electrical resistance measurements were made with the wires immersed in liquid nitrogen. In order to bring the wires to a standard state they were conditioned by holding them at a temperature of about 1700°c for ten minutes before quenching. After this treatment they consisted mainly of grains which were the full diameter of the wire and from one to three diameters long. All quenching was from a temperature of about 1600°c which gave a resistivity increase due to vacancies of about 0·1 microhm-cm (about 5% of the resistance in liquid nitrogen). A single specimen was used for more than one experiment, the wire being conditioned before subsequent quenching and extension.

It was found in preliminary experiments that most conditioned and quenched wires could be extended by about 10% at room temperature without breaking. Accordingly the extensions were limited to this amount and it was first necessary to check that such an extension did not (*a*) introduce a ΔR of the same order as that introduced by quenching, (*b*) seriously reduce the ΔR quenched in. It was found that for conditioned wires extended by about 10% at room temperature (but not quenched) a ΔR could be annealed out, in the same temperature range as the ΔR introduced by quenching, but that the resistivity decrease was only about 0·006 microhm-cm. It was also found that when a quenched wire was extended by 9·2% the ΔR quenched in was reduced by about 10%.

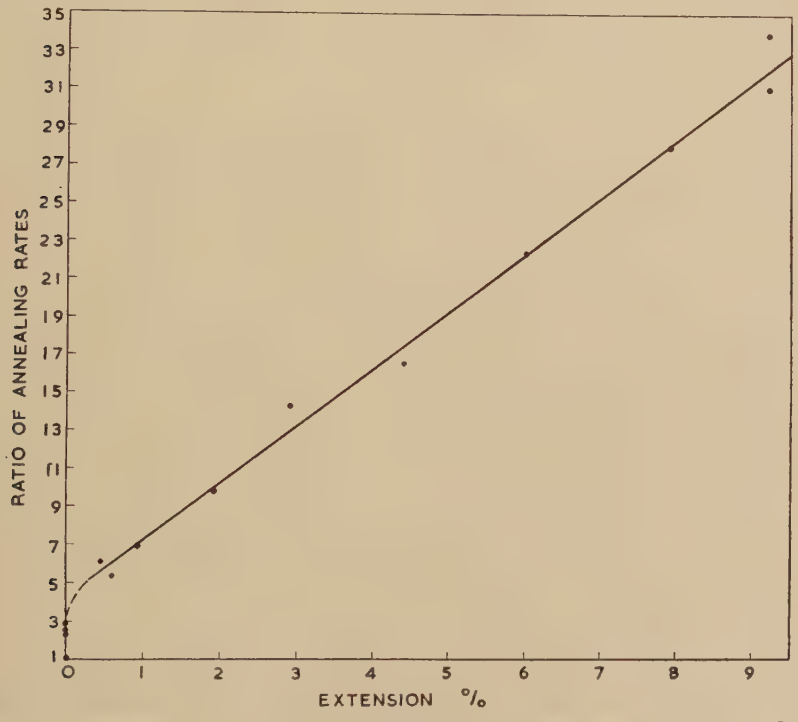

Effect of extension on rate of annealing of excess resistivity quenched in platinum.

The annealing experiments were made on wires which had been conditioned, quenched and stretched by amounts varying from zero to 9·2% and the variation of annealing rate at a standard temperature with extension is shown in the figure. The decay of ΔR with time was not exponential, the initial slope of the logarithmic plot being usually about two to three times that at the end of the anneal. The rates were measured after about 50% of the initial ΔR had annealed out, but as the curves

were all approximately of the same shape, the figure is not significantly altered if the rates are measured for values of ΔR between its initial value and 30% of this. It will be seen that after an initial steep rise the annealing rate increases approximately linearly with extension.

The simplest explanation of the results seems to be that dislocation lines are providing the sinks for the vacancies and that the annealing rate increases because the number of dislocation lines is increased by the deformation. If the relation between annealing rate and number of dislocations is a simple one then it is of interest that the relative increase in annealing rates between 5% and 9% extension is of the same order as the increase in dislocation density obtained by Harper (1951) from measurements of strain ageing of alpha iron stretched by these amounts. His mean dislocation density was about 10^{11} lines cm^2 whereas from recent x-ray measurements (Gay *et al.* 1953, Noggle and Koehler 1955) it seems that the dislocation density for fully annealed platinum would be in the range 10^6–10^8 lines/cm^2.

Acknowledgments

We are grateful to Dr. N. J. Wadsworth for valuable discussions and to Mr. L. G. Carpenter for advice and encouragement.

References

Bradshaw, F. J., and Pearson, S. (in this issue).
Gay, P., Hirsch, P. B., and Kelly, A., 1953, *Acta. Met.*, **1**, 315.
Harper, S., 1951, *Phys. Rev.*, **83**, 709.
Kauffman, J. W., and Koehler, J. S., 1952, *Phys. Rev.*, **88**, 149; 1955, *Ibid.*, **97**, 555.
Lazarev, B. G., and Ovcharenko, O. N., 1955, *Dokl. Akad. Nauk. S.S.S.R.*, **100**, 875.
Noggle, T. S., and Koehler, J. S., 1955, *Acta. Met.*, **3**, 260.

Luminescence of Decorated Dislocations

By W. Van der Vorst and W. Dekeyser

Lab. voor Kristalkunde der Rijksuniversiteit, Rozier, 6, Gent, Belgium

[Received March 5, 1956]

It is well known that the luminescence of phosphors is markedly affected by deformation. It is therefore logical to expect that some relation must exist between luminescence and dislocations.

In order to have some evidence about this, we used the NaCl-Ag system. Single crystals of rocksalt with silver chloride as an addition were prepared; they presented the much studied emission bands when irradiated with x-rays or ultra-violet light (Debrinski and Hinrichs 1955).

Some samples were deformed and annealed in air for several hours at 700°c and 500°c. Careful ultramicroscopic examination of the so treated specimens revealed no precipitation zones nor colloids, the silver is incorporated in the lattice in normal cation sites.

Other samples were deformed, annealed in air at a temperature of 700°c and after cooling reannealed in hydrogen. A good number of combinations of temperature and time were tried out, the temperatures were 700°c, 500°c, 400°c, 300°c, the time 15, 10, 5 and 3 hours.

After such a hydrogen treatment, a thin metallic layer covered the surface of the crystals and the bulk of the crystal was slightly coloured. The thickness of this layer increased with time and temperature. Powder diagrams indicated that it consisted of finely divided silver.

Ultramicroscipic investigation revealed a decoration of the dislocation lines in the specimens treated at 500°c for various periods. The best patterns were observed in the crystals which had been heavily deformed before the first anneal. Decoration is poor in specimens treated at 400°c and 300°c.

The observed networks are similar to those observed by Amelinckx (1956) in additively coloured rocksalt crystals. The net composed of hexagonal and lozenge shaped cells shown on photograph 1 is situated in a plane making a small angle with the (001) plane. Pure rocksalt was heated in hydrogen for a long time at high temperature. Nothing could be detected inside them after this treatment. This proves that the specks are colloidal silver particles.

We suppose that the hydrogen diffuses through the crystals and reduces the silver ions (Pick 1939). The formed silver atoms migrate to the surface. A concentration gradient of Ag is established from the bulk to the surface. On cooling, a supersaturated zone is formed and precipitation occurs. This is consistent with the fact that the specks were only observed in vicinity of the surface. The inside parts of the crystals were optically empty, even if the crystal were thin enough and the hydrogen treatment long enough to allow complete diffusion of the hydrogen.

A microscope was mounted on an x-ray set. A decorated pattern, located near the edge of the crystal, was brought into focus by ultramicroscopy. The intense lines of it could be observed as brighter lines in a blue haze when the crystal was afterwards irradiated with x-rays. Using very long exposure times it was possible to photograph some of them, especially walls seen in the ultramicroscope as a row of dots. Figure 3 (b) (Plate) illustrates this. The same region, photographed with ultramicroscopy, is shown in fig. 3 (a) (Plate). Figure 4 (Plate) is another example. Exposure times are of the order of 12 to 24 hours, the lack of contrast and the poor intensity affect naturally the quality of the pictures.

The question can be raised whether the luminescence occurs around the specks, or if they show up as more intense lines because they scatter the light produced in the bulk of the crystal.

It is certain that the contact zone speck-crystal must have special properties because the bands must be distorted in that contact area, but if this, and other arguments, give credit to the first alternative, we have no clear cut answer yet. Until the phenomenon has been submitted to further study, every attempt to explain the mechanism can only be purely speculative. Experiments in progress will possibly provide more evidence.

Apart from the interest for the better understanding of luminescence, we wish to point out that the described method is a very reliable one for the production of visible dislocation networks in rocksalt and possibly other halides. It is not as tricky as the Rexer method, smaller specimens can be handled and at lower temperature. It will be very well suited for studying the organization of dislocations into networks and their evolution as the anneal proceeds.

Acknowledgments

This work is part of a research programme (C.E.S.) sponsored by the Institut pour l'encouragement de la Recherche Scientifique dans l'Industrie et l'Agriculture (I.R.S.I.A. Brussels), and Gevaert N.V. Fotoprodukten, Antwerp, to which the authors are greatly indebted.

References

Dobrinski, P., and Hinrichs, R., 1955, *Naturforsch.*, **10A**, 620.
Amelinckx, S., 1956, *Phil. Mag.*, **1**, 269.
Pick, H., 1939, *Ann. Phys.*, **35**, 75.

[*The Editors do not hold themselves responsible for the views expressed by their correspondents.*]

Fig. 1

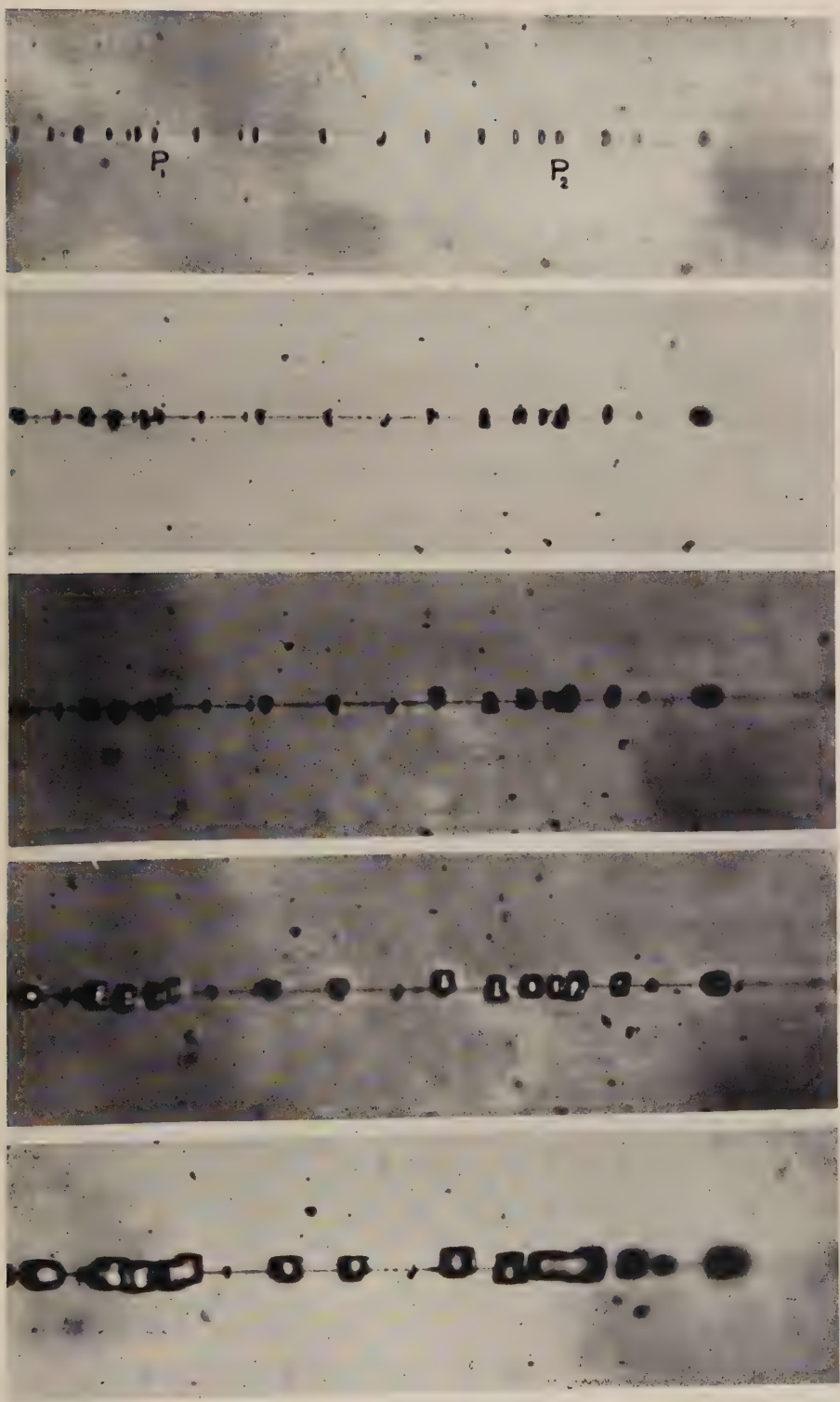

Effect of etching time : (*a*) 5 sec, (*b*) 10 sec, (*c*) 15 sec, (*d*) 30 sec, (*e*) 50 sec. ×1200.

Fig. 2

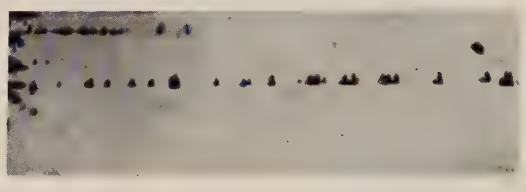

Etchpits along scratch-produced sliplines. ×1000.

Fig. 3

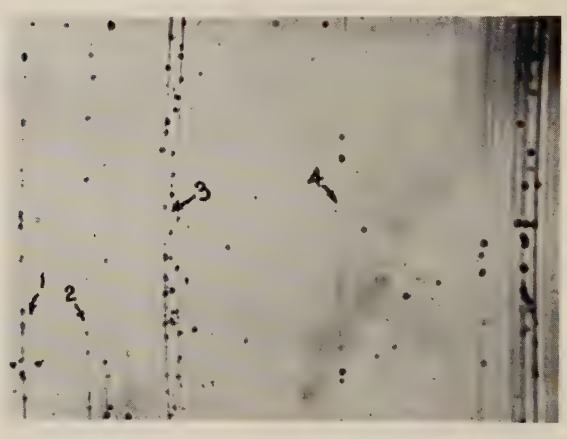

Effect of slip displacement. ×1000.

Fig. 4 (*a*)

Fig. 4 (*b*)

Effect of additional deformation. ×1500. (*a*) σ=50 g/mm². (*b*) σ=85 g/mm².

Fig. 5

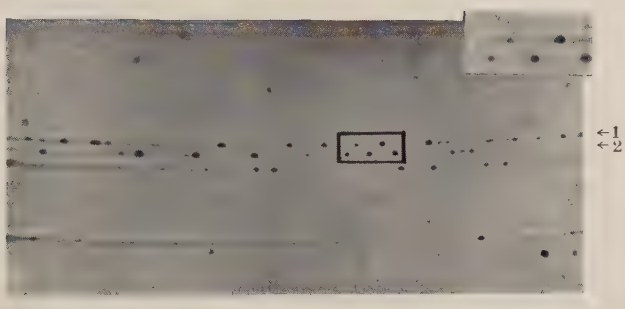

A ' Regular Array ' of etchpits. ×1000.

Fig. 6

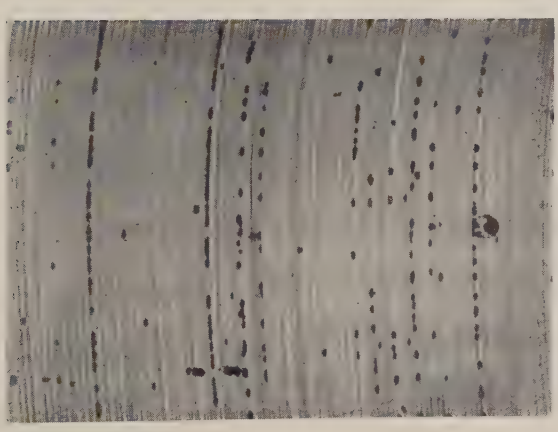

A heavily deformed crystal. ×800.

Fig. 1

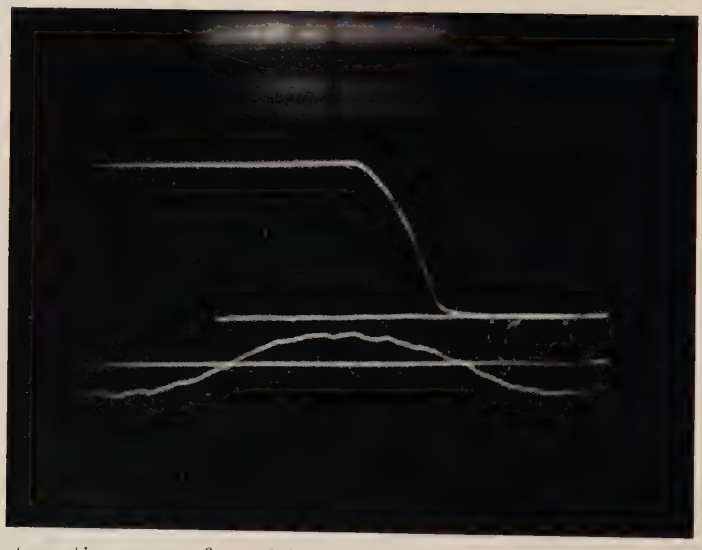

Temperature–time curve for a 0·05 mm dia wire quenched from ~1250°c into water at 4°c. The lower curve is a 50 c/s timing trace.

Fig. 4

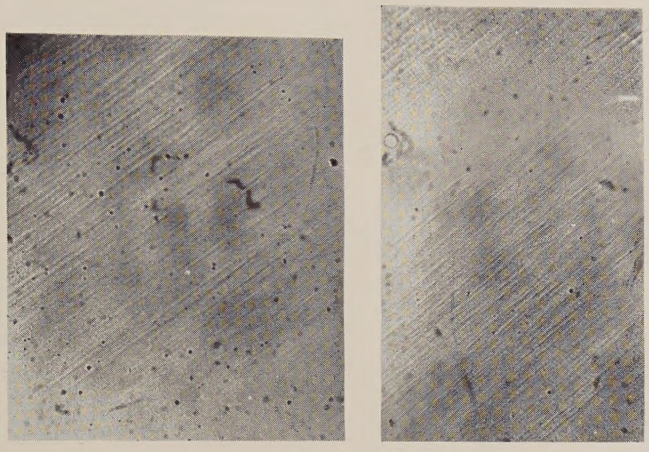

(*a*) (*b*)

Slip traces on the top surface of crystal 2 deformed at 90°K.

(*a*) Total shear strain : 25·8% ; increment visible : 1·9%×360.
(*b*) Total shear strain : 46·4% ; increment visible : 3·1%×360.

Fig. 6

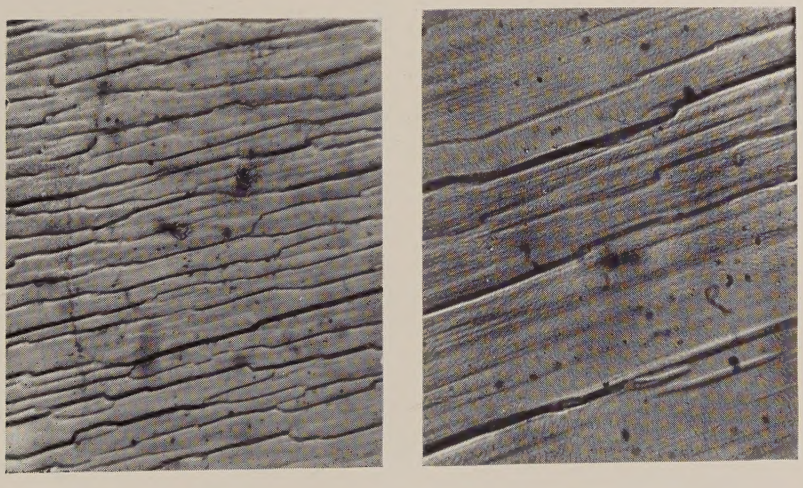

(*a*) (*b*)

Slip traces on top surface of crystal 3 on extending at room temperature after 45·3% shear strain at 90°K. (*a*) ×450. (*b*) ×1230.

Fig. 8

(*a*) (*b*)

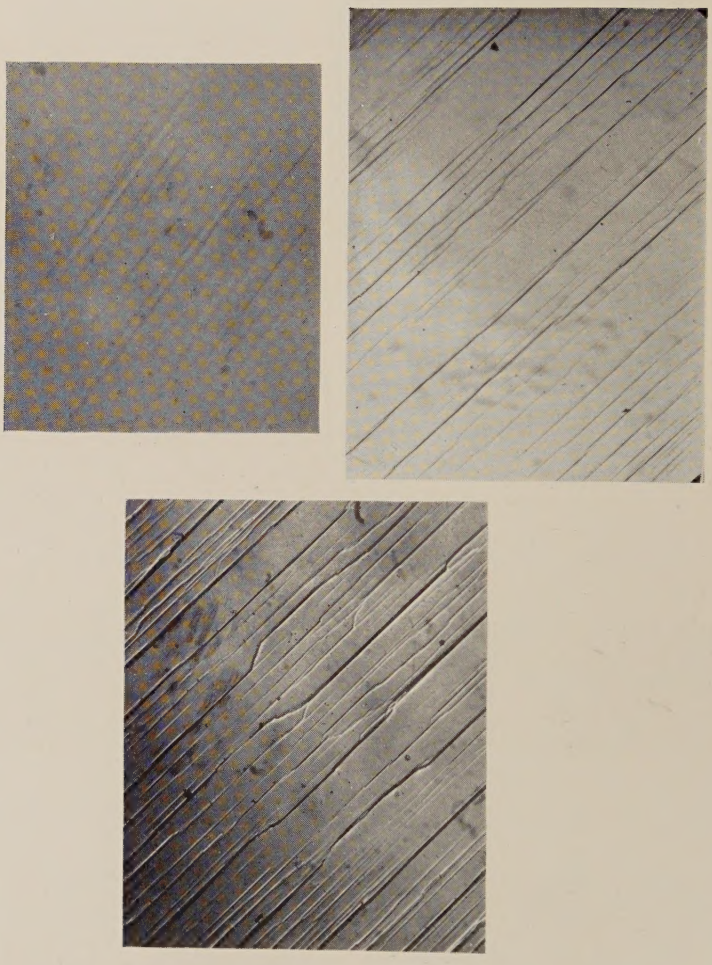

(*c*)

Slip traces on top surface of crystal 13. (*a*) Shear strain : 2·2% ; increment visible : 2·2% ×360. (*b*) Shear strain : 25·2% ; increment visible : 2·7% ×170. (*c*) As (*b*) after additional strain at 453°K.

Fig. 1

Fig. 2
(*a*)

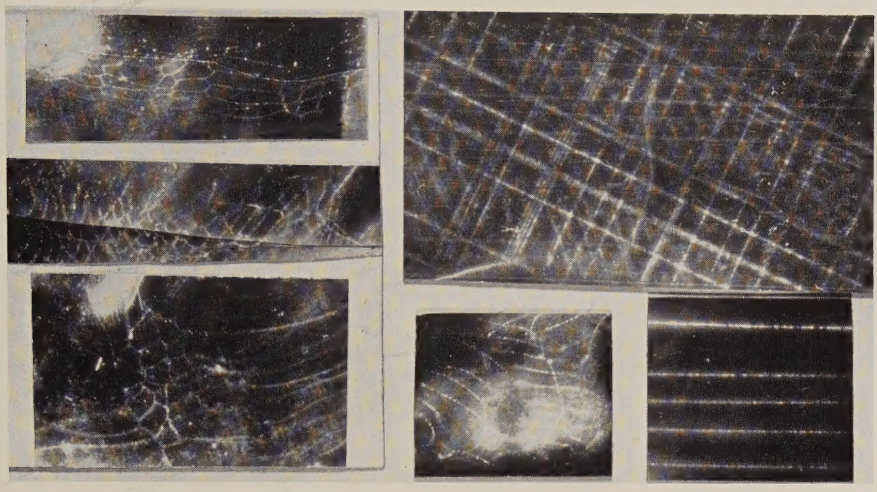

×350. (*b*) (*c*) ×350.

Fig. 3

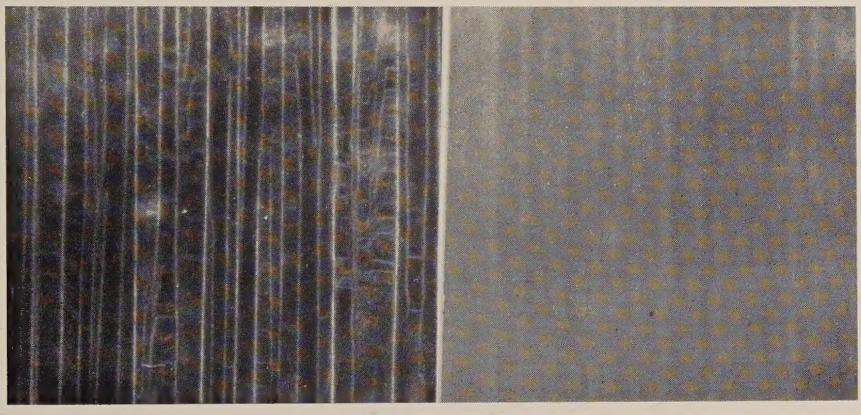

×350. (*a*) (*b*) ×350.

Fig. 4

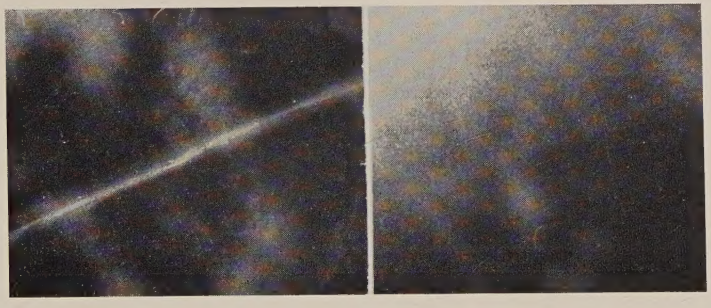

×350. (*a*) (*b*) ×350.

Fig. 1. Networks made visible by precipitation of silver. Fig. 2. (*a*) Decorated slip lines. (*b*) Rows of parallel dislocations. (*c*) Dislocation walls due to polygonization perpendicular to the plane under observation. Fig. 3. (*a*) Ultramicroscopic. (*b*) Luminescence photograph of dislocation walls. Fig. 4. (*a*) Ultramicroscopic. (*b*) Luminescence photograph of a small angle boundary.